

**A New Information Fusion Method for Land-Use Classification
Using High Resolution Satellite Imagery**

An Application in Landau, Germany

Dissertation

zur Erlangung des Grades

“Doktor der Naturwissenschaften”
am Fachbereich Geowissenschaften
der Johannes Gutenberg-Universität
in Mainz

SUN, Wanxiao
geb. in Fushun, VR China

Mainz, 1999

Hiermit versichere ich, die vorliegende Arbeit selbständig und nur mit Hilfe der angegebenen Mittel und Quellen angefertigt zu haben.

Mainz, 01.12.1999

SUN, Wanxiao

Tag der mündlichen Prüfung: 22. 12. 1999

Dedicated to my lovely son, Jiajia and my family

A New Information Fusion Method for Land-Use Classification Using High-Resolution Satellite Imagery

– An Application in Landau, Germany

Abstract

Satellite image classification involves designing and developing efficient image classifiers. With satellite image data and image analysis methods multiplying rapidly, selecting the right mix of data sources and data analysis approaches has become critical to the generation of quality land-use maps.

In this study, a new postprocessing information fusion algorithm for the extraction and representation of land-use information based on high-resolution satellite imagery is presented. This approach can produce land-use maps with sharp interregional boundaries and homogeneous regions. The proposed approach is conducted in five steps.

- First, a GIS layer – ATKIS data – was used to generate two coarse homogeneous regions, i.e. urban and rural areas.
- Second, a thematic (class) map was generated by use of a hybrid spectral classifier combining Gaussian Maximum Likelihood algorithm (GML) and ISODATA classifier.
- Third, a probabilistic relaxation algorithm was performed on the thematic map, resulting in a smoothed thematic map.
- Fourth, edge detection and edge thinning techniques were used to generate a contour map with pixel-width interclass boundaries.
- Fifth, the contour map was superimposed on the thematic map by use of a region-growing algorithm with the contour map and the smoothed thematic map as two constraints.

For the operation of the proposed method, a software package is developed using programming language C. This software package comprises the GML algorithm, a probabilistic relaxation algorithm, TBL edge detector, an edge thresholding algorithm, a fast parallel thinning algorithm, and a region-growing information fusion algorithm. The county of Landau of the State Rheinland-Pfalz, Germany was selected as a test site. The high-resolution IRS-1C imagery was used as the principal input data.

Zusammenfassung

Eine neue Methode der Informationsverknüpfung zur Klassifizierung der Landnutzung auf der Grundlage hochauflösender Satellitenbilddaten

Für die Klassifizierung der Landnutzung existiert eine große Auswahl an Satellitenbilddaten. Die Auflösungsschärfe dieser Daten richtet sich dabei nach der spezifischen räumlichen und spektralen Auflösung der verwendeten Sensoren. Für die eigentliche Klassifizierung ist die Bildverarbeitungsmethode von großer Wichtigkeit. Die Klassifizierung von Satellitenbilddaten umfaßt das Entwerfen und Entwickeln von effizienten Bildklassifizierungsverfahren.

Die bislang nur unzureichend gelöste Problematik in den Bildverarbeitungsmethoden ist die Zuordnung der Mixed Pixel und die Verfeinerung der Kanten (Feldgrenzen). Das Ziel der Arbeit liegt nun darin, Verfahren (Algorithmen) zu entwickeln, die eine möglichst eindeutige Zuordnung von Mixed-Pixel zu einer Landnutzungsklasse ermöglichen, die Problematik der Zuordnung klassenfremder Pixel (Salz und Pfeffer – Phänomen) in einem homogenen Raum lösen und zur Verfeinerung der Kanten führen.

Dieses Ziel wurde in 5 Schritten erreicht:

1. Mit einem GIS-Layer aus ATKIS-Daten ist das Untersuchungsgebiet in zwei homogene Regionen – städtische und ländliche – eingeteilt worden (preprocessing).
2. Eine Landnutzungskarte (Thematic map) wurde durch die Kombination von Gaussian Maximum Likelihood Algorithmus (GML) und ISODATA Clustering Methode erstellt.
3. Anschließend erfolgte mit der Anwendung eines Wahrscheinlichkeits-Relaxation Algorithmus (Probabilistic Relaxation) eine Glättung (= homogene Struktur der Nutzungsklassen) der Thematic map zur Smoothed thematic map.
4. Die genaue Erfassung der Feldgrenzen erfolgte mittels der PAN-Daten (hohe Auflösung). Eine entsprechende Methode existiert allerdings in der Satellitenbilddatenauswertung noch nicht. Das hierfür in der Arbeit entwickelte Verfahren basiert auf der pattern recognition der Methode der Image Segmentation. Über eigene Programmierschritte – Edge Detection, Edge Thresholding und Edge Thinning – ist es gelungen, Kanten in der Breite von 1 Pixel als Feldgrenzen zu erzeugen. Die hohe Zahl der geschlossenen Polygone in der Contour Map unterstreicht die hohe Brauchbarkeit der so entwickelten Methode.
5. Die Modifikation der Region Growing Algorithmen bot nun die Möglichkeit, die Thematic map, Smoothed thematic map und Contour map miteinander zu verschneiden. Bei geschlossenen Polygonen ergab die Zusammenführung von Contour- und Thematic map eindeutig definierte Landnutzungsklassen während bei offenen Polygonen dieses Ziel über eine Kombination von Thematic- und Smoothed thematic map erreicht wurde.

Von den bestehender Methoden konnte lediglich das Verfahren ISODATA unverändert eingesetzt werden. Die Methodik nach GML für Multispektral-Daten dagegen erfuhr eine Ergänzung durch das Hinzufügen eigen entwickelter Programme. Diese und die oben aufgelisteten Programme wurden in der Programmiersprache C selbst geschrieben. Die Satellitenbildscene (weitgehend wolkenfrei !) bestimmte die Stadt Landau in Rheinland-Pfalz und ihre Umgebung als Untersuchungsraum. Die vorliegende Arbeit basiert auf den IRS-1C Daten (PAN 5,8 m; LISS-III 23,5m) des indischen Satelliten.

A New Information Fusion Method for Land-Use Classification
Using High-Resolution Satellite Imagery
– An Application in Landau, Germany

Contents

Abstract	V
Zusammenfassung.....	VI
List of Figures	X
List of Tables.....	XII
Abbreviations	XIII
Acknowledgments	XV
Part I Theoretical and Empirical Background	1
1 Introduction	1
2 Land-Use Classification Using Satellite Imagery	4
2.1 Remote Sensing and Land-Use Mapping	4
2.1.1 Recent developments in remote sensing technology.....	4
2.1.2 Advantages of land-use mapping using satellite imagery	7
2.2 Digital Image Processing and Pattern Recognition.....	7
2.2.1 Pattern recognition systems.....	8
2.2.2 Pattern recognition techniques	9
2.3 Multispectral Satellite Image Classification	11
2.3.1 Conventional spectral classifiers	11
2.3.2 The misclassification problem	13
2.4 Recent Developments in Satellite Image Classification Techniques.....	14
2.4.1 New spectral classification methods	14
2.4.2 Contextual classification techniques	16
2.4.3 Information fusion and GIS integration techniques	17
2.4.4 Knowledge-based classification approaches	18
2.5 The Image Classification Algorithm Proposed in This Study	20
2.5.1 Software architecture	20
2.5.2 Implementation procedures	20
3 The Study Area and Data Acquisition.....	23
3.1 The Study Area	23

3.1.1	Morphological structure	24
3.1.2	Climate	24
3.1.3	Soils and land-use	26
3.2	IRS-1C Satellite Imagery Data.....	26
3.2.1	Background	26
3.2.2	IRS-1C satellite imaging systems.....	27
3.2.3	Payload sensors and IRS-1C imagery data.....	27
3.2.4	Selected satellite scenes	31
3.3	Reference Data.....	33
3.3.1	Digital orthophotos	33
3.3.2	ATKIS	33
3.3.3	Topographic maps - TK 25	34
3.3.4	Field data.....	34
Part II Multispectral Image Classification Methods		35
4	Preprocessing of IRS-1C Imagery	35
4.1	Rectification.....	35
4.1.1	Global Positioning System (GPS).....	37
4.1.2	Rectification of IRS-1C panchromatic image using DGPS	39
4.1.3	Rectification of multispectral images using "image-to-image" registration method.....	48
4.2	Merge of Panchromatic Image and Multispectral Images	51
4.2.1	Intensity-Hue-Saturation (IHS) method	52
4.2.2	Principal Component Substitution (PCS) method	53
4.3	Implementation and Results.....	54
5	Multispectral Classification of IRS-1C Imagery Data	56
5.1	Supervised Classification.....	56
5.1.1	Parallelepiped decision rule	56
5.1.2	Minimum Distance.....	58
5.1.3	Mahalanobis Distance	59
5.1.4	Maximum-Likelihood/Bayesian classification	60
5.2	Unsupervised Classification - ISODATA Clustering	63
5.3	Implementation and Results.....	65
5.3.1	Design of land-use classification system	65
5.3.2	Segmentation of urban and agricultural areas using ATKIS data	66
5.3.3	Classification of agricultural areas.....	69
5.3.3.1	ISODATA clustering	70
5.3.3.2	Training sample selection	70
5.3.3.3	Signature generation and evaluation.....	71
5.3.3.4	Maximum Likelihood classification results.....	76
5.3.4	Classification of urban areas	78
Part III Improved Satellite Image Classification Methods		79
6	Contextual Classification of IRS-1C Imagery	79

6.1	Contextual Classification Techniques	79
6.2	Main Contextual Classifiers	80
6.3	Probabilistic Relaxation Methods.....	82
6.3.1	Probability calculation	83
6.3.2	Compatibility coefficients	83
6.3.3	Neighborhood function	84
6.3.4	Updating rule.....	85
6.4	Implementation and Results.....	86
6.4.1	Implementation procedures	86
6.4.2	Results	90
7	Edge Extraction from IRS-1C PAN Imagery Data	92
7.1	Edge Extraction and Image Classification	92
7.2	Edge Detection Operators	93
7.2.1	Edge detection	93
7.2.2	Edge detection using first-order derivatives.....	94
7.2.3	Edge detection using second-order derivatives	96
7.2.4	Texture boundary locator (TBL)	96
7.3	Edge Thresholding	98
7.4	Thinning of Binary Edge Images	99
7.5	Implementation and Results.....	103
7.5.1	Generation of edge map	103
7.5.2	Generation of pixel-width contour map	106
8	Fusion of Thematic Map and Edge Map Using Region-Growing Algorithm.....	111
8.1	The Basic Concept	111
8.2	Region-growing Algorithms	113
8.3	Implementation and Results.....	115
8.3.1	A modified region-growing algorithm	115
8.3.2	Image fusion.....	115
9	Summary	120
	Literature.....	123

List of Figures

Figure 2-1	The three phases of pattern recognition.....	8
Figure 2-2	Major approaches for image segmentation/classification	9
Figure 2-3	A model for pattern recognition in remote sensing	12
Figure 2-4	Software architecture of the proposed land-use classification algorithm.....	22
Figure 3-1	Location of the study area.....	23
Figure 3-2	Overview of IRS-1C mission	28
Figure 3-3	PAN off-nadir viewing capability	30
Figure 4-1	The constellation of GPS.....	38
Figure 4-2	Workflow for the rectification of panchromatic image using DGPS	40
Figure 4-3	Residuals and RMS error per point	43
Figure 4-4	Relationship between the original image pixels and rectified pixels	45
Figure 4-5	A subset of overlay of rectified panchromatic image and digital orthophotos.....	47
Figure 4-6	A subset of overlay of rectified multispectral image and digital orthophotos.....	50
Figure 4-7	The principle of transform-replace-retransform method	52
Figure 4-8	The HIS transformation process	53
Figure 4-9	A subset of the HIS merge of PAN and multispectral imagery.....	55
Figure 4-10	A subset of the PCS merge of PAN and multispectral imagery.....	55
Figure 5-1	Parallelepiped classification using plus or minus two standard deviations as limits.....	57
Figure 5-2	Minimum spectral distance	58
Figure 5-3	Maximum likelihood decision rule.....	60
Figure 5-4	ISODATA clustering procedure.....	64
Figure 5-5	The procedure for extracting urban areas using GIS	67
Figure 5-6-1	Maximum likelihood classification before segmentation of urban and agricultural areas	68
Figure 5-6-2	Maximum likelihood classification after segmentation of urban and agricultural areas	68
Figure 5-7	The procedure for classification of agricultural areas	69
Figure 5-8	The ellipses for the five signatures of vince in the feature space	72
Figure 5-9	Maximum likelihood and ISODATA classification result.....	76
Figure 5-10	Grassland.....	77
Figure 5-11	Vineyard	77
Figure 5-12	ISODATA classification results of the urban area	78
Figure 6-1	Definition of a simple neighborhood of pixel i	85
Figure 6-2	Three steps for the implementation of probabilistic relaxation.....	87
Figure 6-3	Probabilistic relaxation algorithm	89
Figure 6-4	A subset of the smoothed thematic map generated by use of the probabilistic relaxation algorithm after 10 iterations	91
Figure 6-5	A subset of the original thematic map.....	91
Figure 7-1	(a) Prewitt edge detector masks; (b) Sobel edge detector masks.....	95
Figure 7-2	Window geometry for the texture boundary locator (TBL) algorithm	97
Figure 7-3	The 3×3 neighborhood of the pixel $P(i, j)$	101

Figure 7-4 The flow of cycle 1 of the Chen-Hsu algorithm	102
Figure 7-5 The flow of cycle 2 of the Chen-Hsu algorithm	103
Figure 7-6-1 Result of TBL algorithm: $K = 1, N = 3, T = 10\%$	104
Figure 7-6-2 Result of TBL algorithm: $K = 1, N = 3, T = 15\%$	105
Figure 7-6-3 Result of TBL algorithm: $K = 1, N = 3, T = 20\%$	105
Figure 7-7-1 Result of Chen-Hsu algorithm: $K = 1, N = 3, T = 10\%$	106
Figure 7-7-2 Result of Chen-Hsu algorithm: $K = 1, N = 3, T = 15\%$	107
Figure 7-7-3 Result of Chen-Hsu algorithm: $K = 1, N = 3, T = 20\%$	107
Figure 7-8 Contour map after using Lee-Sigma filter	108
Figure 7-9 Asphalt road	109
Figure 7-10 Field pathway	110
Figure 8-1 A subset of an overlay of the contour map with the rectified PAN image	112
Figure 8-2 Information fusion procedure	113
Figure 8-3-1 Fusion algorithm for the thematic map, contour map and smoothed map	116
Figure 8-3-2 Subroutine region growing	117
Figure 8-4-1 A subset of the original thematic map	118
Figure 8-4-2 A subset of the smoothed map	118
Figure 8-4-3 A subset of the contour map	119
Figure 8-4-4 Improved thematic map by fusion of the thematic map, contour map and smoothed map	119

List of Tables

Table 2-1	Approaches for improving satellite image classification accuracy.....	15
Table 3-1	Key technical parameters of the IRS-1C imaging systems.....	29
Table 3-2	Imaging sensor characteristics on board IRS-1C.....	29
Table 3-3	Overview of IRS-1C data products.....	32
Table 3-4	The path, row number and product code of selected IRS-1C satellite data.....	32
Table 3-5	Explanatory notes on IRS-1C data product code.....	32
Table 3-6	The selected digital orthophotographs.....	33
Table 3-7	TK25 maps used in this study.....	34
Table 4-1	The map projection and coordinate system used for IRS-1C images.....	37
Table 4-2	The source and Gauss-Krueger coordinates of the 25 selected GCPs in panchromatic image.....	44
Table 4-3	The RMS error of the GCPs in the panchromatic image.....	44
Table 4-4	Transformation coefficients of GPS method.....	44
Table 4-5	The selected GCPs coordinates of panchromatic and multispectral images.....	49
Table 4-6	The RMS error of GCPs for the multispectral images.....	49
Table 4-7	Transformation coefficients of "image-to-image" method.....	49
Table 5-1	The land-use classification system used in this study.....	66
Table 5-2	The number, name, source, and the number of pixels of the signatures.....	73
Table 5-3	Separability of the 36 signatures.....	74
Table 5-4	The contingency matrix of the 24 signatures.....	75

Abbreviations

AI	Artificial Intelligence
ATKIS	Amtliches Topographisch Kartographisches Informationssystem
AVHRR	Advanced Very High Resolution Radiometer
CA	Coarse Acquisition
CAD	Computer-Aided Design
CCD	Charge Coupled Devices
CIR	Color Infra Red
DEM	Digital Elevation Model
DGPS	Differential Global Positioning System
ECHO	Extraction and Classification of Homogeneous Objects
EREP	Earth Resources Experiment Package
ERS	European Remote Sensing
ERTS	Earth Resources Technology Satellites
ETM+	Enhanced Thematic Mapper Plus
GIS	Geographic Information System
GAC	Global Area Coverage
GCP	Ground Control Point
GML	Gaussian Maximum Likelihood
GPS	Global Positioning System
HRPT	Resolution Picture Transmission
HRV	High Resolution Visible
IFOV	Instantaneous Field Of View
IHS	Intensity-Hue-Saturation
IR	Infra Red
IRS	Indian Remote Sensing
ISODATA	Self-Organizing Data Analysis Technique
LAC	Local Area Coverage
LBD	Landwirtschaftliche Betriebsdaten Bank
LISS	Linear Imaging and Self Scanning Sensor
MAT	Medial Axis Transformation
MLP	Multi Layer Perceptron
MRF	Markov Random Field
MSS	Multispectral Scanner
NASA	National Agency
NIR	Near Infra Red
NOAA	National Oceanic and Atmospheric Administration
RBV	Return Beam Vidicon
PAN	Panchromatic
PCS	Principal Component Substitution
PPS	Precise Positioning System
RGB	Red-Green-Blue
RMS	Root Mean Square
RS	Remote Sensing
RVS	Regression Variable Substitution
S/A	Selective Availability
SPOT	System Pour l'Observation de la Terre
SVR	Synthetic Variable Ratio

SWIR Short Wave Infra Red
TBL Texture Boundary Locator
TM Thematic Mapper
TK Topographische Karte
TTC Telemetry Tracking and Command
USGS United State Geological Survey
WiFS Wide Field Sensor

Danksagung

Die Möglichkeit, mich im Rahmen meiner Dissertation mit dem vorliegenden Thema zu befassen, verdanke Herrn Prof. Dr. Volker Heidt. Für die Aufnahme in seine Arbeitsgruppe, seine Hilfsbereitschaft, seine stetige Diskussionsbereitschaft, die Bereitstellung von Mitteln für den Ankauf der Satellitenbilder vor allem aber für seine unermüdliche Einsatzbereitschaft möchte ich mich herzlich bedanken.

Außerdem danke ich Herrn Univ. Prof. Dr. Dr. h. c. M. Domrös für seine Unterstützung und seine Bereitschaft, die Arbeit zu begleiten und die Begutachtung zu übernehmen.

Herrn PD Dr. Dieter König sei gedankt für vielfältige Unterstützungen, vor allem für seine Mühen zur Beschaffung der Satellitenbilddaten.

An dieser Stelle möchte ich mich bei den Verantwortlichen, die mir ein Stipendium im Rahmen des Graduiertenkollegs an der Universität Mainz gewährt haben, danken. Durch diese finanzielle Unterstützung ist die Fertigstellung dieser Arbeit im entsprechenden Zeitrahmen erst möglich geworden.

Während meiner Arbeit bin ich vielen Menschen begegnet, denen ich für ihre Hilfestellungen verschiedenster Art zu Dank verpflichtet bin, so Herrn Ohliger von der Kreisverwaltung Südliche Weinstraße, der mir die Unterlagen der Landnutzung bereitstellte und bei der Auswahl der Trainingsgebiete Hilfe geleistet hat. Weiterhin gilt mein Dank den Herren Adam und Bauer vom Amt für Vermessungswesen der Stadt Landau an der Weinstraße, die über die Bereitstellung von Datenmaterial und die Einmessung der Basisstation die Voraussetzung für die Anwendung des Global Positioning System (GPS) schufen. Ebenfalls möchte ich Herrn Rudi Vassel für seine stete Bereitschaft der fachlichen Beratung und seine Hilfe, wenn es um die Bereitstellung von Datenmaterial ging, danken.

Herrn Zhang Yun von der Deutschen Forschungsanstalt für Luft- und Raumfahrt (Berlin) danke ich für seine Hilfeleistung bei der Interfaceerstellung zwischen den C-Programmen und ERDAS Imagine. Herrn Markus Tacke aus dem Zentrum für Datenverarbeitung der Uni Mainz möchte ich an dieser Stelle für die Anwendungsoptimierung der Computerprogramme danken.

Mein besonderer Dank gilt allen Mitarbeitern der Forschungsgruppe Ökologie&Planung, die mir stets mit fachlichen Ratschlägen zu Seite standen und mit ihrer menschlichen Wärme für ein ausgezeichnetes Arbeitsklima sorgten. Insbesondere Paul Hurys, Thorsten Klein, Sabine Krause, Brigitte Leicht, Joachim Merchel, Jamill Sabbagh und Alexander Tillmann.

Schließlich möchte ich an dieser Stelle meinen Eltern, meinem Mann Xu Gang und meinem Sohn Jiajia für ihr großes Verständnis, ihren Beistand und ihre Geduld, sowie ihre tatkräftige Unterstützung während des Werdegangs dieser Dissertation herzlich danken, da sie so manche Entbehrung auf sich nehmen mußten.

Part I Theoretical and Empirical Background

Chapter 1 Introduction

Since the launch of Landsat-1 – the first Earth resource satellite – in 1972, remote sensing has become an increasingly important tool for the inventory, monitoring, and management of earth resources. The increasing availability of information products generated from satellite imagery data has added greatly to our ability to understand the patterns and dynamics of the earth resource systems at all scales of inquiry.

A particularly important application of remote sensing is the generation of land-use/land-cover maps from satellite imagery. Compared to more traditional mapping approaches such as terrestrial survey and basic aerial photointerpretation, land-use mapping using satellite imagery has the advantages of low cost, large area coverage, repetitivity, and computitivity. Consequently, land-use information products obtained from satellite imagery such as land-use maps, data and GIS layers have become an essential tool in many operational programs involving land resource management.

The prospect for the use of satellite imagery data in land-use management and planning is an extremely promising one. As a result of the recent development of sensor technology, the quality of satellite imagery available for land-use mapping is improving rapidly. Particularly noteworthy in this regard is the improved spatial and spectral resolution of the imagery captured by new satellite sensors. In addition to existing imaging systems such as Landsat TM and SPOT HRV, a number of new remote sensing sensors with up to 1-m ground resolution are already in operation. IKONOS of Space Imaging, launched on 24 September 1999, has already sent back its first image with a spatial resolution of 1m.

The increasing availability of satellite imagery with significantly improved spectral and spatial resolution has offered greater potential for more detailed land-use

mapping. It was predicted that in the near future, more than 50 percent of the current aerial photo market will be replaced by high-resolution satellite imagery (Fritz 1996).

At the same time, rapid advances in the computer science as well as other information technology (IT) fields have offered more powerful tools for satellite image processing and analysis. Image processing software and hardware are becoming more efficient and less expensive. Access to faster and more capable computer platforms has aided our ability to store and process larger and more detailed image and attribute data sets. The use of more advanced statistics and probability theories in image processing in such neighboring disciplines as computer vision and artificial intelligence has also generated spill-over effect in satellite imagery classification.

Digital image processing is central to efficient use of satellite imagery in land-use studies. A key task of satellite image processing is to develop image data analysis approaches appropriate to a particular resource management application. The extraction and classification of land-cover types from satellite imagery is probably the most important objective of digital image analysis in the geoscience.

Conventional image classification techniques are based on the spectral response patterns of terrain features captured in satellite imagery. While conventional spectral classifiers are widely used and have achieved a fairly large amount of success, the resulting classification maps are often very noisy.

The enhanced information content of high-resolution satellite imagery and the long-term desire of land-use planners to obtain detailed land-use maps highlight the need for more powerful tools for analyzing multispectral data. As a result, recent years have seen a multiplicity of approaches to satellite image classification. A main thrust in this development is that, in addition to making better use of enhanced spectral information of imagery data, increasing attention is being given to the spatial and semantical characteristics of terrain features. Recent studies demonstrated that the higher information content of imagery data combined with the improvements in image processing power result in significant improvement in classification accuracy.

The objective of this study is to develop an efficient approach for multispectral image classification. We proposed a new information fusion algorithm for the extraction and representation of land-use types from high-resolution satellite imagery. The proposed approach integrates spectral and spatial image classification techniques. This approach can produce land-use maps with sharp interregional boundaries and homogeneous regions.

The county of Landau of the State Rheinland-Pfalz, Germany was selected as a test site. The study area comprises agricultural, forest, grassland, and urban land-use types. This study used the high-resolution IRS-1C imagery as the principal input data. The input image data includes 1/9 PAN scene (5.8-m ground resolution) and the corresponding LISS-III scene. These scenes correspond to a ground area of 23×23 km².

This study is organized into nine chapters. Details of the proposed method as well as a review of image classification techniques are presented in the next chapter. Chapter 3 gives a brief description of the study area and the imagery data used in this study. The preprocessing of IRS-1C imagery data, including image rectification and merging of PAN and LISS-III imagery, is described in Chapter 4. A hybrid method combining GML and ISODATA are presented in Chapter 5. In Chapter 6, a probabilistic relaxation algorithm is described. Edge detection, thresholding and thinning techniques are presented in Chapter 7. In Chapter 8 the procedure for the fusion of the contour map and the thematic map is described. Chapter 9 sums up the main findings of this study.

Chapter 2 Land-use Classification Using Satellite Imagery

2.1 Remote Sensing and Land-Use Mapping

2.1.1 Recent developments in remote sensing technology

Remote sensing is essentially an earth observation technique. It is the science and art of obtaining information about an object through the analysis of data acquired by a device that is not in contact with the object (Lillesand and Kiefer 1994). Since the launch of Landsat-1 in 1972, remote sensing has become an important tool in many resource management areas such as land-cover classification, resource inventory, pollution detection, environmental impact assessment, and environmental modeling.

Generally, a remote sensing system consists of five components. They are the energy source, the sensor, ground objects, the data-handling system, and the multiple data users. According to the source of energy used, two types of remote sensing systems – active and passive – are distinguished. "Active" refers to a sensor that supplies its own source of energy or illumination. Imaging radar sensors are active sensors, which emit a burst of microwave radiation and receive the backscattered radiation. Most commercial satellite sensors are passive solar imaging sensors. In this case, the sun is the source of electromagnetic radiation (ERDAS Field Guide 1997).

Remote sensing systems operate on the principle of electromagnetic radiation. As different types of earth surface features have their own distinctive electromagnetic energy signals, they can be detected, recorded and interpreted on the basis of their electromagnetic reflections. In remote sensing, it is most common to characterize electromagnetic waves by their wavelength location within the electromagnetic spectrum. The wavelength ranges in which the atmosphere is particularly transmissive of energy are referred to as atmospheric windows. Remote sensing data acquisition is limited to the atmospheric windows.

Sensors form the heart of remote sensing systems. They are used to record variations in the way earth surface features reflect and emit electromagnetic energy. Wavelength range and spatial resolution are two major indications of a sensor's technical capabilities. No single sensor is sensitive to all wavelengths. All real sensors are designed to be sensitive to a fixed range within the electromagnetic spectrum. Sensors also have a limit on how small an object on the earth's surface can be and still be "seen" by a sensor as being separate from its surroundings. This limit is called the spatial resolution of a sensor. Spatial resolution is an indication of how well a sensor can record spatial details.

Satellite imaging systems designed for earth resource observation purposes use multispectral scanners. The multispectral scanner (MSS) is a sensor that acquires data from multiple spectral bands simultaneously. Multispectral scanners sense simultaneously through multiple, narrow wavelength ranges that can be located in the visible through the thermal spectral region. Multispectral imagery provides more information than data collected in any single spectral band. When the signals recorded in the multiple bands are analyzed in conjunction with each other, more information becomes available.

A multispectral scanner operates on the same principle of selective sensing in multiple spectral bands. But multispectral scanners have some inherent advantages over their photographic counterparts (Lillesand and Kiefer 1994).

- Using electronic detectors, multispectral scanners can extend the range of sensing from 0.3 to approximately $14\mu m$. This range includes the ultraviolet (UV), visible, near infra red, middle infra red, and thermal spectral regions. MSS systems can also sense in very narrow spectral bands.
- MSS systems use the same optical system to collect data in all spectral bands simultaneously. This ensures that data in separate bands are comparable to one another spatially and radiometrically.
- MSS data are generated electronically and are therefore more amenable to calibration. The electronic format of the scanner output also permits recording over a greater range of values in a digital format.

A main thrust in the recent development of sensor technology has been the increasing spatial and spectral resolution. In addition to existing imaging systems such as Landsat TM and SPOT HRV, a number of new remote sensing sensors with significantly improved geometric resolution are already in operation (Draeger et al 1997). For example, the French SPOT-4, launched in 1997, has incorporated 5-m spatial resolution and along-track stereo imaging capability. The German MOMS-02 sensor system has a designed ground resolution of 4.5m and has adopted the latest three-track technology combined with a stereo- and multispectral module (Fritz 1996).

The Indian IRS-1C has incorporated an advanced imaging system. This system has a panchromatic camera that captures data with a spatial resolution of 5.8m and a ground swath of 70km. In addition to that, the IRS-1C imaging system is equipped with a linear imaging and self scanning (LISS) sensor that provides multispectral data collected in visible, near infra red (NIR) and short wave infra red (SWIR) regions.

A number of high-resolution imaging systems with up to 1-m ground resolution are already in operation (Li 1998). Among these high-resolution satellites are EarlyBird (3-m resolution). The latest development was the launch of IKONOS of Space Imaging, Inc. on 24 September 1999. The IKONOS imaging system has already sent back its first image with a ground resolution of 1m (<http://www.erdas.com>). In the pipeline are QuickBird (1-m resolution) of Earth Watch and OrbView-1 (1-, 2-, and 4-m resolution) of the Orbital Sciences Corporation.

The launch of high-resolution commercial imaging satellites marked the start of a new era of space imaging for Earth observation. The imagery captured by the new sensors will maintain the dominant spectral advantages demonstrated by lower resolution satellite imaging systems. Furthermore, these new sensors can generate imagery that provide strong geometric and radiometric capabilities such as higher spatial resolution, photogrammetric stereo capability and revisit rate that have not been available from existing imaging systems. These advances have opened new horizons for land-use studies.

2.1.2 Advantages of land-use mapping using satellite imagery

Using satellite imagery to extract and represent land-use/land-cover information is a key application of remote sensing technology. Land-use information products generated from multispectral imagery such as maps, data, and GIS layers, have become an essential tool in many land resource management areas such as land-use classification, crop acreage and yield estimation, and land-use planning.

Compared to more traditional mapping approaches such as basic aerial photointerpretation, land-use mapping using satellite imagery has four advantages.

- First, land-use types can be mapped from digital satellite imagery faster and often with lower costs.
- Second, fast and inexpensive updating of land-use map products is possible. This is because satellite images are captured for the same geographic area at a high revisit rate.
- Third, satellite imagery data are captured in digital forms. They can therefore easily be integrated with other types of ground object information through such techniques as GIS.
- Fourth, satellite images cover large geographic areas. The great economies of scale provided by digital image processing make it relatively inexpensive to map large expanses of land, making it easier and more cost effective to generate large amounts of map products.

2.2 Digital Image Processing and Pattern Recognition

Digital image processing is the technique of manipulating and interpreting digital images with the aid of a computer (Swain and Davis 1978). It starts with one image and produces such information products as segmented images, data, and maps. Digital image processing permits rapid and repeatable analysis, allows for statistical treatment of multivariate data and produces quantitative results. The ultimate goal of digital image processing is to identify and interpret patterns in an image, i.e. pattern recognition.

2.2.1 Pattern recognition systems

Pattern recognition is the science and art of finding meaningful patterns in data (ERDAS Field Guide 1997). A pattern is simply any well-defined set of measurements. The pattern recognition process consists of three phases, i.e., 1) image segmentation, 2) feature extraction, and 3) classification (Figure 2-1).

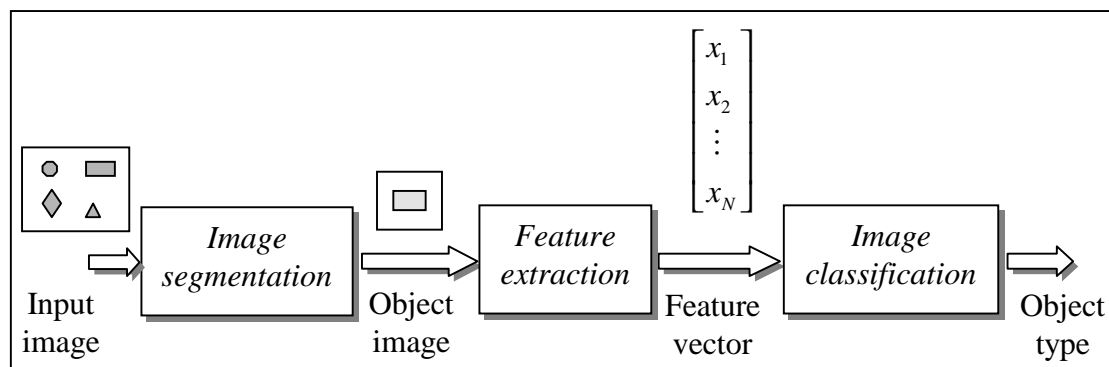


Figure 2-1 The three phases of pattern recognition (Source: after Castleman 1996)

Image segmentation is the first essential step of low level vision (Marr 1982; Rosenfeld and Kak 1982). It is a process of partitioning a digital image into disjoint, connected sets of pixels, one of which corresponds to the background and the remainder to the objects in the image (Hall 1979; Gonzalez and Wintz 1987). There are hundreds of segmentation techniques, but no single method can be considered good for all images (Pal and Pal 1993). Broadly, image segmentation can be approached from three different philosophical perspectives: region, boundary, and edge (Castleman 1996).

- In the region approach, one assigns each pixel to a particular object or region.
- In the boundary approach, one attempts only to locate boundaries that exist between the regions.
- In the edge approach, one seeks to identify edge pixels and then link them together to form the required boundaries.

Following image segmentation is feature extraction. Essentially a feature is a measurement that serves to discriminate between a number of classes. The purpose of extracting feature is to provide some of the information needed for a classification decision rule to operate successfully. Feature extraction is a crucial stage in pattern recognition because the performance of any classification decision rule will depend on how well the feature detector can capture the features of the objects to be classified. The feature extraction process produces a set of features that, taken together, comprise the n -dimension feature vector. Any particular object in an image corresponds to a point in feature space (Swain and David 1978).

Image classification is a process of assigning pixels in an image to one of a number of classes or labels. Classification is based solely on the feature vector. The classification model of recognition is the best understood and it forms the basis for more complex forms of pattern recognition (James 1987; Jaehne 1989). Classification implies the use of a decision rule and it involves establishing mathematical basis of the classification algorithm for the classification procedure. Its output is merely a decision regarding the class to which each object belongs.

2.2.2 Pattern recognition techniques

A variety of approaches for image segmentation and classification are proposed in the literature. Broadly, these approaches can be divided into three major groups (Figure 2-2; Pal and Pal 1993).

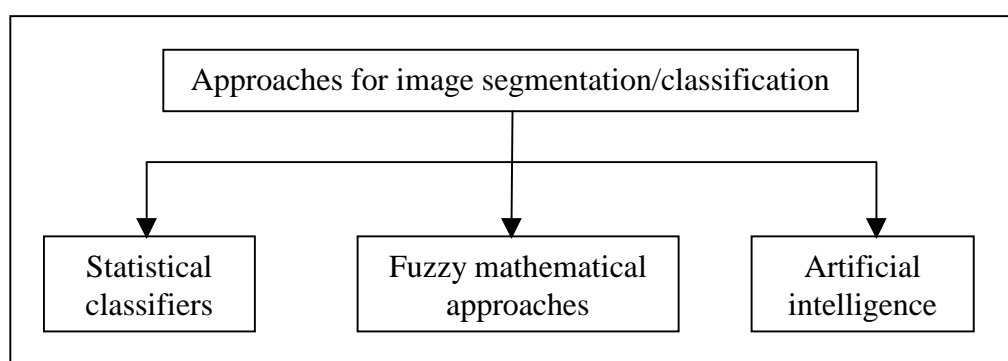


Figure 2-2 Major approaches for image segmentation/classification

(1) Statistical pattern recognition

Statistical pattern recognition is the most widely used approach for image classification/segmentation. Statistical classifiers are based on some quite sophisticated statistics and probability theories. Parametric and nonparametric approaches are two classical statistical pattern recognition methods. Representative of parametric methods is the Bayes Minimal Error Decision Rule. Parzen's Kernel method and the K-Nearest-Neighbor technique are the two most outstanding nonparametric approaches. Tree-based classification was first proposed by Sonquist and Morgan and is widely used in statistical pattern recognition and Machine Learning (Gascuel et al 1993).

(2) Fuzzy mathematical approaches

Zadeh introduced in 1965 the concept of fuzzy sets in which imprecise knowledge can be used to define an event. Fuzzy set theory may be incorporated in handling uncertainties in various stages of a pattern recognition system such as cluster analysis, classifier design, image processing and image recognition. This methodological development has much to do with the realization that many of the basic concepts in image analysis, e.g. the concept of an edge or a boundary, do not lend themselves well to precise definition.

(3) Artificial intelligence (AI)

In the field of artificial intelligence, supervised classification methods were developed from the beginning of the 1970s, with the famous "Arch Concept Learning" problem proposed by Winston (1975). These methods have the capacity to learn from structural example descriptions, thus abandoning the value-attribute model used in other approaches. AI-type models were based on semantic networks and on predicate logic. Use of neural networks is gaining importance in image segmentation in recent years. This development has much to do with the work of Hopfield (1982) on associative memory models. The development of the Multi-Layer-Perceptron (MLP) contributed greatly to the supervised classification. The MLP associates the notion of hidden cells with a learning algorithm of the stochastic gradient type, such as the backpropagation of the error gradient, thus enabling a break-away from the linear framework (Gascuel et al 1993).

2.3 Multispectral Satellite Image Classification

2.3.1 Conventional spectral classifiers

Multispectral satellite image classification is an application of pattern recognition in the geoscience (Figure 2-3). In a satellite image the natural pattern is one ground resolution element or pixel. The receptor may be an airborne or spaceborne multispectral scanner. The feature of a natural pattern is a set of n radiance measurements obtained in the various wavelength bands for each pixel. This set of measurements is referred to as a measurement vector in the measurement space. Classifier or the decision maker assigns the measurement vector to one of a set of classes according to an appropriate decision rule (Swain and David 1978; Lillesand and Kiefer 1994).

The fundamental basis for multispectral satellite image classification is the electromagnetic reflectance properties of earth surface features. Because ground objects have their own characteristic spectral response in different spectral bands of the electromagnetic spectrum, they can be identified and delineated in a multispectral image.

The spectral reflectance characteristics of ground objects are described by spectral reflectance curves. A spectral reflectance curve is a graph of the spectral reflectance of an object as a function of wavelength. Because spectral responses measured by remote sensors over various features often permit an assessment of the type and/or condition of the features, these responses are also referred to as spectral signatures. The configuration of these spectral reflectance curves gives us insight into the spectral characteristics of the objects.

The multispectral approach forms the heart of the application of remote sensing in discrimination of land-cover types and conditions. By analyzing a scene in several spectral bands, we can improve our ability to distinguish the identity and condition of terrain features. For example, water and vegetation might reflect nearly equally in visible wavelengths, yet these features are almost always separable in near-infrared wavelengths.

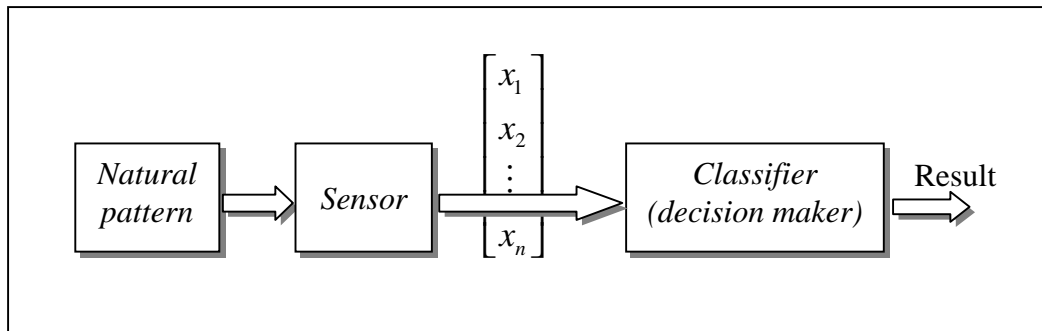


Figure 2-3 A model for pattern recognition in remote sensing (Swain and David 1978)

Many approaches have been developed for the classification of multispectral satellite imagery. These approaches have ranged from pure statistical techniques to pure knowledge-based methods (Gascuel et al 1993; Pal and Pal 1993). A literature survey suggests that until quite recently the research on satellite image classification has focused predominantly on the spectral characteristics of terrain features. Consequently, spectral classifiers are the most commonly used classification method up to date.

Conventional multispectral classification methods make use of spectral response patterns of ground object. In the usual approach, the spectral response vectors of each class are modeled to have multivariate normal distributions, and the parameters of such models are estimated from training samples. Such a technique is known as supervised classification. In an unsupervised classification, these parameters are estimated from all image pixels by a suitable clustering method. Supervised and unsupervised multispectral classifications are two main spectral pattern recognition approaches.

In a supervised spectral classification, the pixel class assignments are based on the likelihood calculated from the observations of each pixel to belong to each of the pre-determined classes. The Maximum Likelihood classifier is the most often used supervised spectral classifier. In this technique, the class of a pixel at a location (i, j) is decided based solely on the observations at that pixel.

2.3.2 The misclassification problem

Conventional spectral classifiers have been widely used for image classification and have given fairly good results for a wide variety of images. Usually conventional spectral classifiers perform well over limited areas where spectral signatures do not vary greatly from those captured in the training data. However, as the size of area to be classified increases, the classification accuracy typically decreases (Carlotto 1998).

In many real applications, the thematic (class) maps generated by conventional spectral classifiers are often found to be very "noisy", with a considerable portion of image pixels being misclassified. This is the so-called misclassification problem in image classification.

Two major factors are responsible for the misclassification problem (Table 2-1). The first is the "noise" contained in a satellite image. Image noise results from many factors. Common sources of image noise include temporal and spatial variations of the same land-cover types, atmospheric distortions, deterioration of sensors, impure spectral information contained in some pixels, etc. The presence of noise causes the spectral response of a particular land-cover class to deviate from its ideal response. For example, the spectral reflectance characteristics of a pixel at (i, j) can be significantly affected by neighboring pixels N at (k, l) . This is so-called compound spectral response problem. There are also cases where different land-cover classes may have very similar spectral reflectance curves. This similarity of spectral features is often referred to as the confusing pixel problem. The presence of confusing pixels complicates the discrimination and often leads to misclassifications.

The second major factor responsible for the misclassification of pixels is the inadequate spatial resolution of imaging sensors. Any real sensor has a finite ground resolution. This finite spatial resolution causes the geographical area subtended by a pixel to contain a mixture of land-cover types. This is particularly true of transitional pixels between land-cover types. As a result of this, the spectral response observed at a pixel is a mixture of the spectral responses of several individual land-cover types. In other words, inadequate spatial resolution of remote sensing sensors often affects the classification of satellite image. This is the so-called mixture-pixel problem.

The presence of image noise and the inadequate spatial resolution of satellite sensors complicate the image classification process and often degrade image classification accuracy. As a result, the thematic maps generated by conventional spectral classifiers have two major defects. The first is a "salt-and-pepper" noise appearance. That is, isolated and, in many cases, misclassified pixels of one class are dispersed within the area of another class. The second defect is a weakly defined inter-class boundaries.

2.4 Recent Developments in Satellite Image Classification Techniques

The major difficulty of image classification is how to partition the noisy image into its constituent classes. In an attempt to reduce classification error rates and to enhance the quality of thematic maps, recent years have seen a rapid proliferation of algorithms for multispectral imagery classification. A survey of the existing literature suggests that four major thrusts can be identified (Table 2-1):

- ❑ Making better use of spectral information,
- ❑ Increasing use of spatial information,
- ❑ Information fusion and GIS integration, and
- ❑ Use of knowledge-based classification techniques.

2.4.1 New spectral classification methods

Spectral information is the most readily available information in a satellite image. Making more efficient use of spectral information is an obvious way to improve classification results. Therefore, considerable efforts are being made in developing new spectral classification methods, in addition to classic spectral classifiers.

Carlotto (1998) proposed a multispectral classifier that is based on an alternative spectral representation. In his approach, spectral classes are represented by their spectral shape; the spectral shape is a vector of binary features that describes the relative values between spectral bands. The classification accuracy of the full-scene spectral shape classifier was shown to be superior to that of a stratified Maximum Likelihood classifier.

Table 2-1 Approaches for improving satellite image classification accuracy

Types of Classification Errors	Possible Causes	Strategy for Error Corrections	Often used Techniques
Class-independent	Scattering and/or absorption of atmosphere		<ul style="list-style-type: none"> • Radiometric correction
	Temporal and spatial variations	<ul style="list-style-type: none"> • Use of ancillary data/ground truth information 	<ul style="list-style-type: none"> • Integration of digital image data and GIS data layers
	Deterioration of sensors		<ul style="list-style-type: none"> • Radiometric correction
Class-dependent			
Compound spectral responses	Spectral reflectance characteristics of a pixel at (i, j) is affected by neighboring pixels <i>N</i> at (k, l)	<ul style="list-style-type: none"> • Extraction and use of contextual/spatial information 	<ul style="list-style-type: none"> • Contextual relaxation • Fuzzy set theory • Neural networks
The mixture-pixel problem	Insufficient spatial resolution; Transitional pixels between land-use types	<ul style="list-style-type: none"> • Edge detection • Extraction and use of contextual/spatial information 	<ul style="list-style-type: none"> • Contextual relaxation • Fuzzy set theory • Neural networks
The confusing pixel problem	Similar spectral reflectance curves of different classes	<ul style="list-style-type: none"> • Multitemporal imagery fusion • Extraction and use of contextual/spatial information 	<ul style="list-style-type: none"> • Contextual relaxation • Fuzzy set theory • Neural networks

Other developments include attempts of using characteristic spectral relationships as expert knowledge in an expert system designed for image classifications. For example, Wharton (1987) developed a prototype expert system to classify multispectral remotely sensed data on the basis of spectral knowledge. In this approach, a knowledge base was developed that describes the target categories in terms of characteristic spectral relationships. Classification decisions are made on the basis of convergent evidence as derived from applying the spectral rules to a multiple spatial resolution representation of the image.

2.4.2 Contextual classification techniques

Conventional multispectral classifiers – both supervised and unsupervised – are point or pixel-specific classifiers in that they make use of the spectral information at each pixel to predict the class of that pixel independently of the observations at other pixels. While conventional spectral classifiers are used extensively, they are likely to lead to misclassifications of pixels in an image. To overcome this problem, a class of techniques called contextual classification methods has been developed for satellite image classification. Contextual classification techniques are also referred to as smoothing methods.

In contrast to conventional methods, contextual techniques make use of the spatial context of a pixel in its classification. The basic idea is that in any real image, adjacent pixels are related and correlated and therefore the context of a pixel should also be considered in the classification process. In a large homogeneous region compared with the pixel size, if an image pixel (not at edge of the region) represents a particular land-use class (e.g. wheat), then it is highly likely that its neighboring pixels are also the same land-use class (in this case, wheat). In a sense, spatial classifiers attempt to replicate the kind of spatial synthesis done by the human analyst during the visual interpretation process.

The context of a pixel (or groups of pixels) refers to its spatial relationship with the surrounding neighboring pixels (Jensen 1986). Spatial information such as pixel proximity, repetition, directionality, location, image texture, feature size, shape, etc. can help identify ground objects. Because contextual classification techniques involve

a more complex decision process, they tend to be much more computationally intensive than spectral pattern recognition procedures (Lillesand and Kiefer 1994).

The advantages and potentialities of contextual classification approaches have been pointed out in many works. Use of contextual techniques will usually result in a reduction of classification error rates (Swain et al 1981; Jhung and Swain 1996). For instance, Lee et al (1992) and Franklin and Peddle (1989) have shown that adding spatial and spectral texture information for coniferous and mixed forest types can significantly improve map classification accuracy. Some of the often used contextual classifiers are discussed in Chapter 6.

It should be noted that while substantial effort is being made in developing spatial classification techniques, practical use of spatial and combined spectral/spatial image classification approaches is still relatively limited compared to spectral pattern recognition approaches. A main reason for this is that the spatial resolution of most existing imaging satellites was inadequate. This situation is changing. With the recent and planned launch of new high-resolution imaging satellites, the outlook for the use of spatial pattern recognition techniques in land-use classification is an extremely promising one.

2.4.3 Information fusion and GIS integration techniques

Another basic strategy for improving image classification accuracy is to add new information to the classification decision process. This is the so-called information fusion technique in satellite image classification.

Broadly, two types of data are used in information fusion techniques. The first is image information. Haralick and Shapiro (1985) presented a technique that combines the edge map and the thematic map. The resulting thematic map has all the contour pixels set to zero, and the noncontour pixels are identified by their class code, as in the original thematic map. Integration of multitemporal and multisensoral digital image data is another approach that is often used in satellite image classification.

The second type of information that can be used to improve classification results are so-called ground truth data or ancillary information. Ancillary data is any type of information used in the classification process that is not directly obtainable from either spatial or spectral characteristics of the remote sensor itself. The most commonly used ground truth information includes DTM, soil data, crop statistics, zoning information, field-check data, statistical data, administrative boundaries, etc.. Integrating imaging data with ground truth information can help better identify and differentiate ground objects and, hence, improve image classification results (Tom et al 1978; Strahler 1980; Schowengerdt 1983; Jensen 1986; Mascarilla et al 1993).

The integration of imagery data and ancillary data is usually done by using Geographic Information System (GIS) technique. One of the most important benefits of a GIS is the ability to spatially interrelate multiple types of information. GIS is capable of handling both locational data and attribute data about such features. GIS permits automated mapping or display of the locations of features; it also provides a relational database capability for recording and analyzing descriptive characteristics about the features.

Ground truth data is commonly compiled as computer files that can be merged with other "layers" of information in a GIS. Remotely sensed data is often used in concert with GIS techniques in many remote sensing applications including land-use classification. Use of multi-source data such as remotely sensed data and non-imaging data gained importance, due to recent advances of GIS technology.

2.4.4 Knowledge-based image classification approaches

The value of knowledge-based techniques for land-use classification in remotely sensed imagery is widely recognized. Knowledge-based image recognition systems have two features in common. First, a database of computed image features is matched with antecedents of production rules (rules are represented as logical statements of the form "if..., then..."). Second, a control system that supervises rule activation.

Knowledge-based techniques have been found to be useful in a number of application areas such as image classification and the labeling of regions. The system developed by Nagao and Matsuyama (1980 and 1987) uses a knowledge base representing contextual and geometric constraints for the task of labeling regions in multispectral imagery. This method is intended for reliable classification of vegetation regions that is independent of the time of year and uses the ratio of two distinct spectral bands to discriminate the vegetation regions from the non-vegetation regions.

Ton et al (1991) demonstrated a knowledge-based segmentation and interpretation methodology for the interpretation of Landsat images. The image interpretation system establishes a coarse segmentation of the imagery using spectral features alone during a stage denoted by category-oriented segmentation, with simple, application-independent spatial constraints. The identified terrain regions are transferred to a second stage, denoted by image-oriented segmentation, where a hierarchical implementation of various image processing operations establishes an accurate segmentation of the image.

Kusaka and Kawata (1991) evaluated a hierarchical, spatial feature-based approach for the detection of linear features in Landsat imagery. Goldberg et al (1985) designed an expert system for the detection of changes in the forests of Newfoundland from Landsat imagery. Other researchers have evaluated Markov Random Field (MRF) based approaches for image texture for the task of multispectral image segmentation (Therrien 1983).

The key to effective use of knowledge-based techniques in satellite image interpretation is the generation of a knowledge base that is suitable for the particular application at hand. Identifying suitable structural rules that are universally valid has been found to be difficult (Swain 1985).

2.5 The Image Classification Algorithm Proposed in This Study

2.5.1 Software Architecture

Successful application of remote sensing is premised on the integration of multiple, interrelated data sources and analysis procedures. With imagery data and image analysis methods multiplying rapidly, selecting the right mix of data sources and data analysis approaches has become critical to the generation of quality land-use maps.

Satellite image classification involves designing and developing efficient classification operators. In a satellite image the features of an object can take many forms – spectral, spatial, radiometric. A robust land-use classification approach should take into account as many features of a land-cover type as possible.

This study aims to develop an efficient algorithm for the extraction and representation of land-use information using high-resolution IRS-1C imagery data. We proposed a new information fusion method that can produce land-use maps with sharp interregional boundaries and homogeneous regions. The proposed approach works by combining results from different multispectral channels in a cooperative and complimentary manner. Figure 2-4 depicts the software architecture of the proposed image classification approach.

2.5.2 Implementation Procedures

The proposed approach is conducted in five steps.

- First, a GIS layer – ATKIS data – was used to generate two coarse homogeneous regions, i.e. urban and rural areas.
- Second, a thematic (class) map was generated using a hybrid spectral classifier combining Gaussian Maximum Likelihood algorithm (GML) and ISODATA classifier.
- Third, a probabilistic relaxation algorithm was performed on the thematic map, resulting in a smoothed thematic map.

- Fourth, edge detection and edge thinning techniques were used to generate a contour map with pixel-width interclass boundaries.
- Fifth, the contour map was superimposed on the thematic map by use of a region-growing algorithm with the contour map and the smoothed thematic map as two constraints.

For the operation of the proposed method, a software package is developed using programming language C. This software package comprises the GML algorithm, a probabilistic relaxation algorithm, TBL edge detector, an edge thresholding algorithm, a fast parallel thinning algorithm, and a region-growing information fusion algorithm. Basic image processing and classification procedures were performed using ERDAS-IMAGINE 8.3.

The county of Landau of the State Rheinland-Pfalz, Germany was selected as a test site. The high-resolution IRS-1C imagery was used as the principal input data. The imagery data used includes 1/9 PAN scene and corresponding multispectral scene. These scenes correspond to a ground area of $23 \times 23 \text{ km}^2$. The imagery data was captured on 29 July 1997.

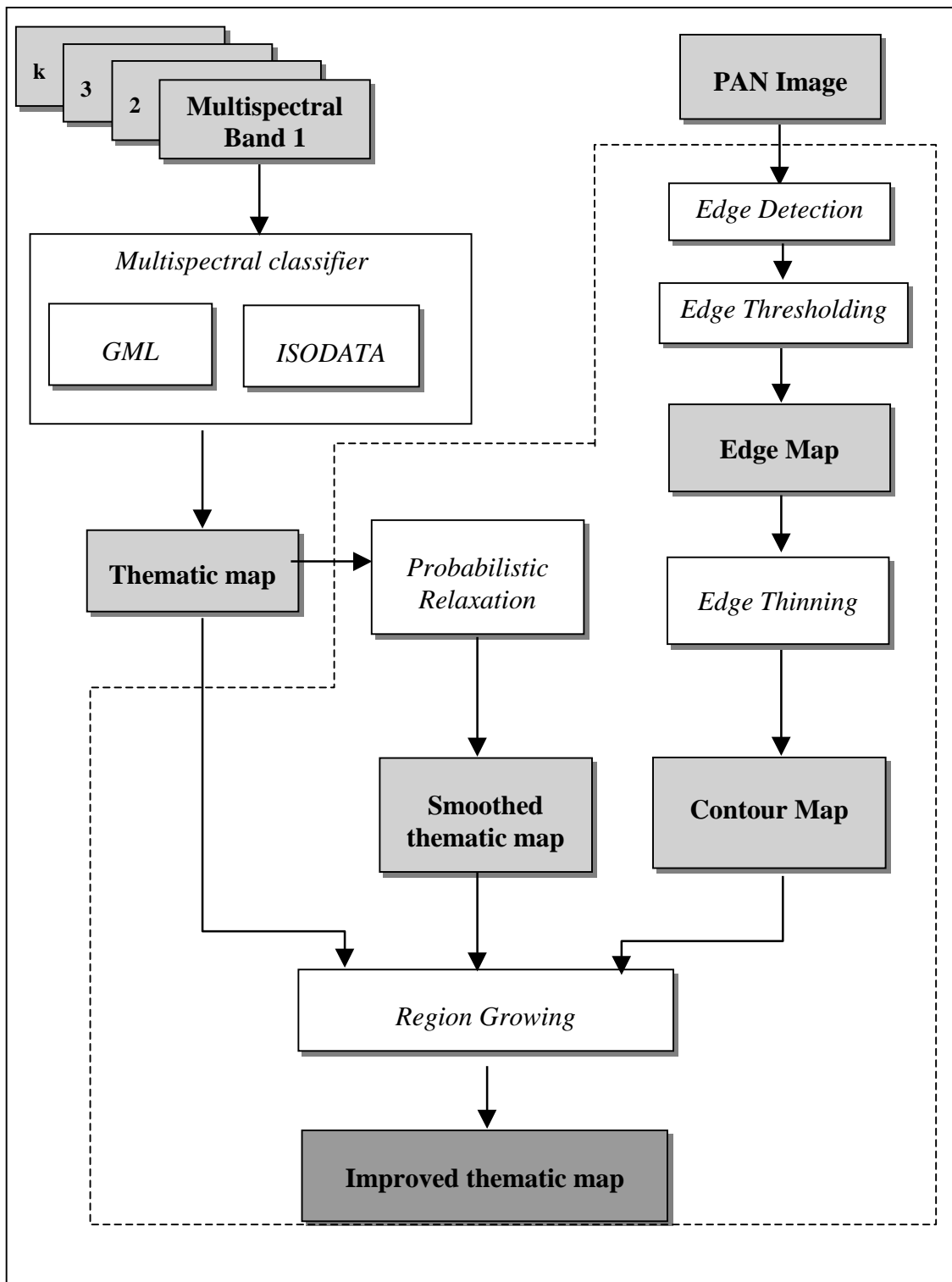


Figure 2-4 Software architecture of the proposed land-use classification algorithm

Chapter 3 The Study Area and Data Acquisition

3.1 The Study Area

The county of Landau of the State Rheinland-Pfalz, Germany was selected as a test site in this study. The geographic location of the study area is shown in Figure 3-1.

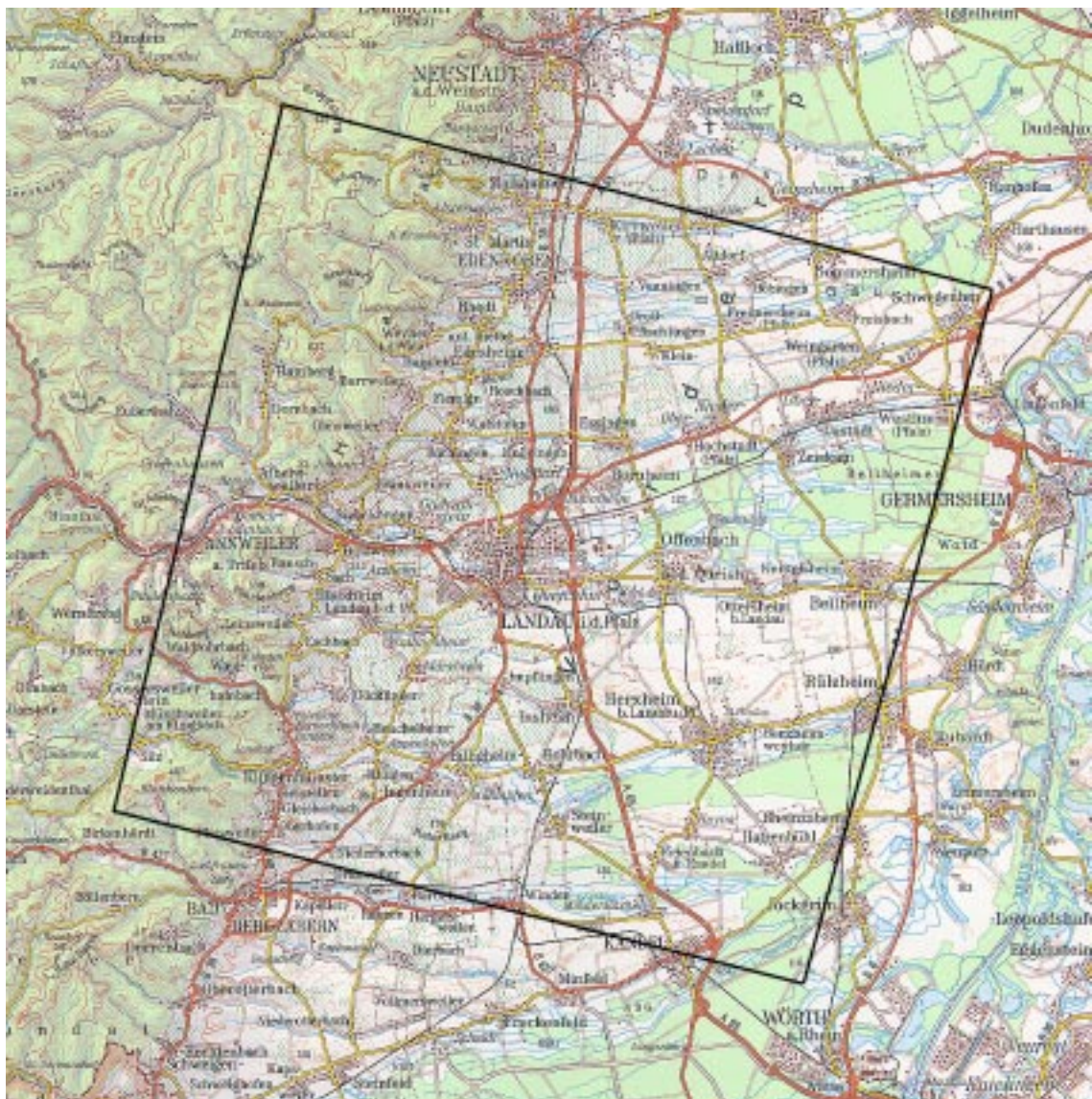


Figure 3-1 Location of the study area
(Source: 1:200 000 Topographische Uebersichtskarte, CC 7110, Mannheim)

The study area of Landau lies between the Palatinate Forest "Haardt" and Rhine lowlands. This area comprises mainly an agricultural environment with a medium-sized city Landau, a few small urban areas, and some forest areas. The test site has an area of 529 km². The multispectral scene of the study area contains 1271×1255 pixels and the corresponding panchromatic image 5143×5082 pixels. The Gauss-Krueger coordinates of the upper left and lower right corners of the study area are as follows:

$$X_{UL} = 3423027 \quad Y_{UL} = 5466126$$

$$X_{LR} = 3452496 \quad Y_{LR} = 5436302$$

3.1.1 Morphological Structure

The landscape of the study area is characterised by the following morphological features.

- In the west is the Haardt with peaks exceeding 600 m. The Haardt constitutes the boundary of the low mountain ranges of the Palatinate Forest; it is structured by step faults and numerous steep V-shaped valleys.
- In the middle are hills of the Weinstraße with relief blocks of heights between 180 to 300 m. These hills are structured by westward oriented V-shaped valleys of depths between 20 and 120 m and cut by the rivers Birnbach, Ranschbach and Queich.
- In the east lies the Palatinatean Rhine-Plain. This part is featured by a terraced landscape that is formed by ledges of loess and alluvial lands. The Rhine Plain gradually descends to 95 to 110 m towards the Rhine River.

3.1.2 Climate

The favourable climatic conditions of the Weinstraße owe much to its geomorphologic positions within the Upper-Rhine valley and, especially, to its positions on the lee-side of the Haardt.

Given the dominant wind direction between West and Southwest, the air masses arriving at the luff-side of the Palatinate Forest are forced to ascend and then descend on the lee-side. Though the difference in elevation at the mountain edge is only about 400 m, the descending winds at the lee-side lead to a foehn-like heating. This explains why this region has a somewhat longer duration of sunlight, fewer cloudy days and fewer rainy days a year, compared to other areas in this climatic zone. The annual precipitation of the study area amounts to around 600 mm.

The favourable climate of high radiation leads to a particularly early beginning of the spring season in the study area. The almond trees are already coming into blossom as early as in March and the growing period in the study area lasts almost one month longer than in the neighboring Palatinate Forest.

Additional advantages result from the particularly favourable climatic conditions of the Upper-Rhine valley. Like other valley landscapes, the Upper-Rhine valley warms up faster than do their neighbouring regions during all seasons. This advantage is particularly important during the summer when the average temperature reaches 18°C or higher. During the daytime the study area is additionally overflowed by ascending warm airs which transport heat from the lower Rhine Plain.

Valleys have a modifying effect on climate. During night radiation from early evening to morning, the study area is constantly covered by cold air masses. Due to its size, the Queich-valley is characterised by a high effectiveness on cold airs. As a result, the risk of late frosts in the spring, which can lead to frostbite on vine and special crops, is very high. A positive effect of these cold air currents is that under high-pressure weather conditions, they supply the settlements with fresh airs. Such weather conditions of slow winds can be accompanied by muggy subtropical air masses coming from the Upper Rhine valley, which can lead to sultriness and heat-stresses. This is especially true of places where settlements are densely built. This is the time when the cold air currents as well as the valley breeze, the land and downslope winds provide the environment with comfortable cooling.

3.1.3 Soils and land-use

At the edge of the Haardt the soils consist of sandy soil mixed with loess. The loess layers in this area varies from a very thin coating to several meters. In the marginal crustal block in the East, limestone is the dominating source rock. But also here, loess covers the relief and determines the smooth surface forms. In this area the sandy soils permit the cultivation of field vegetables and special crops on small, intensively cultivated land parcels. Such a crop pattern is characteristic of this region. Land-use types range from greenland in the leas, intensive cultivation of wheat, sugar beet, special crops (such as vegetables, tobacco, and salad), fruits and vine in the more elevated regions, to forest on the extremely poor soils.

To the west of the region is a predominantly agricultural area which is characterised by large fields of wheat, beets and potatoes. With the beginning of the low mountain ranges, land-use changes to viniculture, which stretches right up to the edge of the Haardt. The viniculture, together with the settlements situated there, forms the typical picture of the cultural landscape of the Weinstraße.

3.2 IRS-1C Satellite Imagery Data

This study uses the Indian IRS-1C satellite imagery as the principal input data for land-use classification.

3.2.1 Background

The development of satellite platforms for acquisition of remotely sensed data in India began with the Bhaskara satellite mission in the late 1970s. Subsequently, India launched a series of satellite imaging systems including IRS-1A, IRS-1B, IRS-P2, and IRS-P3. These missions have realized the primary objective of designing, developing and deploying a three-axis stabilized polar sun-synchronous satellite carrying near state-of-the-art payloads. These missions have also paved the way to establishing and routinely operating ground-based systems services (Kasturirangan 1996).

On 28 December 1995 the Indian Remote Sensing satellite, IRS-1C, was successfully launched using a Russian launch vehicle. One month later IRS-1C was declared operational (<http://www.comlinks.com/satcom/srsintro.htm>). IRS-1C provides one of the highest spatial resolution remote sensing data commercially available today.

IRS-1C data is currently being received at three ground stations: Shadnager (India), Norman, Okla. (USA), and Neustrelitz (Germany). The data received at Neustrelitz covers Europe and part of western Asia and northern Africa.

3.2.2 IRS-1C satellite imaging systems

Figure 3-2 shows an overview of IRS-1C mission. The payload sensor data is transmitted to ground stations in X-band (8025-8400 MHz). Telemetry Tracking and Command (TTC) system works in S-band (2200-2300 MHz). This system is used to monitor the configuration and health of the satellite, including reconfiguring, reorientation and repositioning of the satellite as well as determining the position and velocity of satellite by the spacecraft controllers on the ground (IRS-1C Data Users Handbook 1995). The important technical parameters of the IRS-1C imaging systems are listed in Table 3-1.

3.2.3 Payload sensors and IRS-1C imagery data

IRS-1C offers the remote sensing community a unique combination of payloads consisting of three cameras: Panchromatic camera (PAN), Linear Imaging and Self-Scanning Sensor (LISS-III), and Wide Field Sensor (WiFS). These Payloads operate in a push-broom scanning mode using Charge Coupled Devices (CCD) as detectors (IRS-1C Data Users Handbook 1995). Their characteristics are given in Table 3-2.

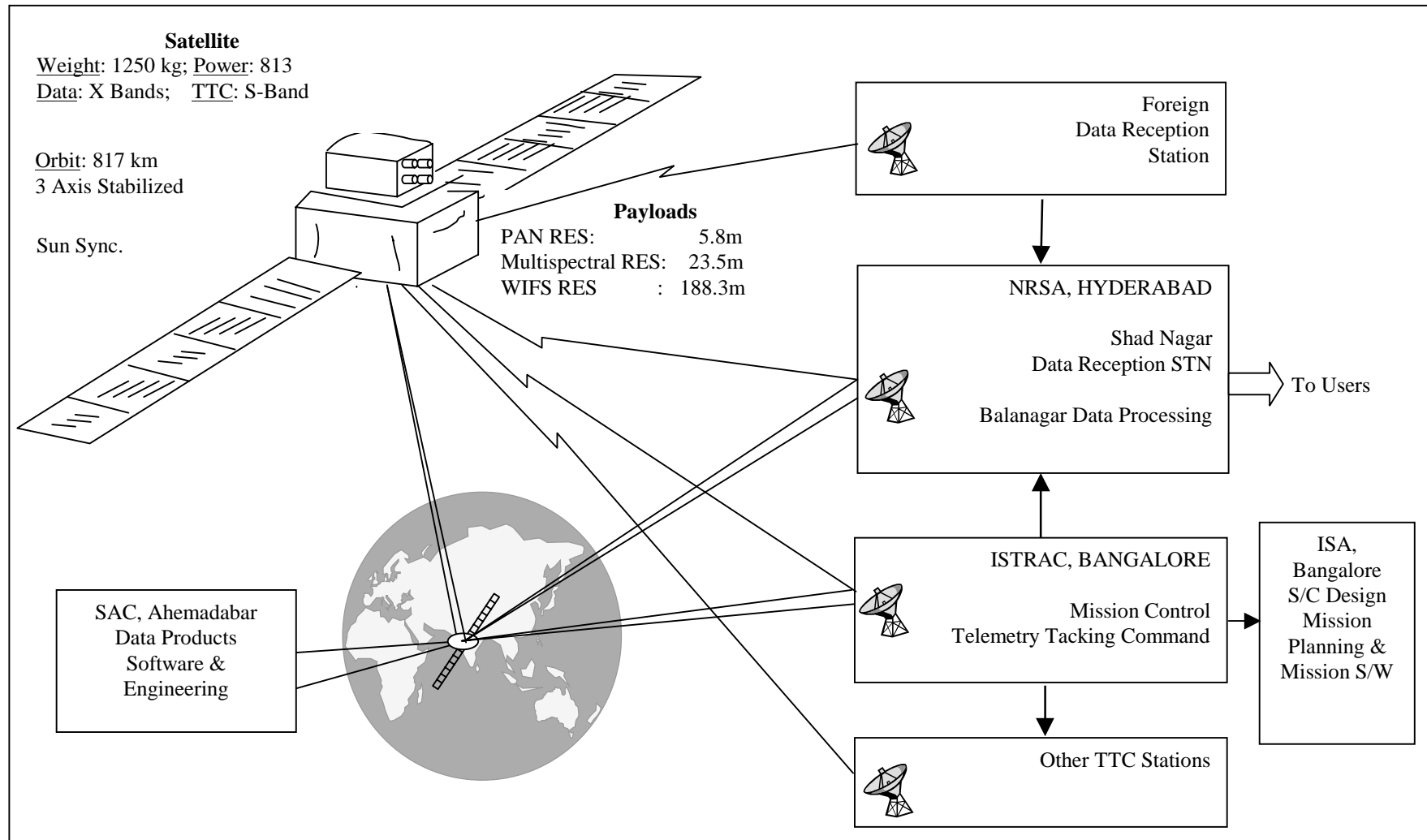


Figure 3-2 Overview of IRS-1C mission (Source: after IRS-1C Data User's Handbook 1995)

Table 3-1 Key technical parameters of the IRS-1C imaging systems

Type	Three-axis, body stabilized satellite
Orbit	Polar, sun synchronous
Altitude	817 km
Weight	1,250 kg
Equatorial crossing time	10:30 a.m., in descending node
Repetivity	24 days between 81 deg north and 81 deg south latitudes
Revisit capability of PAN and WiFS	5 days
Semi-major axis	7,195 km
Inclination	98.69 deg
Period	101.35 minutes; 14 orbits/day
Distance between adjacent traces	117.5 km

Source: IRS-1C Data User's Handbook 1995 p.20 and p.39

Table 3-2 Imaging sensor characteristics on board IRS-1C

Sensor	PAN	LISS-III			WiFS		
Spatial resolution	5.8 m	23.5 m (VIS and NIR) 70.5 m (SWIR)			188 m		
Swath-width	70 km	141/148 km			810 km		
Spectral coverage	Panchromatic	Band 2	520-590 nm	green	Band 3	620-680 nm	Red
		Band 3	620-680 nm	red	Band 4	770-860 nm	NIR
		Band 4	770-860 nm	NIR			
		Band 5	1550-1700 nm	SWIR			
Radiometric Resolution, Quantisation	6 bit	7 bit			7 bit		

Source: IRS-1C Data User's Handbook 1995

PAN camera

The PAN camera enables the acquisition of images at a ground resolution of 5.8 m. Until quite recently this 5.8-m ground resolution was the highest offered by civilian remote sensing satellites. The PAN camera operates in the spectral range of 0.5-0.75 μm and provides a ground coverage of 70 km.

In addition, the PAN camera has off-nadir viewing capability. Off-nadir refers to any point that is not directly beneath the detectors, but off to an angle (ERDAS Field

Guide 1997). With this off-nadir capability the revisit frequency for the same geographic area has been increased to five days, instead of twenty-four days as in the LISS camera system. The off-nadir viewing capability is also very useful for generating stereo images, from which digital terrain model (DTM) can be derived. A maximum tilt angle of ± 26 degrees corresponds to an off-nadir coverage of ± 398 km on the ground (Figure 3-3).

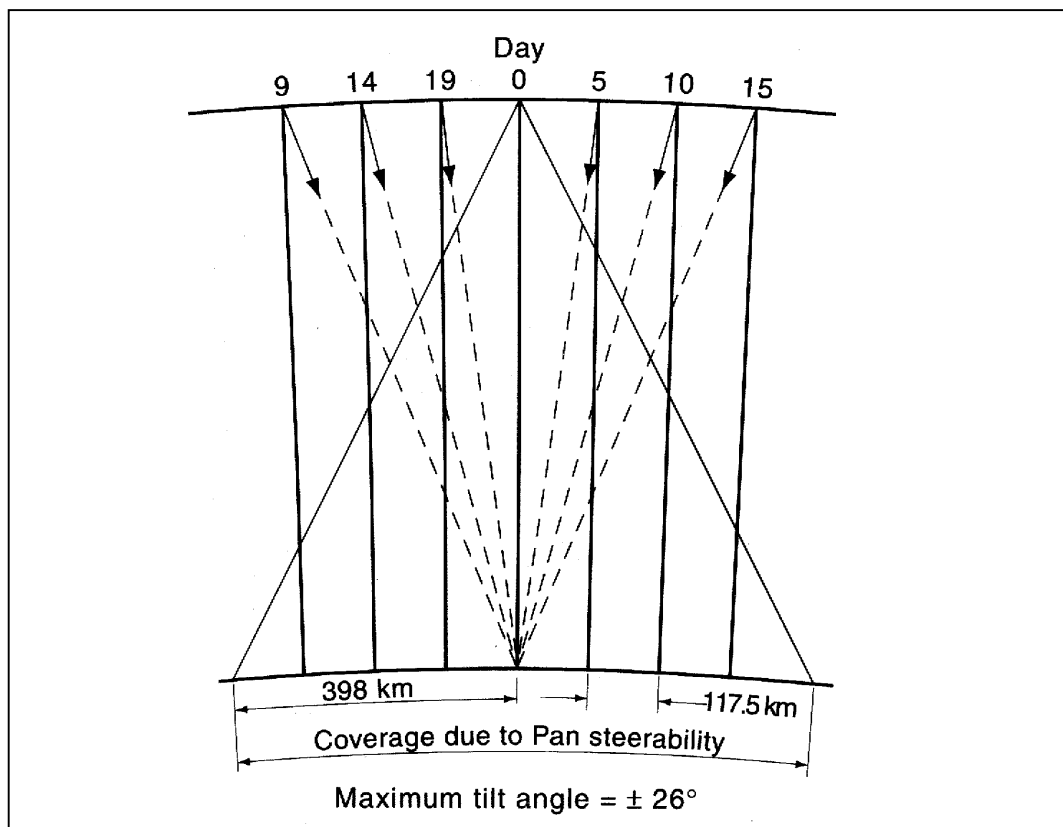


Figure 3-3 PAN off-nadir viewing capability
(Source: IRS-1C Data User's Handbook 1995)

The high-resolution PAN data enables the generation of detailed digital cartographic databases and DTMs that can help provide engineering solutions to complex problems associated with micro-level planning and development. The availability of stereo images from the PAN data has opened up new vistas in urban management. Added to these are the potentials of the PAN data for updating topographical maps as well as mapping at the cadastral level (Kasturirangan 1996).

LISS-III

The four-band multispectral camera, LISS-III, provides data of terrain features in visible, NIR, and SWIR regions within the electromagnetic spectrum. LISS-III has a spatial resolution of 23.5 m each in the visible and NIR bands and 70.5 m in the SWIR band. The swath in the visible and NIR bands is 141 km while the SWIR has a swath of 148 km. Each band has its own collecting optics and linear array CCD.

LISS-III data from visible and NIR bands can significantly improve the separability among various crops and vegetation, enabling the identification of small fields and better classification accuracy. The SWIR data is very useful for agriculture applications, such as the study of crop canopy, water status, and estimation of leaf area index. The LISS-III data can also be used to discriminate crops in the mixed crop regions.

WiFS

WiFS is a two-band camera. It operates in the visible and NIR region with a spatial resolution of 188 m and a swath width of 810 km. The sensor observes the same region once in every five days.

The high repetivity feature of the image data from WiFS is particularly useful in the monitoring of natural resources, especially in the vegetation and dynamic phenomena like flood, droughts, forest fires, and so on.

3.2.4 Selected satellite scenes

Data products

According to the extent of pre-processing performed on the raw image data, four levels of data products are available (Table 3-3).

Table 3-3 Overview of IRS-1C data products

Level 0	Raw data	Uncorrected
Level 1	Browse Product	Radiometrically corrected and Geometrically corrected only for earth rotation
Level 2	Standard Product	Both radiometrically and geometrically corrected
Level 3	Special Product	Special processing like merging, enhancement, etc.

Source: IRS-1C Data User's Handbook 1995 p.96

Selected image scenes

For this study a LISS-III quadrant scene and a 1/9 PAN subscene are selected. These images were acquired on 29 July 1997. The path and row number and product code are given in Table 3-4. and Table 3-5.

The selected image data are both radiometrically and geometrically corrected, standard path oriented products (Level 2). Path oriented products refer to the scenes that are geometrically corrected to the orientation as seen by the spacecraft, parallel to the ground track. Geometric corrections correct distortions resulted from Earth rotation, Earth ellipsoid, satellite attitude, as well as internal distortions (Euromap, 1998).

Table 3-4 The path, row number and product code of selected IRS-1C satellite data

LISS-III	Path 24	Row 33	Quadrant 11	QUSCB02AZ
PAN	Path 24	Row 34	Subscene A3	STSCB02AZ

Table 3-5 Explanatory notes on IRS-1C data product code

Product Type	ST	Standard Scene
	QU	LISS-3 Quadrant
Map Projection	S	Space Oblique Mercator
Resampling	C	Cubic Convolution
Earth Ellipsoid	B	International 1909
Enhancement	0	No Enhancement
Level of Correction	2	System Corrected
Media and Format	AZ	Fast Format BSQ on disk

3.3 Reference Data

3.3.1 Digital orthophotos

Orthophotos are orthographic photographs that do not contain the scale, tilt, or relief distortions characterizing normal aerial photographs. Orthophotos are generated from overlapping conventional aerial photos in a process called differential rectification. This process results in elimination of photo scale variation and image displacement resulting from relief and tilt (Lillisand and Kiefer 1994).

Digital orthophotos are othophotos in digital raster format. In this study digital orthophotos were used not only for the selection of training samples but also for verifying the rectification accuracy of the IRS-1C imagery. Details of the selected four digital orthophotographs are presented in Table 3-6.

Table 3-6 The selected digital orthophotographs

Area	Number	Original Scale	After-scan Scale	Date
Ingenheim	3432 5444	1:13 000	1:5000	1997.08.10
Eschbach	3428 5448	1:13 000	1:5000	1997.08.10
Landau	6814 SW	1:34 000	1:10 000	1992.07.30
Rheinaue/Hördt	6816 NW	1:34 000	1:10 000	1992.07.30

3.3.2 ATKIS (Amtliches Topographisches Kartographisches Informations-system)

ATKIS are a type of GIS data. They are in digital vector format and correspond to the topographic maps at a scale of 1:25000. Objects in ATKIS are classified into six main categories and 80 sub-categories. The six main categories are residential, traffic, vegetation, relief, water, and region.

ATKIS data is useful for selecting training samples and evaluating the classification accuracy. As ancillary data, the ATKIS data can also help improve the quality of automated land-use classification based on satellite imagery data.

3.3.3 Topographic maps - TK25

Six TK25 maps are used in this study (see Table 3-7).

Table 3-7 TK25 maps used in this study

Map series number	Area
TK 6713	Annweiler am Trifels
TK 6714	Edenkoben
TK 6715	Zeiskam
TK 6813	Bad Bergzabern
TK 6814	Landau in der Pfalz
TK 6815	Herxheim bei Landau

3.3.4 Field data

Field data are collected for two purposes, i.e., rectification of imagery data and training sample selection. Differential Global Positioning System (GPS) was used for rectification of the imagery data. Fieldwork was carried out to measure the geographic coordinates of ground control points and select training samples.

Part II Multispectral Image Classification Methods

Chapter 4 Preprocessing of IRS-1C Imagery

The purpose of image preprocessing is to correct distorted or degraded image data. Sensor noises and atmospheric effects are two sources of radiometric distortion.

Sensor errors and atmospheric effects can be corrected before classification by radiometric correction function. Radiometric correction addresses errors in the measured brightness value of the pixels (Richards 1994). Sensor errors are usually already calibrated at the satellite ground stations.

All electromagnetic radiation, before reaching sensors, passes through some distance, or path length of the atmosphere. Due to atmospheric scattering and absorption, the atmosphere can have a profound effect on the intensity and spectral composition of radiation available to any sensing system. This impact of atmosphere on the remotely sensed data is called atmosphere effects. The atmosphere effects vary with the differences in path length and also vary with the magnitude of energy signal being sensed, the atmospheric conditions present, and the wavelengths involved.

The atmospheric effects are not considered "error", since they are part of the signal received by the sensing device (Bernstein 1983). However, for scene matching and change detection analysis, elimination of, or compensation for, atmospheric effects via some form of calibration is particularly important (ERDAS Field Guide 1997).

4.1 Rectification

Rectification is the process of transforming image data so as to create an image oriented to map coordinates in a specific map projection (McCloy 1995). Raw remotely sensed data usually contains geometric errors so significant that they will not

be a good fit to map data. The sources of these errors range from variations in the altitude, attitude, and velocity of the sensor platform, to factors such as panoramic distortion, earth curvature, earth rotation, relief displacement, and nonlinearities in the sweep of a sensor's IFOV (Lillesand and Kiefer 1994).

Geometric errors take two forms: systematic and nonsystematic (Jensen 1986). Systematic errors can be corrected by applying formulas derived by modeling the nature and magnitude of the sources of the distortions mathematically. Usually, systematic errors are removed at the satellite ground stations.

Using an n th order polynomial, rectification procedure corrects nonsystematic errors and georeference image data. An n th order polynomial is a mathematical relationship established between the coordinates of pixels in an image and their corresponding coordinates on the ground. This relationship can be used to correct the image geometry irrespective of the analyst's knowledge of the source and type of distortions (Richards 1994).

Georeferencing is the process of assigning map coordinates to the image data. It is an important process because these map coordinates are essential to locating training samples in the image and overlaying the imagery data with other types of data, such as GIS layers, for the study area,

Rectification is usually done in three steps, i.e. locating ground control points (GCPs), computing a transformation matrix, and resampling the output image (ERDAS Field Guide 1997).

As the IRS-1C PAN data has a higher resolution compared to that of multispectral data, panchromatic image was first rectified using Differential Global Positioning System (DGPS). Using the rectified panchromatic image as a reference image, multispectral images were then rectified using the "image-to-image" registration method. The IRS-1C images were georeferenced to the following map projection and coordinate system (Table 4-1).

Table 4-1 The map projection and coordinate system used for IRS-1C images

Map projection	Coordinate system	Spheroid	Datum	Longitude of central meridian
Transverse Mercator	Gauss-Krueger	Bessel	Potsdam	9 ⁰ E

4.1.1 Global Positioning System (GPS)

GPS is a worldwide, satellite-based positioning and radio navigation system. GPS is very accurate in time, velocity, and in all three dimensions of positions. The achieved positioning accuracy with GPS ranges from 100 meters to millimeters. GPS was developed by the U.S. Department of Defense (Pro XL System 1994; <http://www.lowe.co.uk/gps1.html>).

The constellation of GPS consists of 24 satellites (Figure 4-1). The GPS satellites orbit the Earth twice a day at a height of 20,000 km above the earth, and transmit their precise position and elevation.

Every GPS satellite transmits almanac and ephemeris data. Almanac data is the general information on the location and the health of each satellite in the constellation. A receiver with a current almanac in its memory knows where in the sky to look for satellites, given its last known position and the time of the day. Ephemeris data is the precise satellite positioning information that is used by the GPS receiver to compute its position. Each satellite transmits its own ephemeris data.

GPS receivers on the ground acquire the satellite signals and are able to determine a measurement called pseudorange. The pseudorange is a combination of the distance between the receiver and the satellite and the error in the receiver's clock. At least four satellites are required to compute the receiver's position in three dimensions and the magnitude of the receiver's clock error.

There are two distinct signal types emitted from the satellites: Coarse Acquisition (CA) and Precise Positioning System (PPS). CA coded signals can give 15 m Root Mean Square (RMS) accuracy. However, the U.S. Department of Defense introduced

a random error into the system, known as Selective Availability (S/A). The satellites will randomly give out an error signal, thus degrading the accuracy to 100 m; the usual accuracy is 50 m. S/A error is the greatest source of pseudorange error.

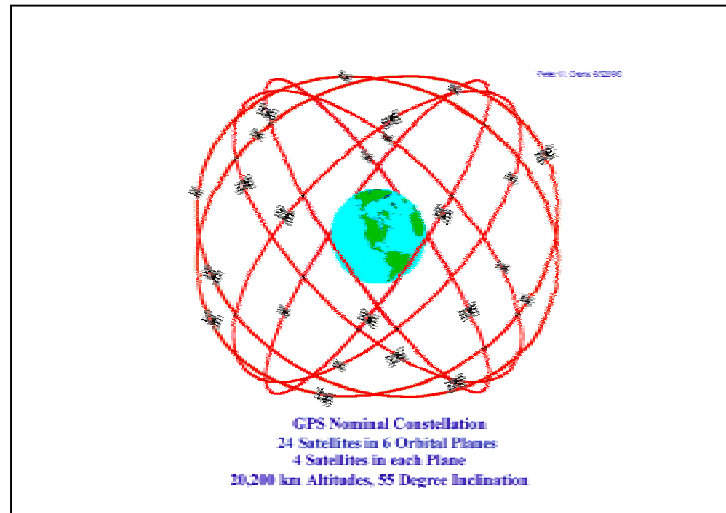


Figure 4-1 The constellation of GPS

(Source: <http://wwwhost.cc.utexas.edu/ftp/pub/grg/gcraft/notes/gps/gps.html>)

DGPS is used to correct the random signal errors caused by Selective Availability to achieve positions with accuracy up to the sub-meter level. DGPS employs two receivers. One is the reference receiver; the other is the rover receiver. The reference receiver, also called base receiver or base station, is located at a known position. The reference receiver is used to determine the errors in the pseudoranges in relation to the satellites. The rover receiver, also called roving receiver, collects data at unknown locations within the vicinity.

Base receiver collects data at the same time a rover receiver does. The difference between the position measured by the base receiver and its actual position is first calculated. Because GPS satellites are in high orbits, the pseudorange errors in the reference receiver and rover receiver are virtually identical if the radius between them is within 50 km. The pseudorange error measured by the base receiver can then be applied to rover receiver to remove pseudorange errors of the rover receive by using differential correction procedure. Differential correction can be performed using either real-time or postprocessing correction.

4.1.2 Rectification of IRS-1C panchromatic image using DGPS

The rectification process begins with locating a sufficiently large number of ground control points both on the image and on the ground. Then a transformation was developed to estimate ground coordinates for every pixel from the image pixel coordinates (McCloy 1995). Figure 4-2 describes the five steps for the rectification of panchromatic image using DGPS.

(1) Locate ground control points in the panchromatic image with the GCP

Editor.

Ground control points (GCPs) are specific pixels in an image for which the output map coordinates are known. As ground control points, they must satisfy the following conditions: 1) clearly identifiable and accurately located both on the image and on the ground; 2) reachable with GPS on the ground; 3) evenly distributed across the study area; and 4) sufficient number of points.

As point features are difficult to be located accurately in the image, it is more appropriate to use as GCPs the objects that are easily to be identified in an image. An example of such ground objects is intersections of linear features. In an image-to-image registration approach, intersections of highways or main roads are often used as GCPs.

In cases where GPS is employed, it is less practical to use highway intersections as GCPs though. This is because obtaining an accurate measurement of GCPs usually requires about three minutes but it might be difficult to stay at the highway intersections for three minutes because of heavy traffic. Therefore, objects such as intersections of field roads and edge elements of large buildings were selected as GCPs for rectifying panchromatic image in this study.

The minimum number of GCPs is usually determined using the following formula.

$$\text{Minimum number of GCPs} = ((n + 1)(n + 2)) / 2$$

Where n is the order of polynomial.

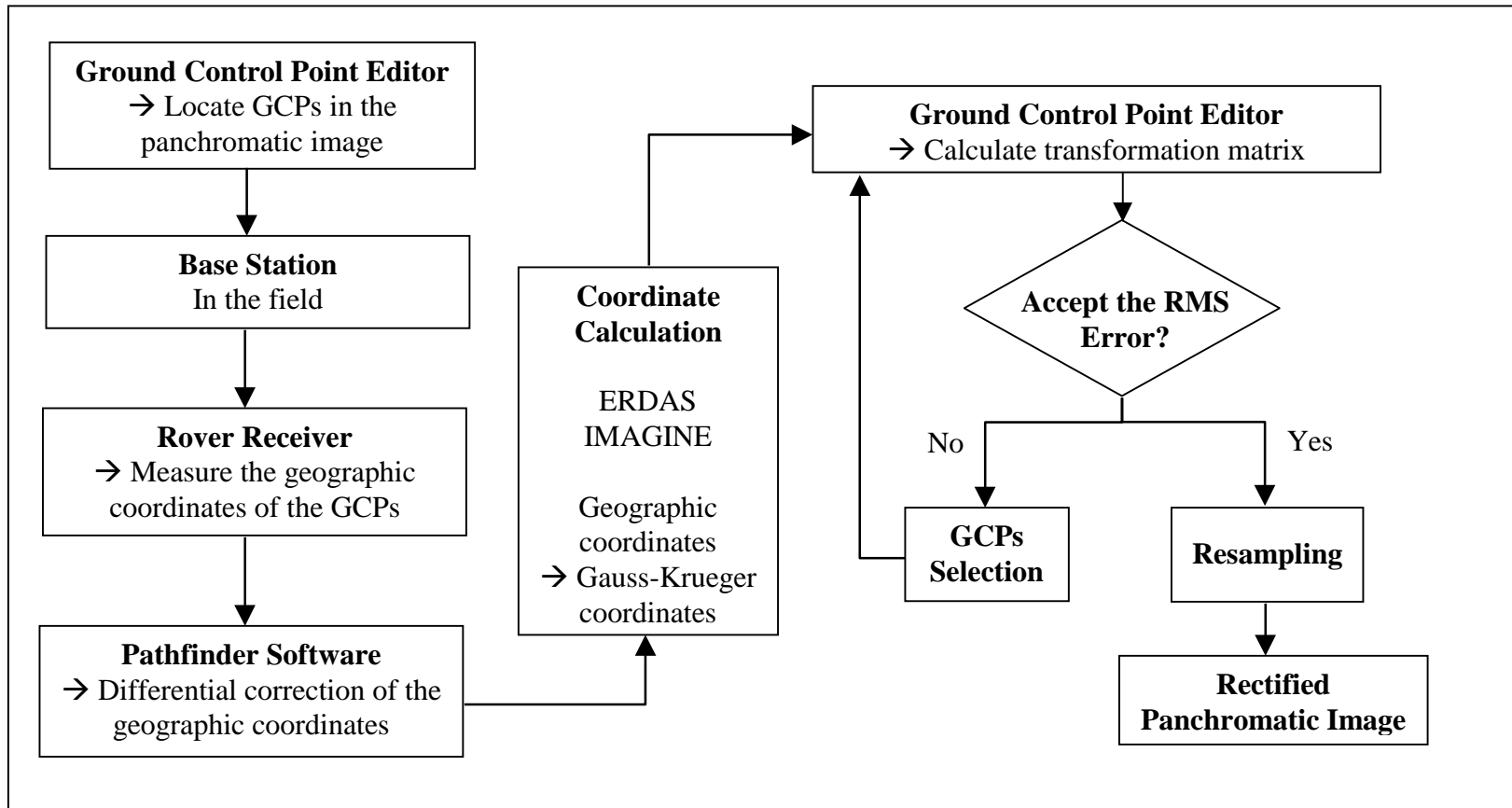


Figure 4-2 Workflow for the rectification of panchromatic image using DGPS

This means that at least six GCPs are required for a second-order polynomial function. In practice, more GCPs than the minimum required are used to achieve better rectification results. In this study twenty-eight GCPs were selected in the panchromatic image.

(2) Measure the geographic coordinates of the GCPs in the field using DGPS.

This study employed the GPS Pathfinder Pro XL System. Asset Surveyor software runs on the field data collector TDC1. The base/reference receiver was placed at Klaeranlage in Landau. The geographic coordinates of the reference receiver are $8^{\circ}10'43.30''E$ and $49^{\circ}12'31.43''N$ at an altitude of 131.586m. The geographic coordinates of the twenty-eight GCPs already identified in step (1) were captured by the rover receiver. Differential corrections were then performed using the postprocessing method. The PFINDER software was employed for this operations.

(3) Convert geographic coordinates to Gauss-Krueger coordinates using Coordinate Calculate.

The geographic coordinates need to be converted to Gauss-Krueger coordinates. This is necessary because Gauss-Krueger coordinates are the destination coordinate system. For the conversion operation two parameters – spheroid and datum – corresponding the geographic coordinate system are specified as WGS84 and WGS84.

(4) Calculate the transformation matrix using GCP Editor and the Transformation Editor until the RMS error is acceptably low.

Polynomial equations are used to convert the source file coordinates to rectified map coordinates. Polynomial equations are normally expressed as an n th-order bivariate polynomial:

$$X = a_0 + a_1x^n + a_2x^{n-1}y + a_3x^{n-2}y^2 + \dots + a_{j-1}x^i y^j + \dots + a_{n+1}y^n$$

$$Y = b_0 + b_1x^n + b_2x^{n-1}y + b_3x^{n-2}y^2 + \dots + b_{j-1}x^i y^j + \dots + b_{n+1}y^n$$

where:

- X, Y : coordinates of rectified image;
- x, y : coordinates of source image;
- a_0, a_1, \dots, a_{n+1} and b_0, b_1, \dots, b_{n+1} : coefficients;

n : the order of the polynomial;
 i, j : exponent.

A transformation matrix consists of coefficients that are used in polynomial equations for converting the coordinates. The least square regression method is used to calculate the transformation matrix from the GCPs (ERDAS Field Guide 1997). The least square method uses all of the equations to derive estimates of the unknowns that are a best fit to all of the equations. The criterion used to decide on best fit is to minimize the sums of squares of the residuals at all of the GCPs.

The order of the polynomial is simply the highest exponent used in the polynomial equations. It describes the degree of complexity of the polynomial. A first-order polynomial is simply a linear transformation. It can be used to project raw image to a planar map projection or convert a planar map projection to another planar map projection (ERDAS Field Guide 1997). A second-order transformation is more complex than a first-order transformation. A second-order polynomial function can describe many of the geometric errors. In this study the first-order polynomial was found to be adequate for the transformation.

Accurate measurement of ground control points is essential to efficient rectification. Inaccurate measurement of some GCPs is possible. To control the accuracy of GCPs an error measurement called Root Mean Square (RMS) error needs to be computed. Before calculating the RMS error, the reference coordinates of the GCPs must be transformed back to the source coordinate system using the inverse of the transformation matrix. The RMS error is the distance between the input (source) location of a GCP and the re-transformed location for the same GCP (Figure 4-3).

RMS error is calculated using the following distance equation:

$$RMS\ error = \sqrt{(x_r - x_i)^2 + (y_r - y_i)^2}$$

where:

x_i, y_i : the input source coordinates;
 x_r, y_r : the retransformed coordinates

RMS error is first calculated for each GCP. Then the total RMS error is obtained by adding up the RMS error of all GCPs. The RMS error will be checked. If the total RMS error is not acceptable, then those GCPs with high RMS errors must be deleted. This process repeats until the RMS error is acceptable.

In this study, three GCPs with high RMS error were deleted. Consequently, twenty-five GCPs were used for computing the transformation matrix. Table 4-2 lists the twenty-five GCPs coordinates of source and GPS measurements. Table 4-3 presents the results of the RMS error calculation. It should be noted that RMS errors are reported in pixels. The total RMS error is 1.14 pixels, which corresponds to about 6.6m on the ground. This result suggests that the use of DGPS has improved the accuracy of image rectification to a significant extent. The final calculated coefficients of the polynomial equation are given in Table 4-4.

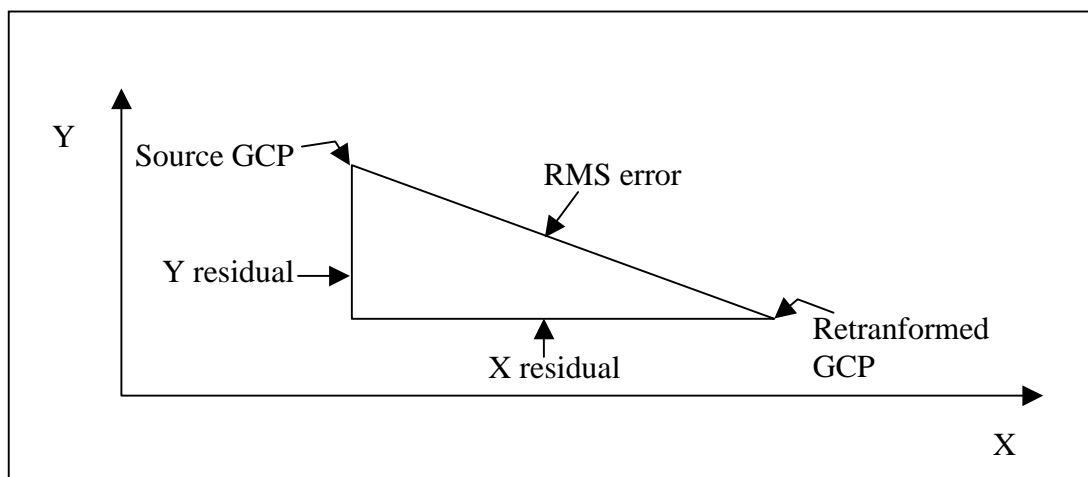


Figure 4-3 Residuals and RMS error per point

Table 4-2 The source and Gauss-Krueger coordinates of the 25 selected GCPs in panchromatic image

Number	GCP number	X Source	Y Source	X Destination	Y Destination
1	GCP#1	1844	4536	3436926	5462478
2	GCP#2	538	3662	3429556	5459814
3	GCP#3	150	2197	3425884	5453200
4	GCP#4	3161	4745	3443572	5461873
5	GCP#6	4469	4736	3449912	5460231
6	GCP#7	1483	3450	3433868	5457649
7	GCP#8	2851	2867	3439798	5453145
8	GCP#11	4803	2635	3448989	5449619
9	GCP#12	4103	2493	3445419	5449793
10	GCP#13	2931	1257	3438237	5445229
11	GCP#14	2267	2906	3437009	5454048
12	GCP#15	1088	1746	3429884	5449862
13	GCP#17	2730	2312	3438533	5450598
14	GCP#18	1925	709	3432696	5443805
15	GCP#19	2061	1471	3434272	5447336
16	GCP#20	4516	779	3445356	5440963
17	GCP#21	4353	1777	3445765	5446010
18	GCP#22	1418	584	3430085	5443817
19	GCP#23	3517	723	3440438	5441920
20	GCP#24	1826	205	3431613	5441481
21	GCP#25	2397	3766	3438682	5458063
22	GCP#26	4896	3371	3450338	5453076
23	GCP#27	4035	3963	3446867	5457007
24	GCP#28	1200	1225	3429808	5447199
25	GCP#29	1789	1936	3433514	5449921

Table 4-3 The RMS error of the GCPs in the panchromatic image

X-RMS Error (pixel)	Y-RMS Error (pixel)	Total RMS Error (pixel)
0.97694	0.58867	1.14059

Table 4-4 Transformation coefficients of GPS method

	X'	Y'
Const.	-694595.582392	-1313606.791787
X	0.235613	0.059752
Y	0.033220	0.059752

(5) Resample the image data.

The pixels in the source image are in a different position, orientation, and are of a different size to the pixels to be derived for the rectified image (Figure 4-4). This problem can be solved using the resampling method. Resampling is the process of calculating the data file values for the pixels in the rectified image by use of data file values in the source image data (McCloy 1995).

The rectified coordinates (x_0, y_0) of each pixel are transformed back to the source coordinate system. The retransformed coordinates (x_r, y_r) are usually fractional image coordinates. The data file values of the retransformed coordinates are derived by using the resampling method. The calculation of a pixel's retransformed coordinates (x_r, y_r) is based on its neighborhood relationships. There are three resampling methods: nearest neighbor, bilinear interpolation, and cubic convolution.

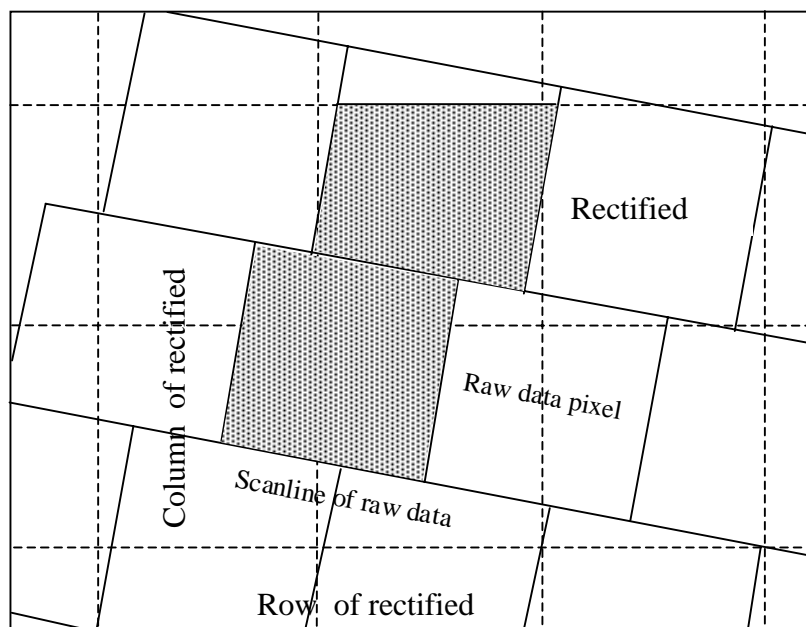


Figure 4-4 Relationship between the original image pixels and rectified pixels

Nearest neighbor

In this approach, the data file value of the nearest pixel to the retransformed pixel in the source image is adopted as the data file value for the output rectified pixel. Contrary to the bilinear interpolation and cubic convolution methods, the nearest neighbor approach does not change the data file value. The nearest neighbor method is suitable for use before classification. It is the easiest and fastest of the three methods. One of the disadvantages of this method is that a “stair stepped” effect may be produced.

Bilinear interpolation

The data file value of the rectified pixel is computed from the four closest pixels in the source image by use of three linear interpolations (Richards 1994). This method is considered more spatially accurate than the nearest neighbor. But it has the effect of a low frequency convolution. Edges are smoothed, and some extremes of the data file values are lost.

Cubic Convolution

The data file value of the rectified pixel is derived from a set of 16 pixels in the source image by use of cubic function. This method is quite similar to bilinear interpolation. The image resulted from the cubic convolution method is generally smooth in appearance. It is the most computationally intensive method.

The nearest neighbor method was applied in this study to ensure that no change in data file value occurs. This is important for the subsequent classification operations. A good match between the rectified panchromatic image and digital orthophotos is illustrated in Figure 4-5.



Figure 4-5 A subset of overlay of rectified panchromatic image and digital orthophotos

4.1.3 Rectification of multispectral images using "image-to-image" registration method

Using the rectified panchromatic image as a reference image, multispectral images were rectified using the "image-to-image" registration method. Compared to the panchromatic image, the rectification of multispectral images is a relatively simple process.

The registration of the multispectral images is conducted in three steps.

- (1) Locate GCPs both in the panchromatic image and the multispectral images using the GCP Editor. In this study, twenty-six GCPs were interactively selected.
- (2) Calculate the transformation matrix using GCP Editor and the Transformation Editor until the RMS error is acceptably low. The first-order polynomial was adequate for the transformation. Two GCPs with higher RMS errors were deleted. Twenty-four GCPs were used to compute the transformation matrix. Table 4-5 lists twenty-four GCPs coordinates of panchromatic and multispectral image. Table 4-6 presents the results of the RMS error calculation. The total RMS error is 0.333 pixels, or about 7.8m on the ground. This accuracy level is quite satisfactory. The final calculated coefficients of the polynomial equation are given in Table 4-7.
- (3) Resample the image data. As in the panchromatic image rectification, the nearest neighbor resampling method was used for rectifying the multispectral images, so that no change in data file value occurs.

A good match between the rectified multispectral image and digital orthophotos is illustrated in Figure 4-6.

Table 4-5 The selected GCPs coordinates of panchromatic and multispectral images

Number	GCP number	X Source	Y Source	X Destination	Y Destination
1	GCP #1	369	929	3437548	5462424
2	GCP #2	440	763	3438233	5457980
3	GCP #3	13	486	3426216	5453809
4	GCP #4	609	966	3443579	5461872
5	GCP #5	45	48	3424371	5442994
6	GCP #6	856	963	3449570	5460331
7	GCP #7	244	695	3433079	5457507
8	GCP #8	590	603	3440915	5453202
9	GCP #9	270	557	3432879	5453989
10	GCP #10	88	750	3429641	5459776
11	GCP #11	944	500	3448905	5448553
12	GCP #12	811	650	3446564	5453014
13	GCP #13	601	271	3439187	5445061
14	GCP #14	420	575	3436621	5453538
15	GCP #15	153	263	3428275	5447582
16	GCP #17	795	524	3445420	5450029
17	GCP #19	377	294	3433907	5446972
18	GCP #20	880	171	3445365	5440965
19	GCP #21	717	284	3442085	5444685
20	GCP #22	524	64	3436072	5440509
21	GCP #23	685	130	3440372	5441128
22	GCP #24	690	808	3444587	5457568
23	GCP #25	788	30	3442273	5438078
24	GCP #26	957	689	3450335	5453069

Table 4-6 The RMS error of GCPs for the multispectral images

X-RMS Error (pixel)	Y-RMS Error (pixel)	Total RMS Error (pixel)
0.3652	0.2419	0.438

Table 4-7 Transformation coefficients of "image-to-image" method

	X'	Y'
Const.	-278183.984545	-218553.949671
X	0.072140	-0.002306
Y	0.041906	0.036929

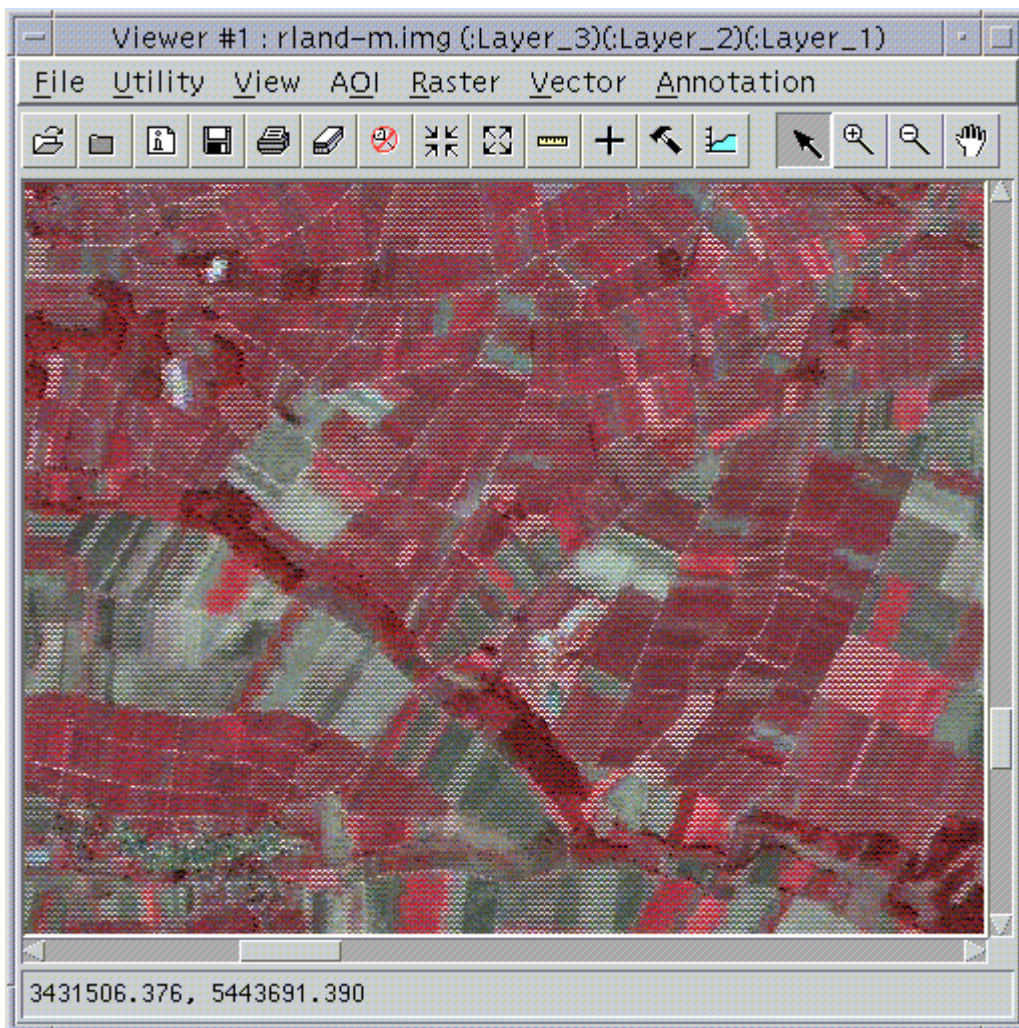


Figure 4-6 A subset of overlay of rectified multispectral image and digital orthophotos

4.2 Merge of Panchromatic Image and Multispectral Images

Merging information from different imaging sensors is a widely used image processing technique. The purpose of image fusion is to make the best use of the complementary information acquired in different imagery data sets about the same terrain features. A popular image merging approach is the fusion of panchromatic and multispectral images. The basic idea underlying this approach is that the features of ground objects can be better described by combining panchromatic and multispectral data because the panchromatic data usually has higher spatial resolution while multispectral data higher spectral resolution. IRS-1C satellite system offers both types of imagery data.

Merging PAN and multispectral data involves two distinct steps. First, the low-resolution multispectral images are geometrically registered to the high-resolution panchromatic image. As described in Section 4.1, both multispectral and panchromatic images are rectified to the Gauss-Krueger coordinate system. Second, the information contents – spatial and spectral – are merged to generate a single data set that contains the best of the two input data sets.

Several image merging methods have been proposed in the literature. Examples include IHS (Intensity-Hue-Saturation), PCS (Principal Component Substitution), HPF (High-Pass Filter), RVS (Regression Variable Substitution), and SVR (Synthetic Variable Ratio). In this study, the IHS and PCS methods were used to merge the PAN and multispectral data.

The principle underlying the IHS and PCS methods is similar (Figure 4-7). Multispectral images are first forward transformed into a replace-space. One of the components of the transformed images is then replaced with the high-resolution panchromatic image in the replace-space. Finally, the replaced images are transformed back into the original space.

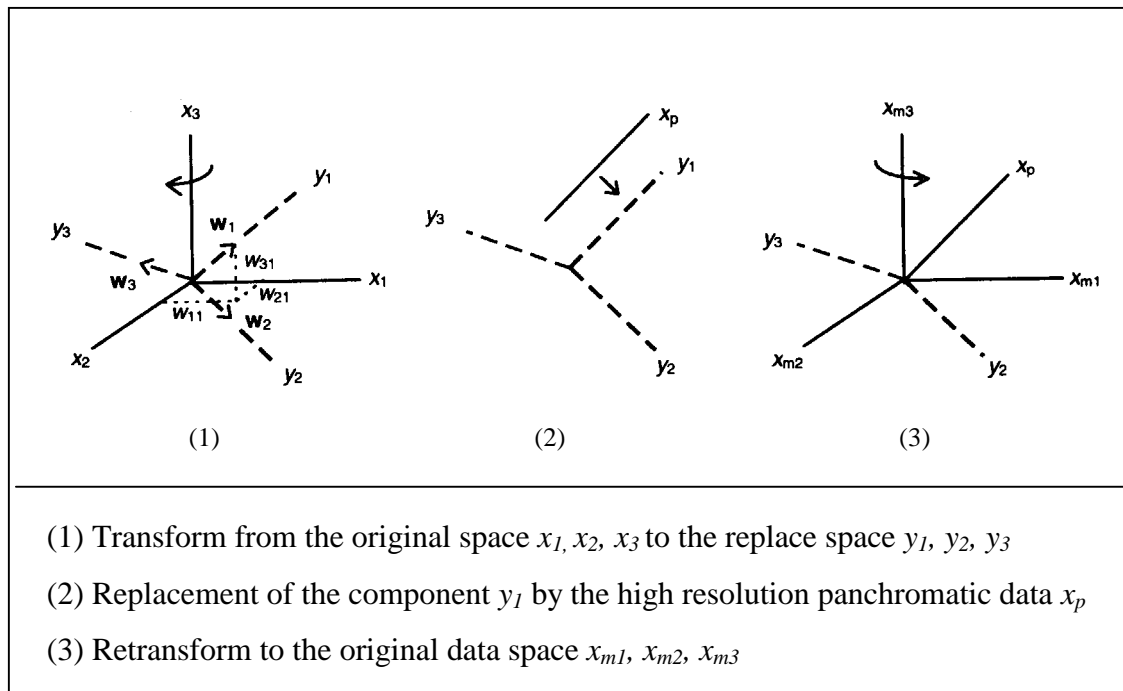


Figure 4-7 The principle of transform-replace-retransform method
(Source: Shettigara 1992)

4.2.1 Intensity-Hue-Saturation (IHS) method

IHS is one of the most often used methods for merging multisensor imagery data. The IHS method has been used in merging Landsat MSS and Return Beam Vidicon (RBV) data (Haydn et al 1982), Landsat TM and SPOT PAN data (Welch and Ehlers 1987), and SPOT multispectral and PAN data (Thormodsgrad and Feuquay 1987).

The IHS transformation process is illustrated in Figure 4-8. It is assumed that the intensity component is spectrally equivalent to the PAN image, and that all the spectral information is contained in H and S components.

The implementation of IHS involves four steps.

- (1) The multispectral bands 4, 3 and 2 were first displayed in RGB (Red-Green-Blue) system and were then transformed into IHS space as intensity, hue and saturation image.

- (2) A two standard deviation linear contrast stretch was applied to the higher spatial resolution panchromatic image so that it has approximately the same variance and average as the intensity component image.
- (3) The stretched, higher spatial resolution panchromatic image replaced the intensity component image.
- (4) Finally, the replaced images in IHS space were transformed back into the original space.

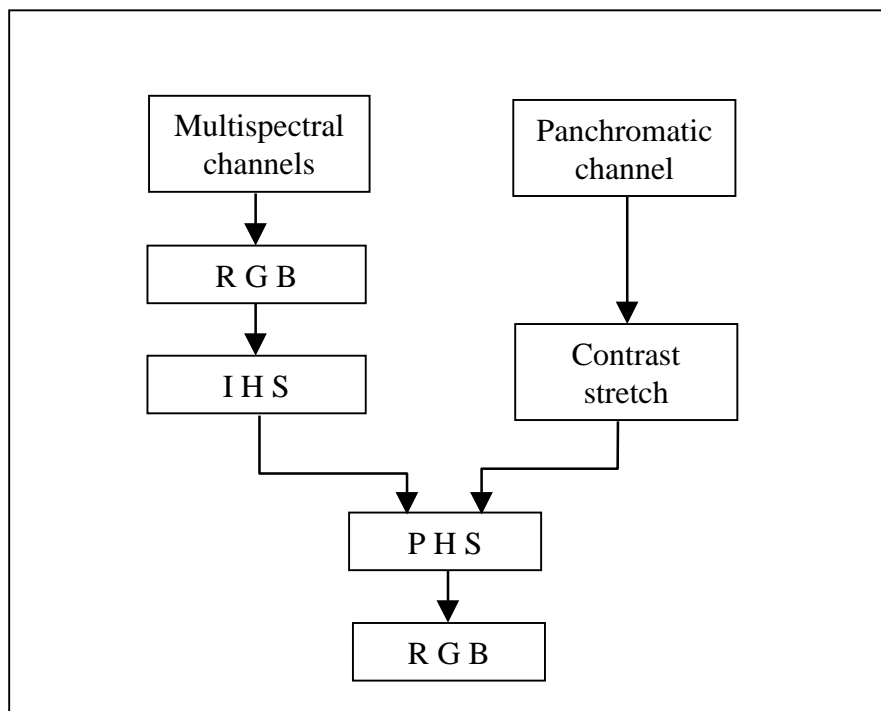


Figure 4-8 The IHS transformation process

4.2.2 Principal Component Substitution (PCS) method

The procedure for the merging of the multispectral and PAN data using the PCS method is similar to that of the IHS method. The justification used for replacing the first principal component image with the stretched PAN image is that the PAN image is approximately equal to the first principal component image. This assumption is made because the first principal component image will have the information that is common to all the bands used as input to PCA, while spectral information unique to

any of the bands is mapped to the other components. The multispectral data spectrally overlaps the PAN data so that its spectral information will be represented in the first principal component image.

The implementation of PCS was conducted in four steps.

- (1) The forward transform of LISS-III bands 2, 3, and 4 into principal components was made.
- (2) A two standard deviation linear contrast stretch was performed on the higher spatial resolution panchromatic image so that it has approximately the same variance and average as the first principal component.
- (3) The first principal component image was substituted by the stretched PAN image.
- (4) Finally, the reverse transform is performed.

4.3 Implementation and Results

Figures 4-9 and 4-10 present two subsets of the results of IHS and PCS merging operations. A visual comparison of the resulted merge images shows that the IHS method produced better color environment and more spatial details. However, the IHS technique is limited to three bands.

A major problem resulted from the image transformation operation is the distortion of spectral characteristics of the high spectral resolution data. Chavez et al (1991) analyzed the distortion of spectral characteristics of merged images from statistical, visual, and graphical point of view. In his study three methods – IHS, PCS, and HPF – were applied for the merging of Landsat TM and SPOT panchromatic data. It was found that the three methods have all caused distortions. The HPF method had the least distortion while the IHS method the greatest. Wald et al (1997) proposed a formal approach and some criteria for quantitative assessment of the synthetic images.

The merged data are not suitable for further digital classifications because the spectral separability of the merged data is different from the original data. Therefore, merged images are used mainly for visual interpretation.

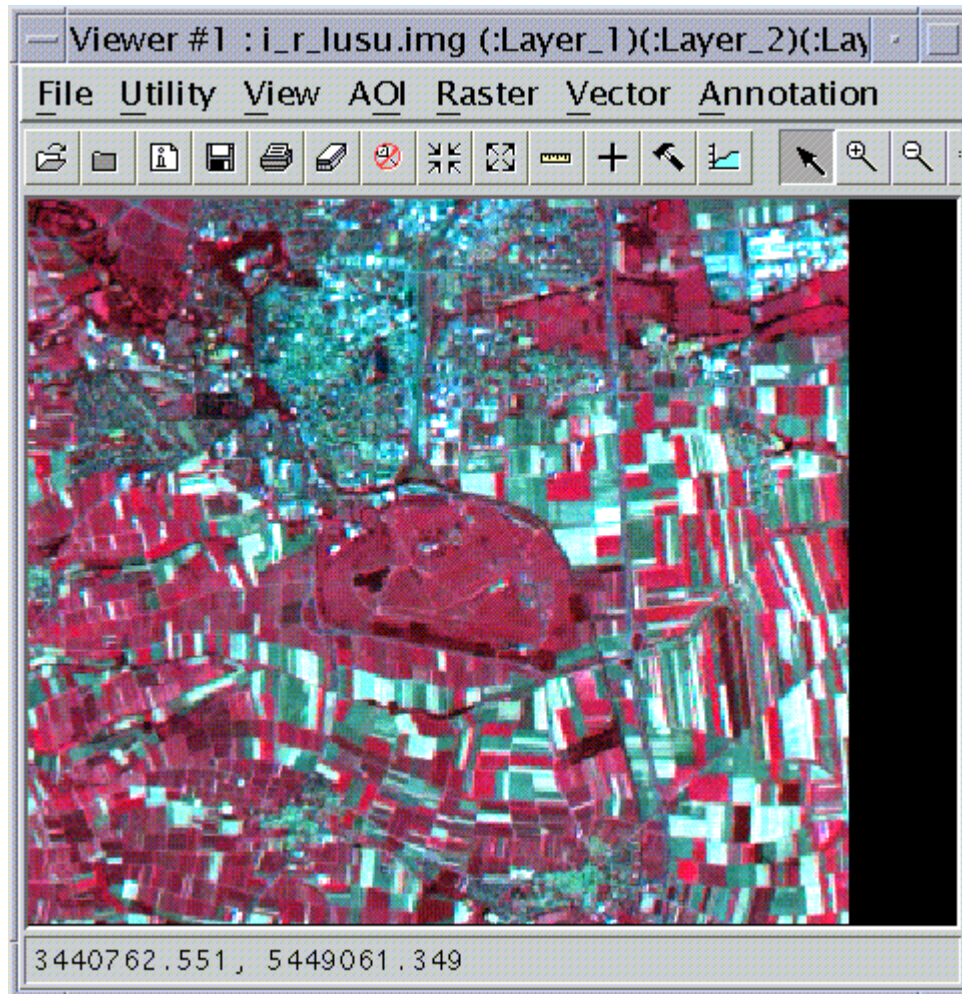


Figure 4-9 A subset of the IHS merge of PAN and multispectral imagery

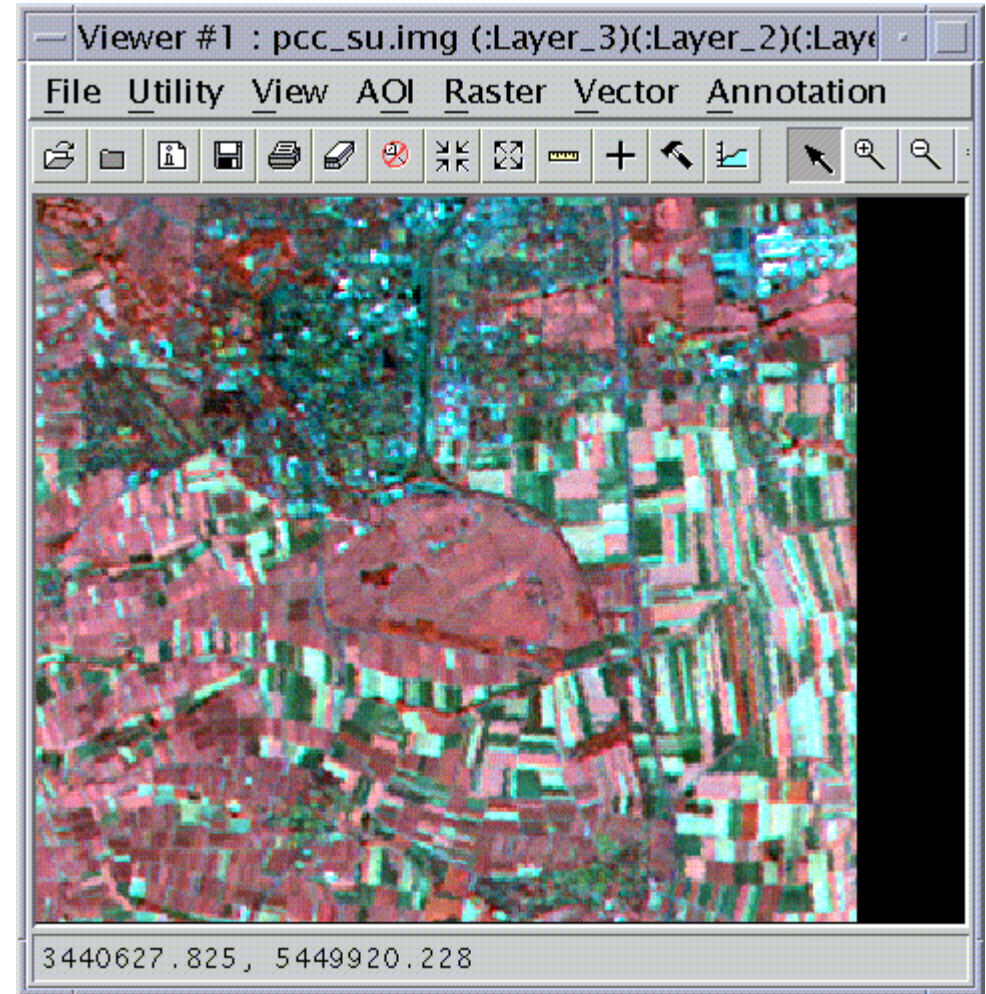


Figure 4-10 A subset of the PCS merge of PAN and multispectral imagery

Chapter 5 Multispectral Classification of IRS-1C Imagery Data

5.1 Supervised Classification

Supervised and unsupervised multispectral classifications are two main spectral pattern recognition approaches. Supervised classification requires *a priori* knowledge about the image data, such as which types of land-use exist in the study area and spatial locations of reliable samples for each land-use type. The procedure of supervised classification will be more controlled by the user than unsupervised classification. Supervised classification starts with training, which results in various signatures, and followed by class assignment using a decision rule (ERDAS Field Guide 1997).

Training is the process of defining the criteria by which patterns are recognized (Hord 1982). The computer must be trained to recognize patterns in the data. Training samples for each land-use type are first selected by use of ground truth data, aerial photos, and maps. Signatures for each class are then generated from the training samples. Signatures are statistical criteria for corresponding classes. Finally the pixels in the image are sorted into classes based on the signatures, by use of a classification decision rule. The decision rule is a mathematical algorithm that performs the actual sorting of pixels into distinct classes.

The often-used decision rules in supervised classification are Parallelepiped, Minimum Distance, Mahalanobis Distance, and Maximum Likelihood/ Bayesian. These decision rules are discussed in the following sections (ERDAS Field Guide 1997).

5.1.1 Parallelepiped decision rule

There are upper and lower limits for every signature in every band. Figure 5-1 is a two-dimensional example of a parallelepiped classification. The large rectangles are

called parallelepipeds. If pixels are found to lie in such a parallelepiped, then they are assigned to that signature's class.

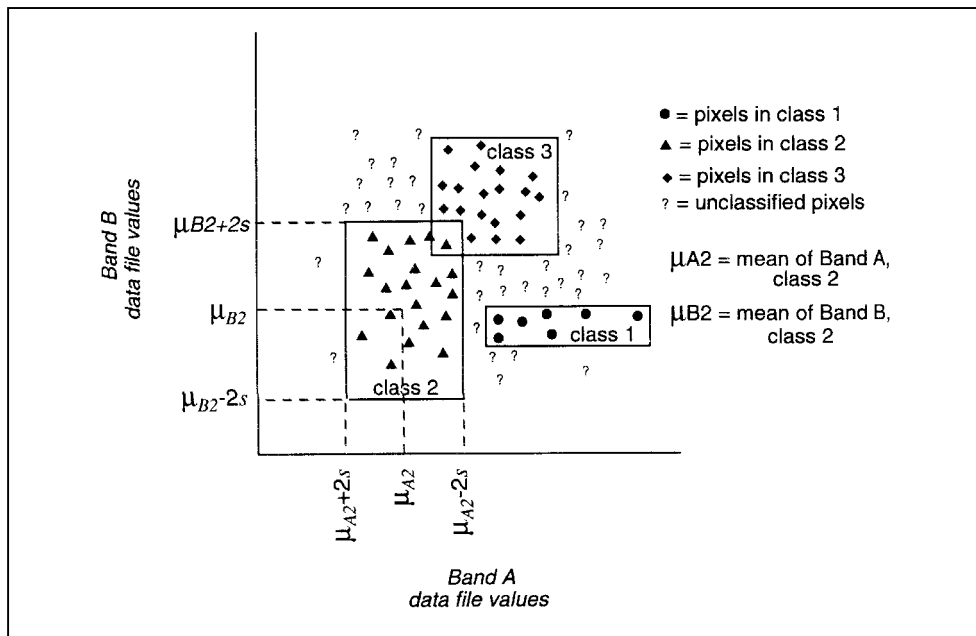


Figure 5-1 Parallelepiped classification using plus or minus two standard deviations as limits (Source: ERDAS Field Guide 1997 p. 244)

The limits for every signature can be either the minimum and maximum data file values of each band in the signature, the mean of each band, plus and minus a number of standard deviations, or any limits that the user specifies, based on the user's knowledge of the data and signatures.

The parallelepiped classifier is a very simple, and fast supervised classifier. It is often useful for a first-class, broad classification. The parallelepiped classifier has two main drawbacks though. One is that there can be considerable gaps between parallelepipeds and, as a result, pixels in these gap regions will not be classified. Secondly, pixels may be classified which are actually quite far, spectrally, from the mean of the signatures due to "corners" in parallelepipeds.

5.1.2 Minimum Distance

The minimum distance decision rule calculates the spectral distance between the measurement vector for the pixel to be classified and the mean vector for each signature (Figure 5-2). Generally, spectral distance is based upon the squared Euclidean distance.

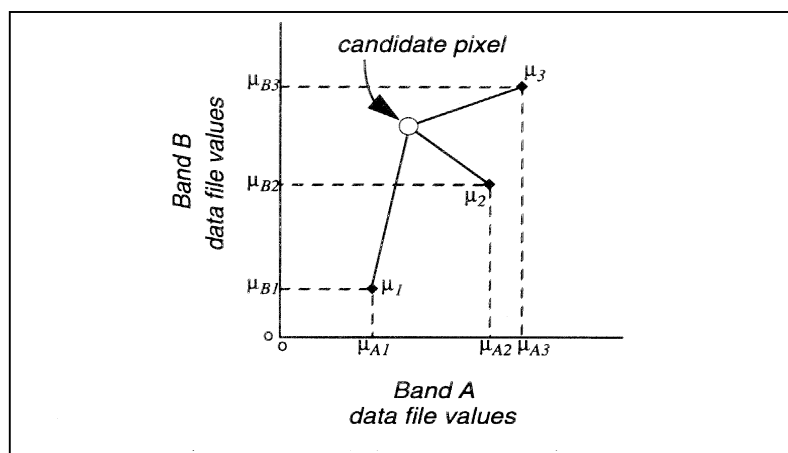


Figure 5-2 Minimum spectral distance
(Source: ERDAS Field Guide 1997 p.248)

Formula

Classification is performed on the basis of

$$x \in \omega_i \quad \text{if } d(x, m_i)^2 < d(x, m_j)^2 \quad \text{for all } j \neq i$$

where:

- x : the measurement vector for the pixel to be classified;
- ω_i : $\omega_i = 1, 2, \dots, M$, the spectral classes for an image, M is the total number of classes;
- m_i : $i = 1, 2, \dots, M$, are the mean vectors for each class;
- $d(x, m_i)^2$: squared Euclidean distance,

$$d(x, m_i)^2 = (x - m_i)^t (x - m_i),$$
 where t is the transposition function (matrix algebra).

The pixel at position x belongs to class ω_i , if $d(x, m_i)^2$ is the closest (lowest).

There are no unclassified pixels in the minimum distance classification as every pixel is spectrally close to one sample mean. Minimum distance is a fast decision rule. A

disadvantage of this technique is that pixels which should be unclassified, because they are not spectrally close to the mean of any sample, will become classified. This problem can be alleviated by thresholding out the pixels that are farthest from the means of their classes.

Another limitation of this method is that it does not consider class variability. For example, an urban class may be improperly classified, because an urban area consists of pixels with high variance, which may tend to be far from the mean of the signature. Inversely, a class with less variance, like water, may tend to be overclassified, since the pixels that belong to the class are usually spectrally closer to their mean.

5.1.3 Mahalanobis Distance

The Mahalanobis distance algorithm assumes the histograms of the bands have normal distributions. Mahalanobis distance is similar to minimum distance, except that the covariance matrix is used in the discriminant function. Variance and covariance are figured in so that clusters that are highly varied will lead to similarly varied classes.

Formula

Classification is performed on the basis of

$$x \in \omega_i \quad \text{if } d(x, m_i)^2 < d(x, m_j)^2 \quad \text{for all } j \neq i$$

where:

- x : the measurement vector for the pixel to be classified;
- ω_i : $\omega_i = 1, 2, \dots, M$, the spectral classes for an image, M is the total number of classes;
- m_i : $i = 1, 2, \dots, M$, are the mean vectors for each class;
- $d(x, m_i)^2$: Mahalanobis distance;

$$d(x, m_i)^2 = (x - m_i)^t \Sigma_i^{-1} (x - m_i),$$

where:

- t : the transposition function;
- Σ_i^{-1} : inverse of the covariance matrix of the data in class ω_i .

The pixel at position x belongs to class ω_i , if $d(x, m_i)^2$ is the closest.

Unlike minimum distance or parallelepiped, the Mahalanobis distance classifier takes into account the variability of classes. It may be more useful than minimum distance in cases where statistical criteria must be taken into account, but the weighting factors that are available with the Maximum Likelihood/Bayesian option are not needed.

There are several disadvantages of the Mahalanobis distance classifier. First, it tends to overclassify signatures with relatively large values in the covariance matrix. If there is a large dispersion of the pixels in a cluster or training sample, then the covariance matrix of that signature will contain large values. Second, it is slower to compute than minimum distance and parallelepiped classifier. Third, Mahalanobis distance is parametric, meaning that it relies heavily on a normal distribution of the data in each band. If this is not the case, better results can be achieved with minimum distance or parallelepiped decision rule.

5.1.4 Maximum Likelihood/Bayesian classification

The maximum likelihood algorithm is the most common decision rule for supervised classification. This decision rule is based on the probability that a pixel belongs to a particular class. It assumes that these probabilities are equal for all classes, and that the input bands have normal distributions (Figure 5-3).

If the user has *a priori* knowledge that the probabilities are not equal for all classes, the user can specify weight factors for particular classes. This variation of the maximum likelihood decision rule is known as Bayesian decision rule (Hord 1982).

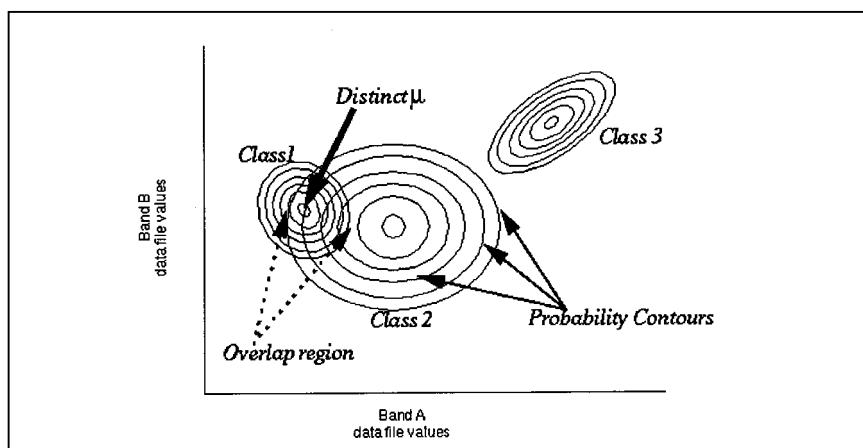


Figure 5-3 Maximum likelihood decision rule
(Source: ERDAS IMAGINE V8.3 Professional Training Reference Manual 1997 p.29)

Formula

The maximum likelihood classification is performed according to the following decision rule:

$$x \in \omega_i \quad \text{if } p(\omega_i | x) > p(\omega_j | x) \quad \text{for all } j \neq i \quad (5.1)$$

where

x : the *position vector*, a column vector of brightness values for the pixel;

ω_i : the *spectral classes* for an image, $\omega_i = 1, 2, \dots, M$, where M is the total number of classes;

$p(\omega_i | x)$: the *conditional probabilities*, which gives the likelihood that the correct class is ω_i for a pixel at position x .

The pixel at x belongs to class ω_i , if $p(\omega_i | x)$ is the largest.

To obtain $p(\omega_i | x)$ in (5.1), a probability distribution $p(x | \omega_i)$ can be estimated from training data for each ground cover type. The desired $p(\omega_i | x)$ in (5.1) and the available $p(x | \omega_i)$ are related by Bayes' theorem (Freund and Walpole 1987):

$$p(\omega_i | x) = p(x | \omega_i) p(\omega_i) / p(x) \quad (5.2)$$

where:

$p(\omega_i)$: the probability that class ω_i occurs in the image;

$p(x)$: the probability of finding a pixel from any class at location x .

It is of interest to note that

$$p(x) = \sum_{i=1}^M p(x | \omega_i) p(\omega_i)$$

The $p(\omega_i)$ are called *a priori* or prior probabilities, since they are the probabilities with which class membership of a pixel could be guessed before classification. By comparison, the $p(\omega_i | x)$ are *posterior* probabilities. Using (5.2) it can be seen that the decision (classification) rule of (5.1) is modified as:

$$x \in \omega_i \quad \text{if } p(x | \omega_i)p(\omega_i) > p(x | \omega_j)p(\omega_j) \quad \text{for all } j \neq i \quad (5.3)$$

where $p(x)$ has been removed as a common factor.

The maximum likelihood decision rule assumes that the probability distributions for the classes are of the form of multivariate normal models, therefore,

$$p(x | \omega_i) = (2\pi)^{-N/2} |\Sigma_i|^{-1/2} \exp\left\{-\frac{1}{2}(x - m_i)^t \Sigma_i^{-1}(x - m_i)\right\} \quad (5.4)$$

where m_i and Σ_i are the mean vector and covariance matrix of the data in class ω_i .

Resulting from applying natural logarithm to (5.4) and mathematical simplifications, the discriminant function for the maximum likelihood/Bayesian classifier is:

$$g_i(x) = \ln p(\omega_i) - \frac{1}{2} \ln(|\Sigma_i|) - \frac{1}{2}(x - m_i)^t \Sigma_i^{-1}(x - m_i)$$

where:

- ω_i : a particular class;
- x : the measurement vector of the candidate pixel;
- m_i : the mean vector of the data in class ω_i ;
- $p(\omega_i)$: the probability that class ω_i occurs in the image (equal for all classes, or is entered from a priori knowledge);
- Σ_i : the covariance matrix of the data in class ω_i ;
- $|\Sigma_i|$: determinant of Σ ;
- Σ_i^{-1} : inverse of Σ ;
- \ln : natural logarithm function;
- t : transposition function.

The pixel is assigned to the class ω_i , for which $g_i(x)$ is the largest.

The maximum likelihood /Bayesian algorithm is the most accurate classifier in the ERDAS IMAGINE system, because it takes most variables into account (ERDAS Field Guide 1997). It should be noted, though, that the maximum likelihood algorithm assumes the histograms of the bands of data to take normal distributions. If this is not the case, the parallelepiped or minimum distance decision rule may generate better results.

5.2 Unsupervised Classification - ISODATA Clustering

Unsupervised classification, also called clustering, is more computer-automated than supervised classification. Only some parameters are required to specify from the user to begin this process. Then the computer uses these parameters to uncover statistical patterns that are inherent in the data.

It should be noted that the statistical patterns identified are just clusters of pixels with similar spectral characteristics. They do not necessarily correspond to any meaningful characteristics of ground objects. Consequently, after unsupervised classification the user must attach the actual meaning to the resulting classes (Jensen 1986).

Sequential, statistic, ISODATA (Self-Organizing Data Analysis Technique), and RGB (Red-Green-Blue) decision rules are often used in unsupervised classification. Details of the ISODATA clustering algorithm are given below (ERDAS Field Guide 1997).

The ISODATA method uses minimum spectral distance to assign a cluster for each candidate pixel. This algorithm is iterative in that it repeatedly performs an entire classification and recalculates statistics. Three parameters must be specified for ISODATA clustering:

- N – the maximum number of clusters to be considered. Since each cluster is the basis for a class, this number becomes the maximum number of classes to be formed;
- T – a convergence threshold, which is the maximum percentage of the pixels whose class values are allowed to be unchanged between iterations; and
- M – the maximum number of iterations to be performed.

ISODATA process (Figure 5-4) begins by determining N arbitrary cluster means. The spectral distance between the candidate pixel and each cluster means is calculated. The pixel is assigned to the cluster whose mean is the closest.

After each iteration, the means for each cluster are recalculated, based on the actual spectral locations of the pixels in the clusters, causing them to shift in feature space.

Then these new means are used for defining clusters in the next iteration. The entire process is repeated—each candidate pixel is compared to the new cluster means, and assigned to the closest cluster mean. The process will terminate until either the convergence threshold T or the maximum number of iterations M is reached.

The ISODATA method has three major advantages. First, Clustering is not geographically biased to the top or bottom pixels of the data file, because it is iterative. Second, this algorithm is highly successful at finding the spectral clusters that inherent in the data. It does not matter where the initial arbitrary cluster means are located, as long as enough iterations are allowed. Third, The resulting thematic raster layer from ISODATA clustering method is similar to using minimum distance classifier. This thematic layer can be used for analyzing and manipulating the signatures before actual classification is performed.

Time consuming is a major disadvantage of this algorithm. Obviously, this is a result of the iterations needed. Another deficit of the ISODATA clustering method is that it does not account for pixel spatial homogeneity.

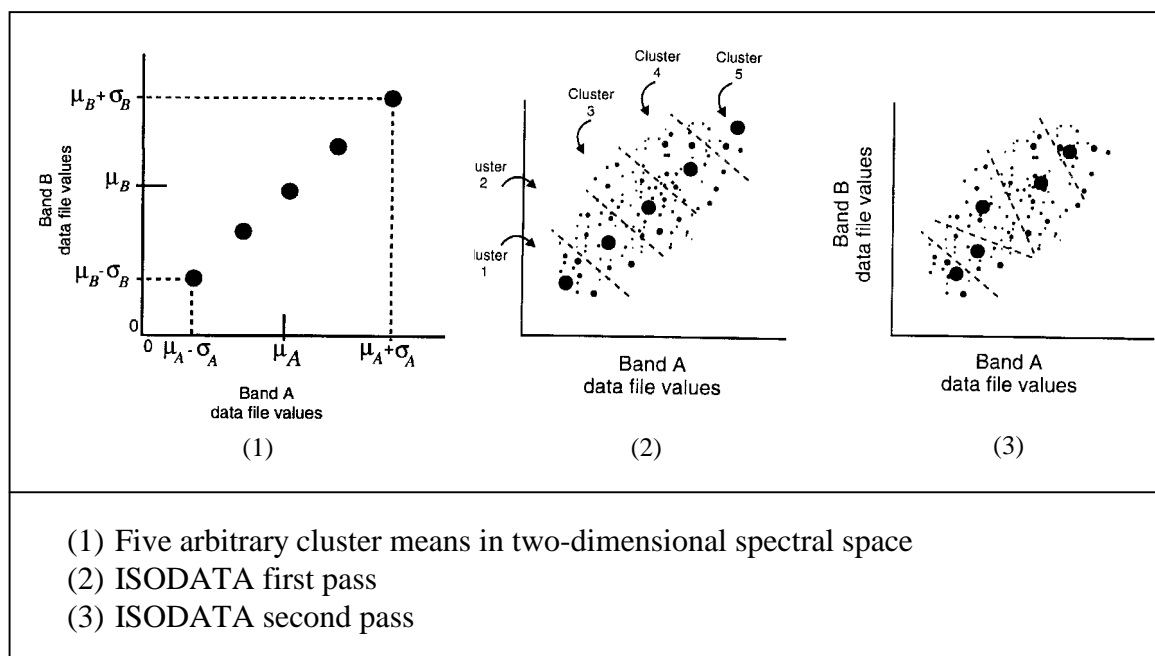


Figure 5-4 ISODATA clustering procedure

(Source: ERDAS Field Guide 1997 pp. 227-228)

5.3 Implementation and Results

Because Band 5 of LISS-III has a spatial resolution of 70.5 m, it is inadequate for the objective of this study. Therefore, Band 5 was not used for the land-use classification.

5.3.1 Design of land-use classification system

A classification process begins with defining a classification system. A land-use classification system categorizes all land-use types into classes in the system. A classification system should be mutually exclusive and totally exhaustive. A system is mutually exclusive if any point on the map/ground falls into one and only one land-use category. A system is totally exhaustive if every place on the ground has a label.

A hierarchical structure for the land-use classification system of the study area was developed. The hierarchical system is used to increase the flexibility of classification procedure. This hierarchical system contains three levels of detail of the land-use types: six classes in the first level, ten classes in the second level and seventeen classes in the third level (Table 5-1).

It should be noted that all subclasses within the agriculture class such as wheat, barley, sugar beet, corn, oat do not correspond to the unique land-use type of the fields, they represent only the dominant land-use types. It was difficult to differentiate pasture from grassland in a satellite imagery captured in July. Therefore the class "grassland" contains land-use type "pasture".

Table 5-1 The land-use classification system used in this study

Level 1	Level 2	Level 3
Urban or built-up	Residential	Low density Medium density High density
	Industrial	Industrial area
	Green space	Green space
Agriculture	Cropland	Barley
		Corn
		Oat
		Sugar beet
		Vine
		Wheat
Grassland	Grassland	Grassland
Forest land	Evergreen	Conifer
	Deciduous	Deciduous
	Mixed forest	Mixed forest
Water	Water	Water
Transport	Highway	Highway

5.3.2 Segmentation of urban and agricultural areas using ATKIS data

The purpose of segmenting urban and agricultural areas in the PAN and multispectral images is to generate two coarse homogeneous regions, i.e. urban and agricultural land-use types. This operation is useful because after the segmentation of operation, further land-use classification of the urban and agricultural areas can be conducted separately. This in turn can help reduce classification errors that might have resulted from similar spectral response patterns of some urban and agricultural land-use types – the confusing pixel problem.

The extraction of urban area is conducted in three steps (Figure 5-5). First, a vector urban file was extracted from ATKIS data. Second, the vector urban file was transformed into raster urban file. Third, urban areas were masked out from the whole image using raster urban file as mask file.

The extraction of vector urban file from ATKIS was implemented using Arc/Info software. The extraction process is conducted in three steps. First, select all data

records under the category “residential” that begins with the number “2” (urban areas) in the ATKIS data; add new item called *urban* and assigning the selected records the value “2”. Second, select all polygons with item *urban* != “2” and delete these polygons; save the remaining polygons (i.e. urban areas) to a new urban file. Third, dissolve the polygon boundaries in file urban areas.

The transformation of vector file into raster file and the masking of urban areas are performed in ERDAS Imagine. After masking operation, two new image files were generated, i.e., urban file and agriculture file. The urban file comprises only the “urban and built-up area” classes. All other classes appear in the agriculture file.

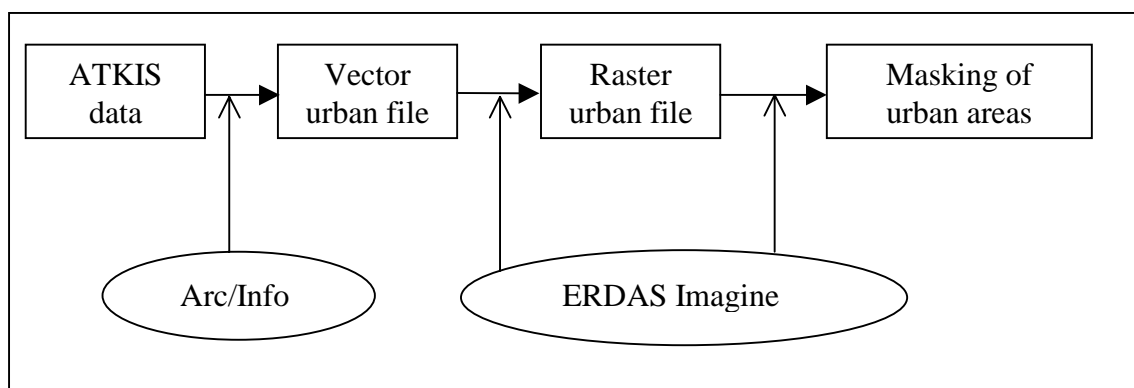


Figure 5-5 The procedure for extracting urban areas using GIS

Figures 5-6-1 and 5-6-2 compare the maximum likelihood classification before and after the segmentation of urban and agricultural areas. The confusing pixel problem in harvest fields and urban areas was eliminated. In addition, the mixed pixels between two land-use classes were greatly reduced.

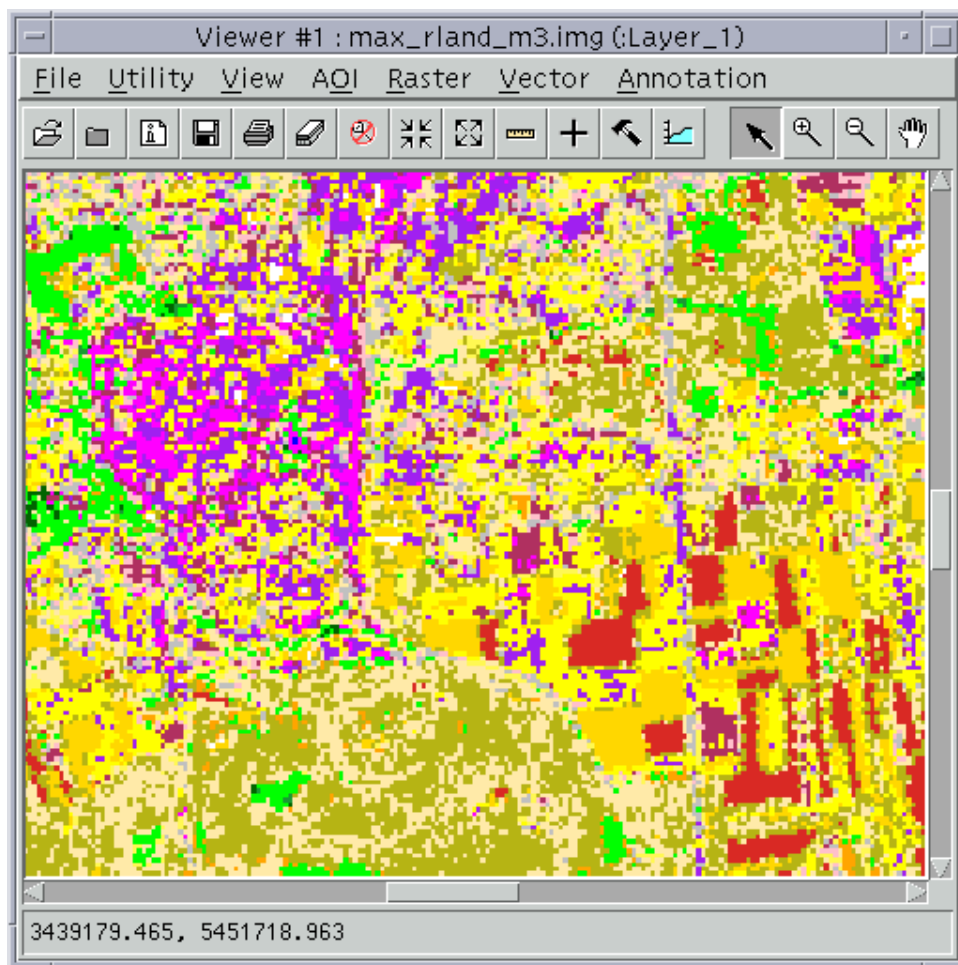


Figure 5-6-1 Maximum likelihood classification before segmentation of urban and agricultural areas

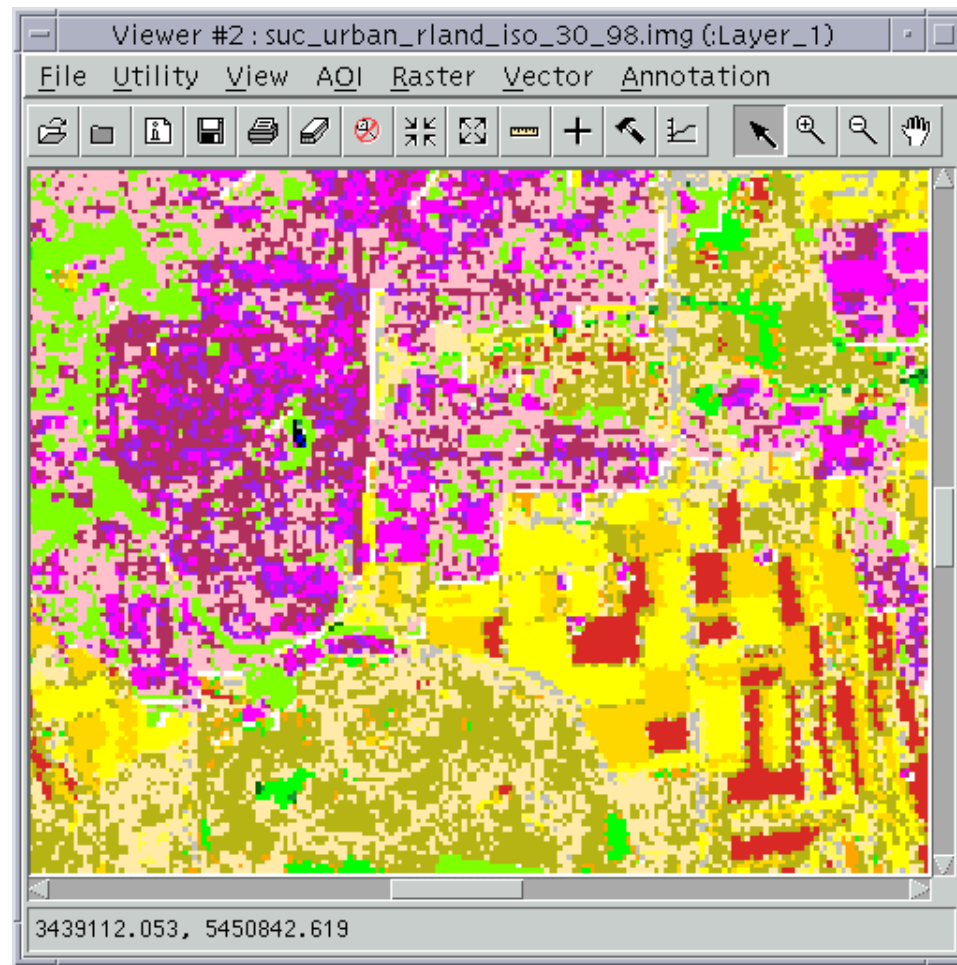


Figure 5-6-2 Maximum likelihood classification after segmentation of urban and agricultural areas

5.3.3 Classification of agriculture areas

The parallelepiped, minimum distance, Mahalanobis distance, and maximum likelihood/Bayesian algorithms and ISODATA methods were performed on the three bands of LISS-III imagery data of the agriculture file.

It was found that the hybrid method combining ISODATA method and the maximum likelihood/Bayesian algorithm produced the best results. The classification procedure is described in Figure 5-7.

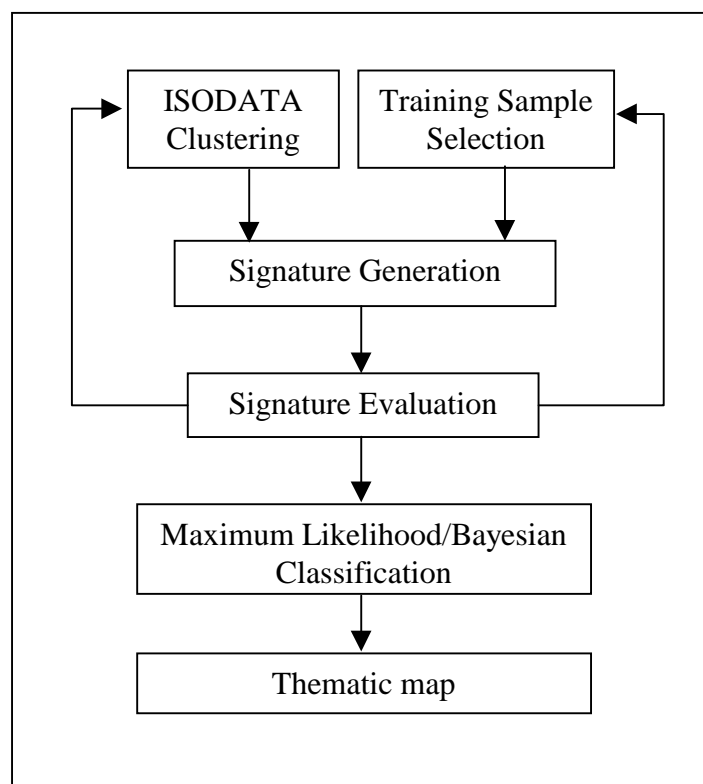


Figure 5-7 The procedure for classification of agriculture areas

5.3.3.1 ISODATA clustering

For the implementation of ISODATA algorithm, the parameters were given as follows:

Number of classes = 50;
Maximum iterations = 30;
Convergence threshold = 0.98.

A thematic raster layer and a signature file were created from the ISODATA clustering. The 50 classes in the thematic raster layer were then assigned the actual class names by comparing the original image data with the individual classes of the thematic raster layer. In addition to the land-use classes displayed in the land-use classification system, two more classes were classified: cloud and shadows.

It was found that conifer, deciduous, barley, cloud, and shadows can clearly be identified using the ISODATA clustering method. A heavy spectral mixture occurred between vine and grassland. There are also mixtures between conifer, water rim, and shadows; deciduous and grassland; between deciduous and ripe crop such as sugar beets and corn; and between vine and sugar beet, grassland and sugar beet.

5.3.3.2 Training sample selection

A total number of 400 samples were selected. Fieldwork for the selection of training samples was done in 1998; one year after the satellite data was acquired. For land-use types that change little over a short period of time, such as forest and vineyard, training samples were selected by use of various maps and data as reference basis. These maps and data include the TK 25, digital orthophotos, original PAN and LISS-III data, merged PAN and LISS-III data, as well as ATKIS data.

For crop types, the method described above is less appropriate. This is because, first, the type of crops on a field may change from year to year and, second, the fieldwork was not conducted at the same time the imagery data was acquired. To overcome this

problem an agricultural database of the town Suedliche Weinstrasse was used. This database records the actual crop types of fields in the study area for 1997. 102 training samples were selected from the agricultural database. Of these training samples 25 fields of crops, which either have small area, or do not have homogeneity in satellite imagery, or the types of the fields do not belong to any class of the classification system, were not used.

5.3.3.3 Signature generation and evaluation

For the maximum likelihood classification signatures were generated from both the ISODATA clustering procedure and the training samples. Because of the inherent spectral differences in land-use classes, level-3 classes in the land-use classification system were further differentiated. For example, eight subclasses under the vine class were distinguished according to their different spectral signatures.

Thirteen signatures including conifer, deciduous, mix-forest, barley, wheat, cloud and shadows from the ISODATA clustering procedure were first incorporated in the maximum likelihood signature file. Signatures for all other land-use types were generated from the training samples.

Following signature generation, signatures from the training samples were evaluated mainly by comparing ISODATA clustering results. Signatures of each land-use class that corresponds to the same ISODATA class, were merged while noise signatures were deleted.

Figure 5-8 displays an example of merge five similar signatures of the land-use class vine in the feature space.

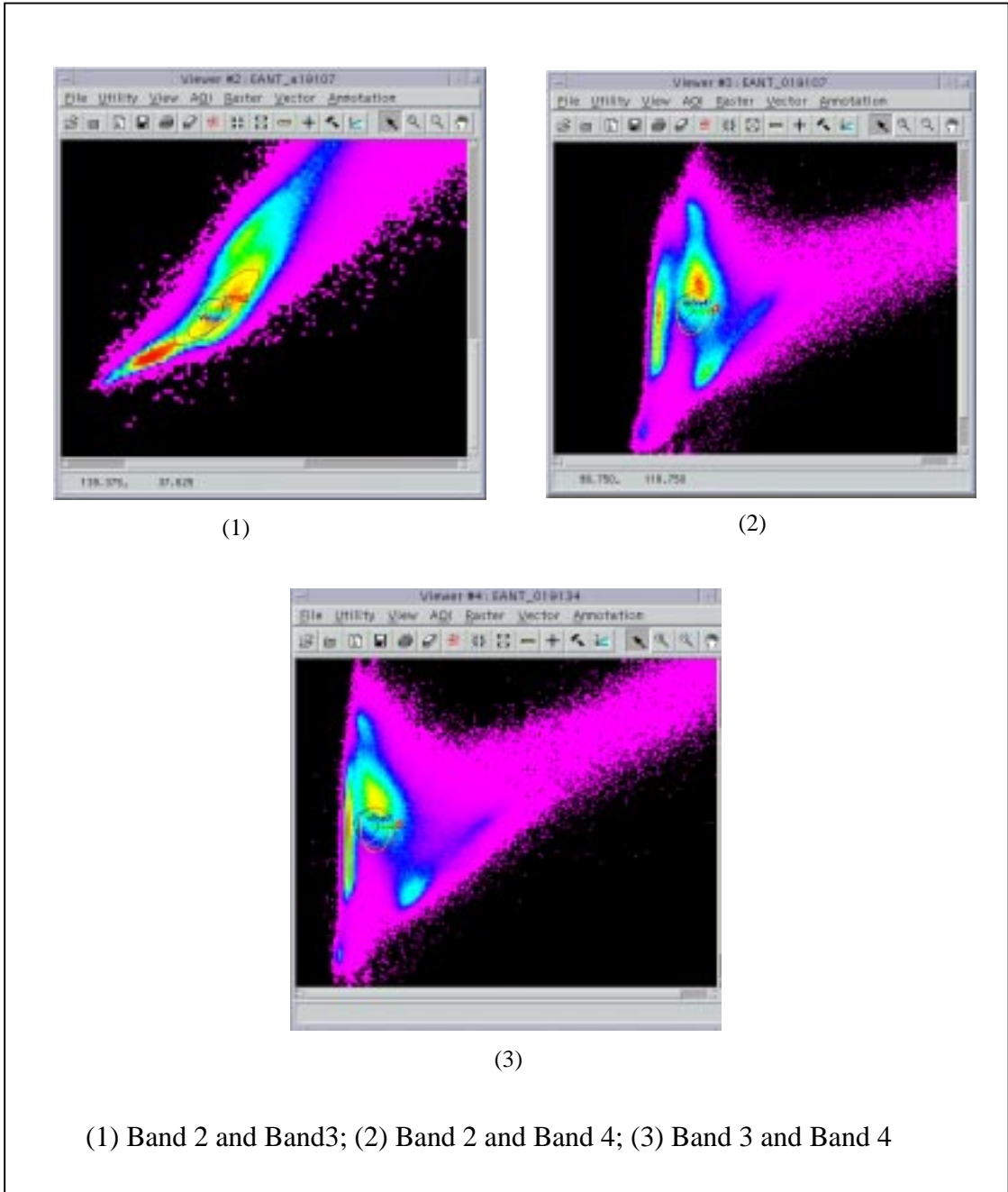


Figure 5-8 The ellipses for the five signatures of vine in the feature space

Signature generation and evaluation is an iterative process. As a result, a signature file containing 36 signatures was constructed. Table 5-2 presents the number, the name and the source of the signatures and their corresponding numbers of pixels. The separability of the 36 signatures based on the transformed divergence is illustrated in Table 5-3. The contingency matrix for the signatures captured from the training samples was calculated in Table 5-4.

Table 5-2 The number, name, source, and the number of pixels of the signatures

Class number	Class name	Number of pixels	Source
1	barley1	11387	ISODATA
2	barley2	22717	ISODATA
3	cloud1	8031	ISODATA
4	cloud2	41108	ISODATA
5	conifer	45255	ISODATA
6	corn	98	TS
7	deciduous1	29396	ISODATA
8	deciduous2	33192	ISODATA
9	deciduous3	34313	ISODATA
10	deciduous4	29917	ISODATA
11	grassland1	801	TS
12	grassland2	782	TS
13	grassland3	496	TS
14	grassland4	511	TS
15	grassland5	85	TS
16	grassland6	382	TS
17	highway1	11	TS
18	highway2	16	TS
19	mixed forest	25223	ISODATA
20	oat	92	TS
21	shadows1	10986	ISODATA
22	shadows2	340	ISODATA
23	sugar beet	439	TS
24	vine1	897	TS
25	vine2	505	TS
26	vine3	120	TS
27	vine4	208	TS
28	vine5	14	TS
29	vine6	206	TS
30	vine7	112	TS
31	vine8	35	TS
32	water1	32	TS
33	water2	26	TS
34	wheat1	29482	ISODATA
35	wheat2	102	TS
36	wheat3	9	TS

TS: training samples

Table 5-4 The contingency matrix of the 24 signatures

Class	6	11	12	13	14	15	16	17	18	20	23	24	25	26	27	28	29	30	31	32	33	35	36	
6	90.82	0.25	0	0	0	0	0	0	0	0	0	0	0	0	0	0	0	0	0	0	0	0	0	
11	0	64.43	6.98	10.04	0	0	0	0	0	0	0	0	0	0	4.29	0	4.33	2.68	0	0	0	0	0	0
12	0	12.06	62.18	0.2	0	0	7.07	0	0	0	0	0	3.56	0	2.86	0	30.77	0	0	0	0	0	0	0
13	0	9.33	0	58.4	0	0	0	0	0	0	0	0	0	0	0	0	0	30.36	0	0	0	0	0	0
14	0	0	0	0	85.77	0	0	0	0	0	0	0	0	0	0	0	0	0	0	0	0	0	0	0
15	0	0	0	0	0	77.65	0	0	0	0	0	0	0	0	5	14.29	0	0	0	0	0	0	0	0
16	0	1.49	6.85	0	0	0	63.87	0	0	0	0	4.43	34.98	0	0	0	8.17	0	0	0	0	0	0	0
17	0	0	0	0	0	0	0	100	6.25	0	0	0	0	0	0	0	0	0	0	0	0	0	0	0
18	0	0	0	0	0	0	0	0	87.5	1.09	0	0	0	0	0	0	0	0	0	0	0	0	0	0
20	0	0	0	0	0	0	0	0	6.25	95.65	0	1.44	0	0	0	0	0	0	0	0	0	0	0	0
23	0	0	0	0.61	0	0	0	0	0	0	100	0	0	0	0	0	0	0	0	0	0	0	0	0
24	0	0	0	0	0	0	4.45	0	0	3.26	0	82.5	11.86	0	0	0	0	0	0	0	0	0	0	0
25	0	1	0.63	0	0	0	16.75	0	0	0	0	10.85	45.85	0	0	0	0.48	0	0	0	0	0	0	0
26	0	0	1.65	0	0.4	0	0	0	0	0	0	0	0	94.17	0	0	6.25	0	0	0	0	0	0	0
27	0	8.46	4.95	1.64	0.2	4.71	0	0	0	0	0	0.22	0	0.83	82.86	0	6.25	4.46	0	0	0	0	0	0
28	0	0	0	0	0	16.47	0	0	0	0	0	0	0	0	0	85.71	0	0	0	0	0	0	0	0
29	0	1.12	16.75	0	0	0	7.85	0	0	0	0	0.22	3.56	5	2.14	0	43.75	0	0	0	0	0	0	0
30	0	1.62	0	29.1	0	1.18	0	0	0	0	0	0	0	0	2.86	0	0	62.5	0	0	0	0	0	0
31	0	0	0	0	13.63	0	0	0	0	0	0	0	0.2	0	0	0	0	0	100	0	0	0	0	0
32	0	0	0	0	0	0	0	0	0	0	0	0	0	0	0	0	0	0	0	100	0	0	0	0
33	0	0	0	0	0	0	0	0	0	0	0	0	0	0	0	0	0	0	0	0	100	0	0	0
35	0	0	0	0	0	0	0	0	0	0	0	0	0	0	0	0	0	0	0	0	0	94.12	0	0
36	0	0	0	0	0	0	0	0	0	0	0	0	0	0	0	0	0	0	0	0	0	0	0	100

5.3.3.4 Maximum likelihood classification results

The maximum likelihood/Bayesian classification was performed. A subset of the classified thematic map is given in Figure 5-9. A total number of fourteen land-use classes were extracted. Forest, wheat, barley, sugar beet, water, cloud and shadows have been well classified. Corn and oat have only small area and they were also relatively well identified.

Mixture occurred between sugar beet and grassland. In the middle of Figure 5-9, for example grassland was misclassified as sugar beet. Vineyard and grassland are heavy mixed because during this season, they have similar spectral reflections. Figure 5-10 shows grassland of the military training site. It was partly correctly classified as grassland but part of it was misclassified as vine. Figure 5-11 is a picture of vineyard.

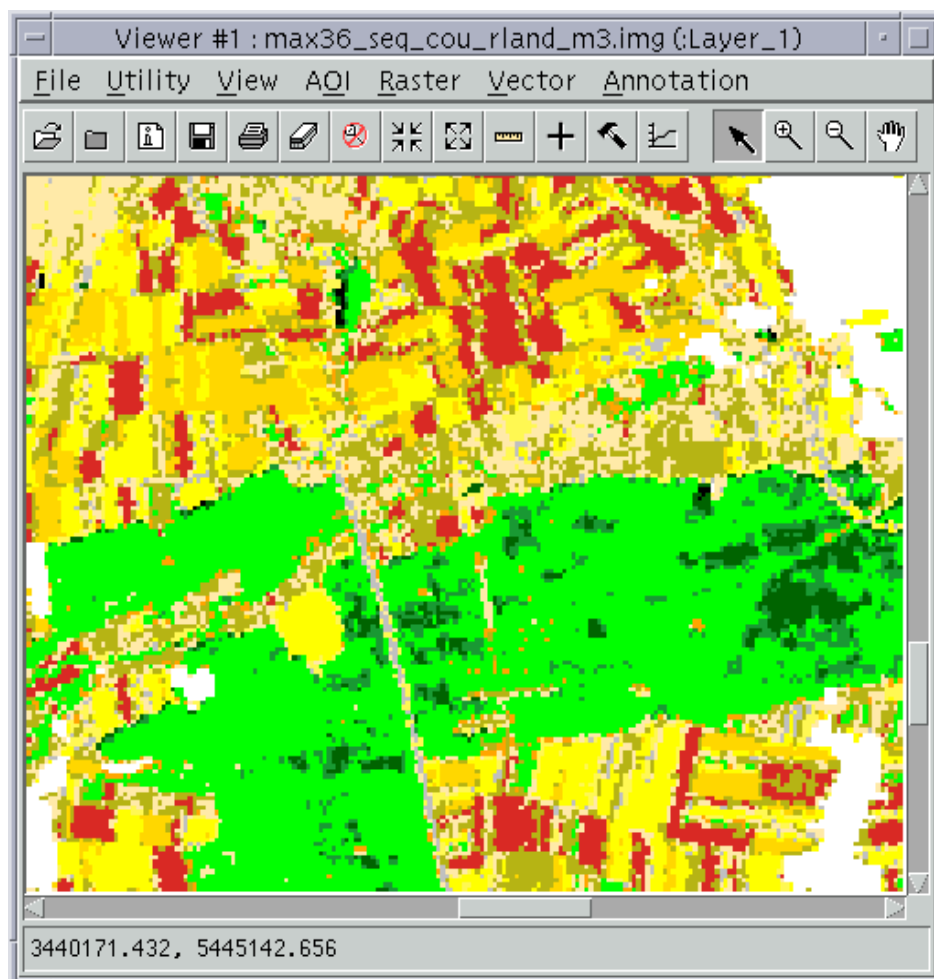


Figure 5-9 Maximum likelihood and ISODATA classification result



Figure 5-10 Grassland



Figure 5-11 Vineyard

5.3.4 Classification of urban areas

ISODATA clustering method was found to be suitable for the classification of the urban land-use types. The parameters for the implementation of ISODATA algorithm were given as follows: Number of classes = 30; Maximum iterations = 30; Convergence threshold = 0.98.

A thematic raster layer was created. The 30 classes in the thematic raster layer were then assigned the actual class names by comparing the original image data with the individual classes of the thematic raster layer. A subset of the ISODATA clustering operation is given in Figure 5-12. Five classes were extracted; they are residential of low density, medium density, and high density, industrial area, and green space.

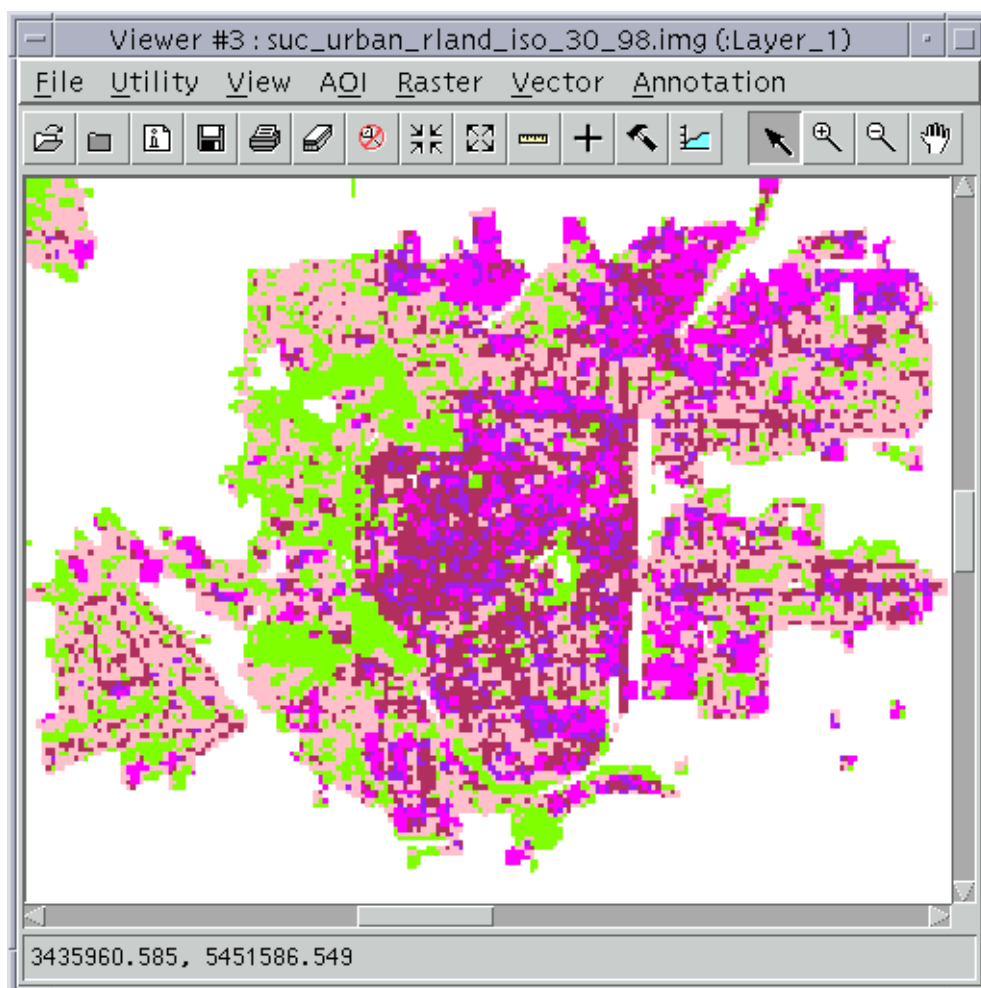


Figure 5-12 ISODATA classification results of the urban area

Part III Improved Satellite Image Classification Techniques

Chapter 6 Contextual Classification of IRS-1C Imagery

6.1 Contextual Classification Techniques

In any real image, the response and class of two spatially neighboring pixels are highly related. There are two reasons for this spatial correlation. First, imaging sensors acquire a significant portion of energy from adjacent pixels. In other words, the spectral reflectance characteristics of a pixel is significantly affected by its neighboring pixels. This effect is characterized as compound spectral response.

The second reason for the spatial correlation between image pixels is that, due to finite resolution of satellite sensors, land-cover types often occur over a region that is large compared with the size of a pixel. Consequently, in a large homogeneous region compared with the pixel size, if an image pixel (not at edge of the region) represents a particular land-use class, it is highly likely that its neighboring pixels are also the same land-use class. For example, if i and j are two neighboring pixels and if pixel i , belongs to class ω_k , then there is a high probability that pixel j also belongs to class ω_k . Thus, the decision for a pixel is to be made based not only on the observation at pixel i , but also on all pixels j where j is a neighbor of pixel i .

To take into account the spatial correlation between pixels in an image, a class of classification methods called contextual techniques are developed. Contextual techniques use both spectral and spatial information to improve the classification accuracy. Contextual classifiers take into account contextual information when seeking to determine the most appropriate class for a pixel. They attempt to produce a thematic map that is consistent both spectrally and spatially.

6.2 Main Contextual Classifiers

The approaches adopted by the researchers during the past few years to incorporate context in the classification of remotely sensed data can be grouped as follows (Rosenfeld et al 1976; Pal and Pal 1993; Kartikeyan et al 1994; Deng and Iyengar 1996):

- Methods based on the classification of homogeneous objects,
- Techniques based on probabilistic relaxation,
- Methods derived using compound decision theory and sequential compound decision theory, and
- Methods derived based on a stochastic model for the distribution of classes in the scene.

Using filters before classification is the simplest method to exploit and enhance the spatial context of image data. For example, a median filter will reduce salt and pepper noise that would lead to inconsistent class labels. Simple averaging filters (possibly with edge preserving thresholds) can be used to impose a degree of homogeneity among the brightness values of adjacent pixels thereby increasing the chance that neighboring pixels may be given the same label (Richards 1994).

Generating a separate channel of data is another preprocessing contextual method. In an attempt to improve the accuracy of classification of image data containing urban segments, Gong and Howarth (1990) set up a "structural information" channel to bias a classification according to the density of high spatial frequency data.

Kettig and Landgrebe (1976) proposed a spatial preprocessing technique called ECHO (Extraction and Classification of Homogeneous Objects). In this approach, regions of similar spectral properties are "growing" before classification. These regions are then classified by comparing with class spectral signatures. The CASCADE algorithm of Merickel et al (1984) and the agglomerative clustering technique of Amadsun and King (1988) are other examples of such an approach.

Following ECHO method, Supervised Extraction and Classification of Homogeneous Objects (SECHO), one of the early and best known contextual classifiers, was presented by Landgrebe (1980). It can be seen as a "per field" classifier. It first divides the scene into homogeneous image segments and then classifies these segments using an extended version of the Gaussian maximum-likelihood (GML) algorithm. This technique is known to be efficient for classifying data sets that contain homogeneous objects that are large compared to the spatial resolution provided by the sensor.

Another type of contextual classification approach is postprocessing contextual classification techniques. Logical filters can be applied to a thematic map generated using a simple classifier (Duda and Hart 1973). Majority filter is another useful method (Townsend 1986; Schowengerdt 1983). Some contextual methods make use of neural networks (Bischof et al 1992). In this approach, the degree of smoothing depends on the confidence of classification of the individual pixels. The network is trained over the same data as for the classification.

Toussaint (1978) introduced an approach under the theme of sequential compound decision theory, which attempts to decide the label for one pixel based on the observation at all other pixels in the image. Some of the approximations and methods suggested by Toussaint (1978) can be found in Swain et al (1981), Tilton et al. (1982), Haslett (1985), Haralick and Joo (1986), Kaleyeh and Landgrebe (1987) and Khazenie and Grawford (1990).

Another powerful smoothing method is the Nagao filter (Nagao and Matsuyama 1979). The Nagao filter is an edge-preserving smoothing filter. This filter makes use of eight cliques surrounding each pixel and is generally applied on gray-level images. Solaiman et al (1998) proposed a modification of the Nagao filter that is applicable in smoothing thematic maps.

Zhang et al (1990) empirically evaluated the reliability of stochastic relaxation algorithm for region classification in Landsat imagery where a Markov-Gibbs distribution was used to establish constraints on region adjacency. A similar approach was used in Jhung and Swain (1996).

More complex contextual classification algorithms involve some quite sophisticated statistical and probabilistic theories. A good example of more complex contextual methods is the probabilistic label relaxation technique. Previous work on probabilistic relaxation shall be discussed in the following section.

6.3 Probabilistic Relaxation Methods

The possibility of using probabilistic relaxation for contextual classification of remotely sensed data was first discussed by Peleg (1980), Eklundh et al (1980), Faugeras and Berthod (1981), and Richards et al (1981a).

Relaxation is an iterative technique. This technique allows the spatial properties of a region to be carried into the classification process in a logically consistent way and, therefore, it is robust to image noise. The probabilities of neighboring pixels are used iteratively to update the probabilities for a given pixel based on a relation between the pixel labels specified by compatibility coefficients which describe the context of the neighbor. Context is incorporated in pairwise manner. This approach is computationally intensive. Contextual techniques based on relaxation methods iteratively adjust some initial estimates of class membership probabilities by reference to spatial context.

The process of probabilistic relaxation does not use measurement information except in the initialization stage when the measurement information is used to obtain the initial class membership probabilities for each pixel. The probabilistic technique is more complicate. If a map is examined in $N \times N$ windows, a label at the center of the window will be modified by the surrounding $N \times N$ pixels.

DiZenzo et al (1987) proposed an efficient implementation of the probabilistic relaxation method suited to the needs of actual remote sensing applications. This method is based on the key concepts of probability, compatibility coefficient, neighborhood function, and updating rule. Probabilities for each pixel describe the chance that the pixel belongs to each of the possible land-use classes. In the initial

stage, a set of probabilities could be computed from point or pixel-specific classifiers based on spectral data alone. A compatibility coefficient describes how compatible it is to have pixel m classified as ω_i and neighboring pixel n classified as ω_j . A neighborhood function allows the neighborhood pixels to influence the possible classification of the center pixel. The neighborhood function depends on the label probabilities of the neighboring pixels, and can be derived from compatibility coefficients and neighborhood weights. Neighborhood weights means that some neighbors may be more influential than others.

Details of the probabilistic relaxation scheme proposed by DiZenzo et al (1987) are given below (Richards 1994; DiZenzo et al 1987).

6.3.1 Probability calculation

Let $i = 1, 2, \dots, N$ be the N pixels to be classified;
 $l = \omega_1, \omega_2, \dots, \omega_K$ be the K classes, the classes are assumed to be mutually exclusive and exhaustive;
 $[P_i(\omega_1), P_i(\omega_2), \dots, P_i(\omega_K)]$ the vector denotes the probabilities of pixel i belongs to classes $\omega_1, \omega_2, \dots, \omega_K$;

where: $0 \leq P_i(\omega_l) \leq 1$

$$\sum_{l=1}^K P_i(\omega_l) = 1$$

In the initial stage, a set of probabilities can be computed from pixel-specific spectral classifiers such as Gaussian Maximum Likelihood (GML) classification.

6.3.2 Compatibility coefficients

The classes are assumed to be mutually exclusive and exhaustive. For each pair of neighboring pixels i and j and each pair of classes ω_k and ω_l , there is a compatibility measure $r_{ij}(\omega_k, \omega_l)$. These compatibility coefficients indicate the degree to which classifying pixel i as (to) ω_k and its neighboring pixel j as (to) ω_l are compatible. The

compatibility coefficient r_{ij} ranges from -1 , strong incompatibility, through 0 , neutral compatibility, to $+1$, strong compatibility (James 1987).

The r_{ij} can be chosen empirically. One possibility is to use estimates of the mutual information of the pair events $i \in \omega_k, j \in \omega_l$ as $r_{ij}(\omega_k, \omega_l)$. Empirically, it can be estimated from the GML classification as:

$$r_{ij}(\omega_k, \omega_l) = \lg \frac{N_{ij}(\omega_k, \omega_l)}{\sum_{k=1}^K N_i(\omega_k, \omega_l) \sum_{l=1}^K N_j(\omega_k, \omega_l)} \quad (6-1)$$

where:

- $N_{ij}(\omega_k, \omega_l)$: the frequency of occurrence of class ω_k and ω_l as neighbors at pixel i and j ;
- lg: the base-10 logarithm.

$r_{ij}(\omega_k, \omega_l)$ is defined as -1 , in cases where the frequency of occurrence of class ω_k and ω_l is zero.

In order to obtain reliable estimates of r_{ij} , it is important that the GML classification is reasonably accurate. If this requirement is not met, the compatibility coefficients r_{ij} will not reflect the actual characteristics of the image. In that case they can not be expected to promote true improvements of classification accuracy (DiZenzo et al 1987).

6.3.3 Neighborhood function

A neighborhood is defined surrounding center pixel i . This can be of any size and, in principle, should be large enough to ensure that all the pixels considered to have any spatial correlation with pixel i are included. Usually 3×3 window is used. For high-resolution imagery simple neighborhoods (Figure 6-1) are often adopted.

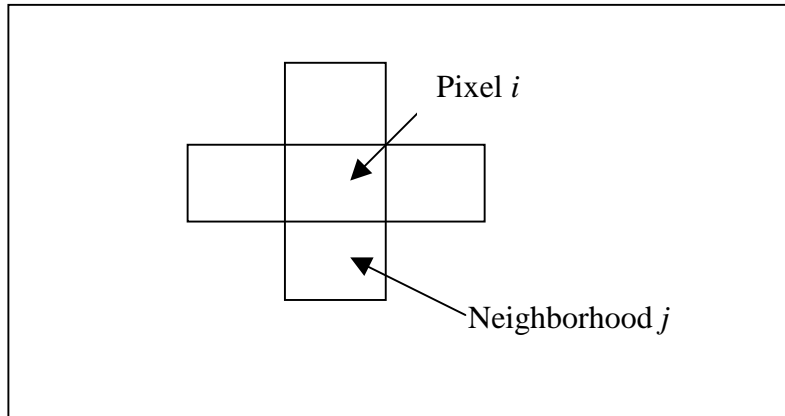


Figure 6-1 Definition of a simple neighborhood of pixel i

A neighborhood function is a function of the label probabilities of the neighboring pixels, compatibility coefficients, and neighborhood weights. It is defined as:

$$q_i^{(t)}(\omega_k) = \sum_{j=1}^{N_b} d_{ij} \sum_{l=1}^K r_{ij}(\omega_k, \omega_l) p_j^{(t)}(\omega_l)$$

where:

- N_b : the number of neighbors considered for pixel i ;
- d_{ij} : the weight factor of neighbors, indicating that some neigh may be more influential than others;
- K : the total number of classes;
- $r_{ij}(\omega_k, \omega_l)$: compatibility coefficient between neighboring pixel i and j ;
- $p_j(\omega_l)$: the probability of pixel j belongs to class ω_l ;
- t : number of iteration.

6.3.4 Updating rule

A neighborhood function allows the neighborhoods to influence the possible classification of the center pixel by multiplying the label probabilities by the neighborhood function. These new values are divided by their sum so that the new set of label probabilities sums to one.

$$P_i^{(t+1)}(\omega_k) = \frac{P_i^{(t)}(\omega_k)[1 + q_i^{(t)}(\omega_k)]}{\sum_{l=1}^K P_i^{(t)}(\omega_l)[1 + q_i^{(t)}(\omega_l)]}$$

where:

- $P_i^{(t)}(\omega_k)$: the probability of pixel i belongs to class ω_k of the t -th iteration;
- $q_i^{(t)}(\omega_k)$: neighborhood function of pixel i belongs to class ω_k of the t -th iteration;
- K : the total number of classes.

Such modification is an iterative process. Theoretically, it will stop until no changes in the label probabilities for all pixels. This can, however, lead up to several hundreds of iterations, which is very costly. In practice, it is observed that the classification results will be improved in the first few iterations (Richards et al 1981b).

6.4 Implementation and Results

6.4.1 Implementation procedure

The probabilistic relaxation was performed on the agricultural thematic map. The implementation of this algorithm was conducted in three steps (Figure 6-2).

First, probability calculation using Gaussian Maximum Likelihood algorithm. The purpose of calculating the probabilities of each pixel belonging to 36 signatures is to initiate the probabilistic relaxation process. A computer program for the GML algorithm was written using C. The means and covariances of the 36 signatures were used as input for the GML classification of the three bands of the agriculture file.

Second, calculating compatibility coefficients $r_{ij}(\omega_k, \omega_l)$ of 36 signatures from GML classified thematic map by using formula (6-1). The compatibility coefficients were then projected to the range (-1,1).

The third step is the implementation of the probabilistic relaxation process. This process is iterative. Details of this algorithm are illustrated in Figure 6-3.

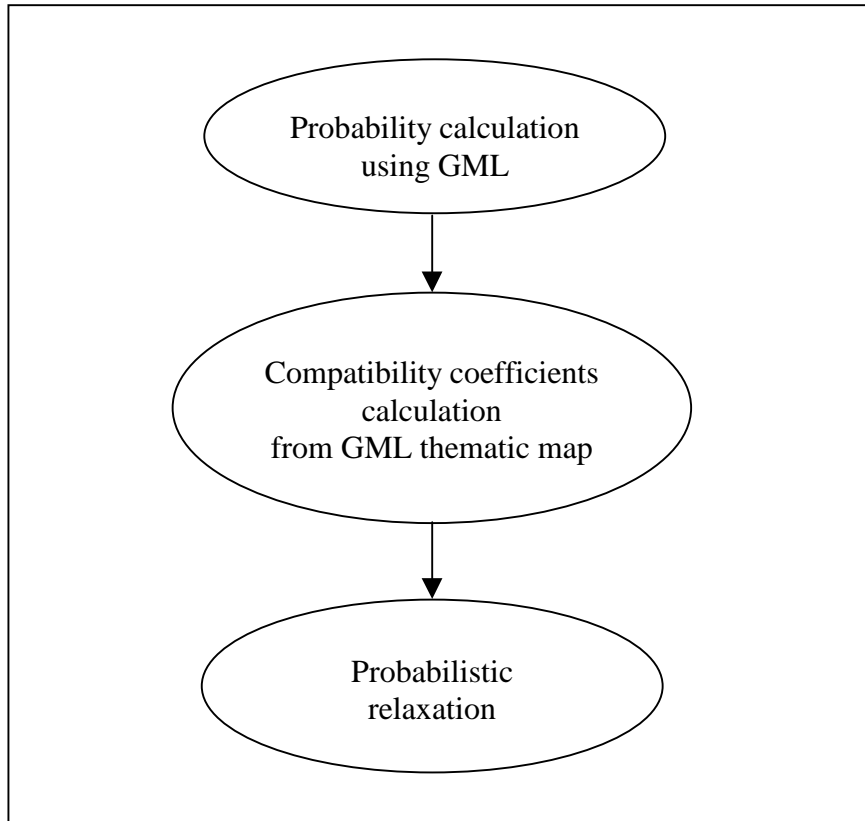
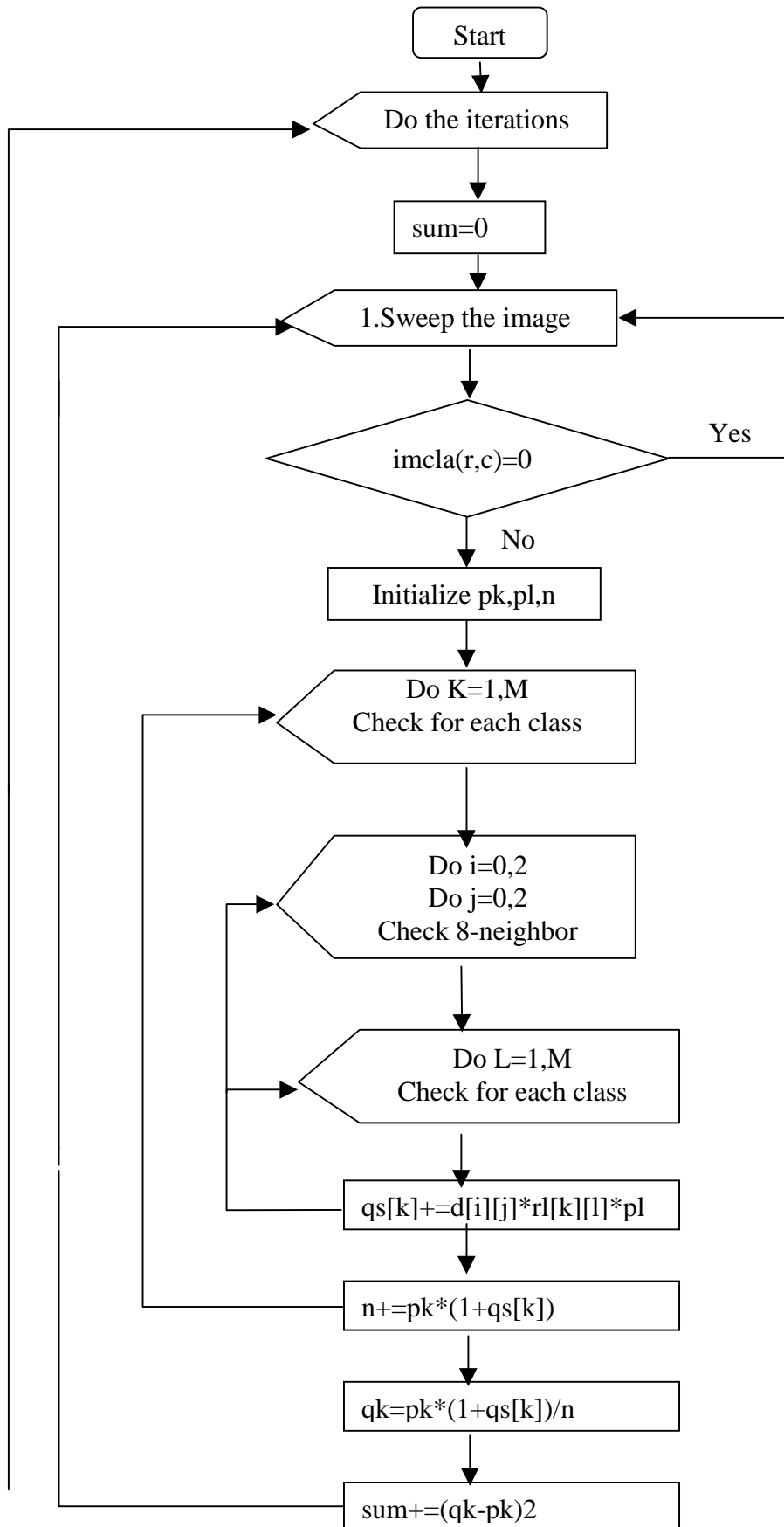


Figure 6-2 Three steps for the implementation of probabilistic relaxation



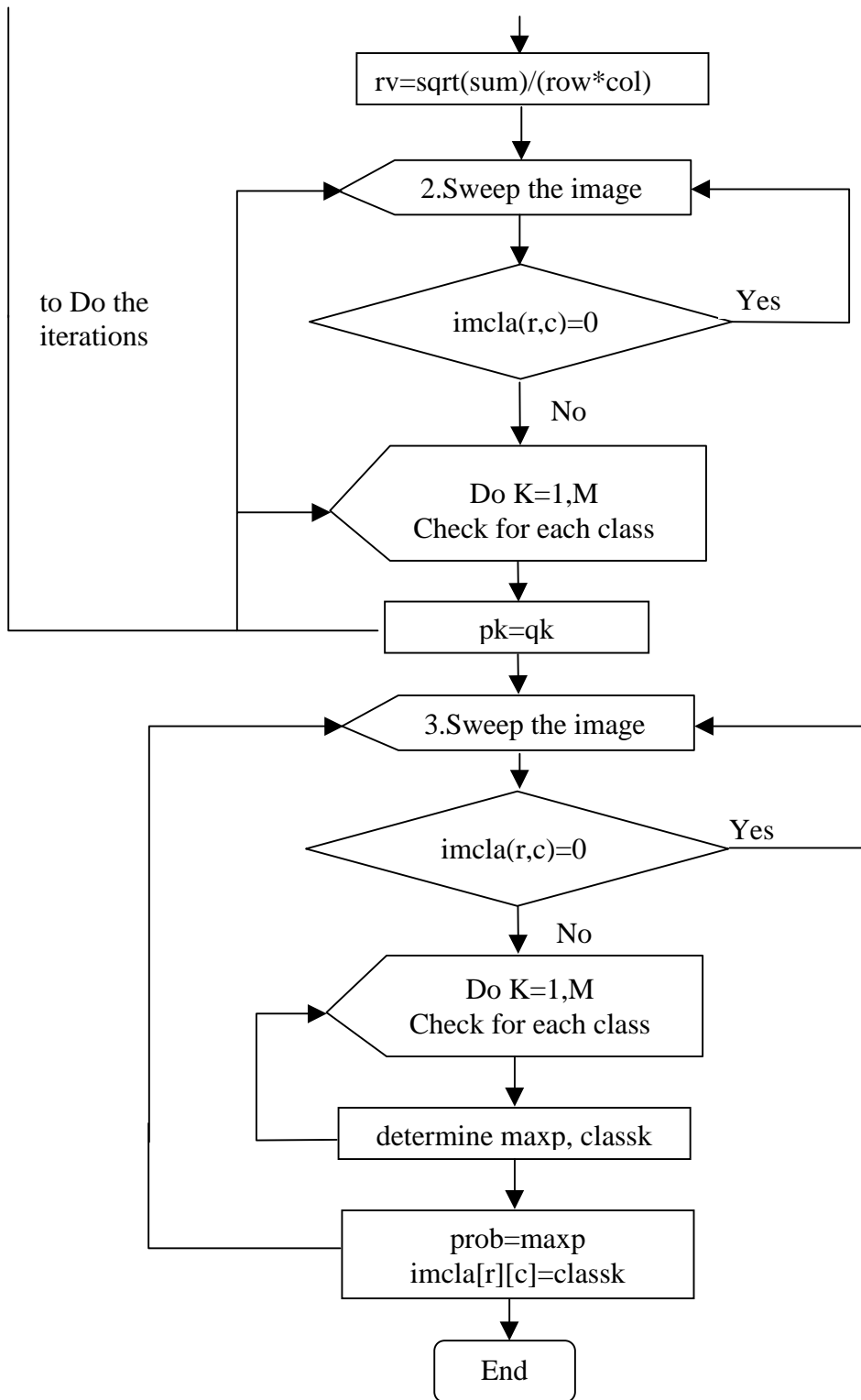


Figure 6-3 Probabilistic relaxation algorithm

6.4.2 Results

Experiment results show that after initial probabilistic relaxation, cloud, shadows, and highway tended to be overclassified. To overcome this problem, a modification of compatibility coefficients was conducted. Compatibility coefficients between cloud, shadows, and highway and each of the 36 signatures were set to zero. This means if the class of a pixel belongs to any of the classes of cloud, shadows or highway, the class probabilities of that pixel would not be influenced by the neighboring pixels in the relaxation process.

The best result was achieved after ten iterations. In cases where a pixel possesses a high class probability, there is no change in class reassignment after the relaxation. Otherwise, if a pixel has low class probabilities, its class probabilities are strongly affected by its neighboring pixels. The class of neighboring pixels may replace the class of the central pixel. The probabilistic relaxation process is computationally intensive. For the implementation of the probabilistic relaxation algorithm for a 5000×5000 pixel image each iteration takes about one hour.

A subset of the class map after probabilistic relaxation is given in Figure 6-4. A comparison of the smoothed thematic map (Figure 6-4) and the original thematic map (Figure 6-5) suggests that the probabilistic relaxation operation has resulted in a significant reduction of the "salt-and-pepper" noise appearance in the original thematic map. Furthermore, the number of mixed pixels has reduced. Consequently, regions in the image have become more homogeneous, while line elements are maintained.

It should be noted that the number of pixels of the land-use class "corn" was reduced to zero. Two factors explain this result. First, there are only very few fields of corn in the study area. This leads to a negative compatibility coefficient between corn and other signatures. Second, GML classification results contain many isolated pixels; these isolated pixels disappeared after the relaxation process.

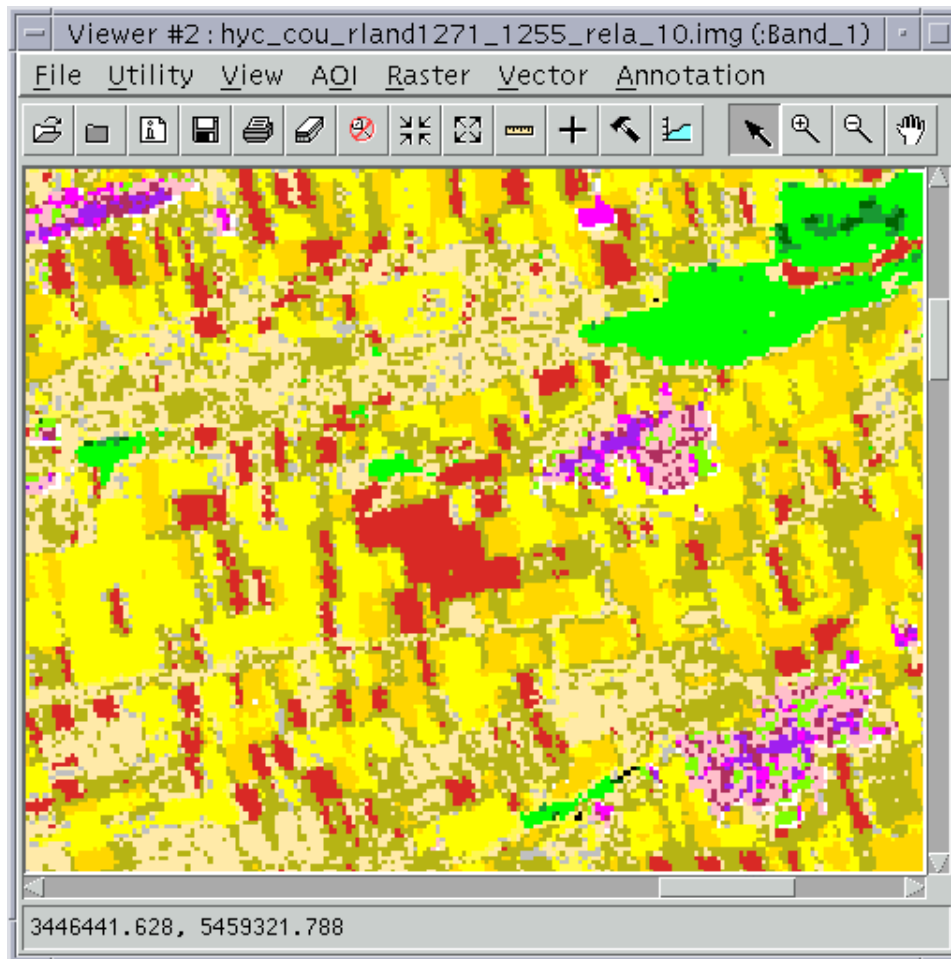


Figure 6-4 A subset of the smoothed thematic map generated by use of the probabilistic relaxation algorithm after 10 iterations

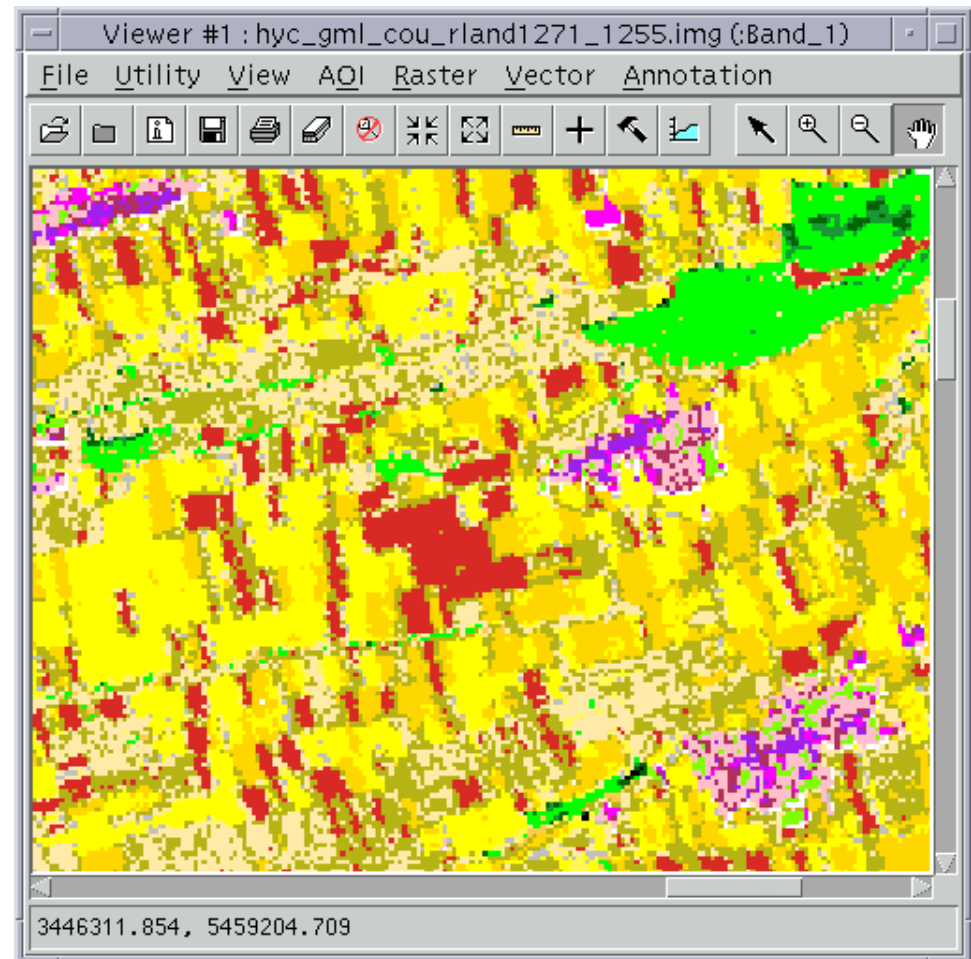


Figure 6-5 A subset of the original thematic map

Chapter 7 Edge Extraction from IRS-1C PAN Imagery Data

7.1 Edge Extraction and Image Classification

Digital image classification results in a thematic (or class) map in which each pixel is assigned a class label. A main defect of the resultant thematic map is that the inter-class boundaries are often blurred, i.e. weakly defined interregion boundaries (Solaiman et al 1998).

The lack of sharp inter-class boundaries in the classified image is a result of the inadequate ground resolution of the multispectral imagery data. In an IRS-1C multispectral image, a pixel footprint is of the order of 23 m for LISS-III. Boundary pixels often contain a variety of small-scale land-use types, leading to impure spectral information. This also makes the classification of boundary pixels extremely difficult and often results in classification errors.

A good strategy to produce sharp inter-class boundaries and reduce classification errors in boundary regions is to extract edge elements from the IRS-1C PAN image and then fuse the detected edge map and the thematic map. This idea makes good sense because the panchromatic imagery data has a much higher spatial resolution of 5.8 m compared to the 23-m ground resolution of the multispectral image. Making fuller use of the high-resolution feature of the PAN imagery data can help generate sharp interregion boundaries and reduce mixed pixels appeared in the transitional areas of land-use types.

The generation of a boundary map is usually conducted in three steps. First, edge elements are extracted from the PAN image. Second, the extracted thick edges are then thinned. Third, in cases where broken edges may affect further image classification operation, edge-linking algorithms are implemented.

An edge image normally shows each object outlined edge points, but these seldom form the closed, connected boundaries that are required for image segmentation. Thus,

another step is required before extraction of object is complete. Edge point linking is the process of associating nearby edge points so as to create a closed, connected boundary. This process fills the gaps left by noise and shading effects (Castleman 1996).

As the edge detector and edge-thinning algorithm used in this study have produced a pixel-width contour map with reasonably good connectedness, edge-linking operation has not been implemented in this study. The following three sections describes the techniques and procedures used for extracting connected and sharp region boundaries from the high-resolution panchromatic imagery data.

7.2 Edge Detection Operators

7.2.1 Edge detection

The first step in edge map generation is edge extraction. Edges are a basic image feature. An edge is considered as the border between two homogeneous image regions that have different illumination intensities (Pitas 1993). Edge detection is a useful approach to establishing the boundaries of the objects in an image. Edge detection results in an edge image.

Edges carry useful information about object boundaries that can be used for image analysis, object identification and image filtering applications. Detecting edge within an image may be sufficient in itself to classify the entire image or it may have to be used in combination with other features as part of a classification rule (James 1987; Pal and Pal 1993; Deng and Iyengar 1996).

An image in which gray level reflects how strongly each corresponding pixel meets the requirements of an edge pixel is called an edge image or edge map. This can also be displayed as a binary edge image showing only the location of the edge points. An image that encodes the direction of the edge, is a directional edge image.

Edge detectors are used to find edge segments. Edges are extracted on the basis of local variations of illumination. If a pixel falls on the boundary of an object in an image, then its neighborhood will be a zone of gray-level transition. The slope and direction of that transition are two principle characteristics. These are the magnitude and direction of the gradient vector respectively.

Edge detection operators examine each pixel neighborhood and quantify the slope, and often the direction as well, of the gray-level transition. There are several ways to do this, most of which are based on convolution with a set of directional derivative masks.

Several edge detectors have been proposed in the literature (Ballard and Brown 1982; Gonzalez and Wintz 1987; James 1987; Jain 1989; Richards 1994; ERDAS Field Guide 1997). Usually, edge detectors use first- or second-order derivatives.

7.2.2 Edge detection using first-order derivatives

The image gradient $\nabla f(x, y)$:

$$\nabla f(x, y) = [\partial f / \partial x \quad \partial f / \partial y]^T \triangleq [f_x \quad f_y]^T \quad (7.1)$$

provides useful information about local intensity variations.

Its magnitude $e(x, y)$:

$$e(x, y) = \sqrt{f_x^2(x, y) + f_y^2(x, y)} \quad (7.2)$$

can be used as an edge detector.

Local edge direction can be described by the direction angle:

$$\phi(x, y) = \arctan(f_y / f_x) \quad (7.3)$$

The direction of the gradient is usually of interest only in contouring applications or in determining aspect in digital terrain models (Richards 1994).

Gradient estimates can be obtained by using gradient operators of the form:

$$\hat{f}_x = W_1^T X \quad (7.4)$$

$$\hat{f}_y = W_2^T X \quad (7.5)$$

where:

- X : the vector containing image pixels in a local image neighborhood;
- W_1, W_2 : weight vectors that are described by gradient masks.

Such masks are shown in Figure 7-1 for the Prewitt and Sobel edge detectors respectively. Relations (7.4 - 7.5) are essentially two-dimensional linear convolutions with the 3×3 kernels shown in Figure 7-1.

The Sobel edge detector provides good performance and is relatively insensitive to noise. Better noise characteristics can be achieved by using large neighborhoods at the expense of computational effort. However, large neighborhoods tend to produce thick edges.

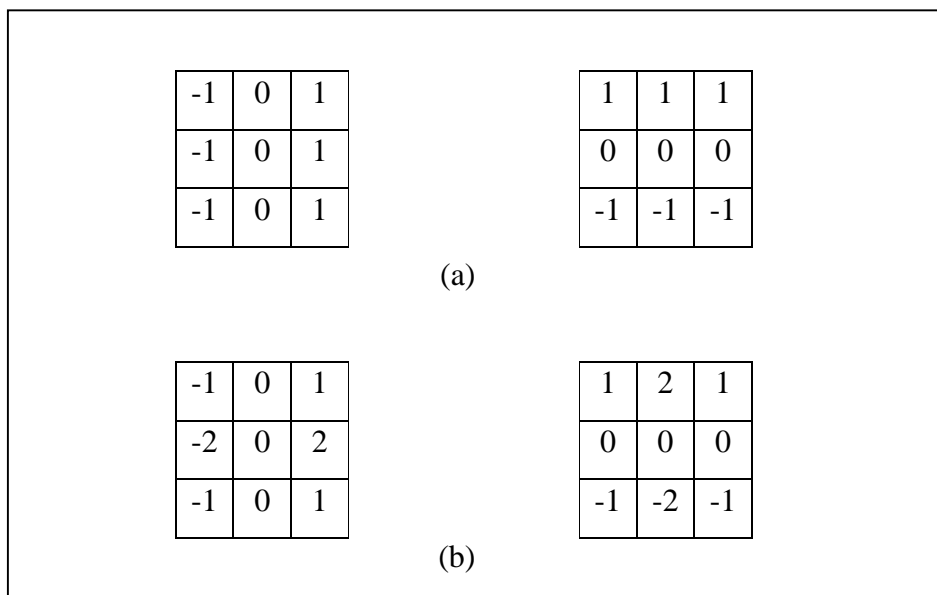


Figure 7-1 (a) Prewitt edge detector masks; (b) Sobel edge detector masks

7.2.3 Edge detection using second-order derivatives

Laplacian operator is defined in terms of the second-order partial derivatives of $f(x, y)$ with respect to x, y respectively:

$$\nabla^2 f(x, y) = \frac{\partial^2 f}{\partial x^2} + \frac{\partial^2 f}{\partial y^2} \quad (7.6)$$

The first-order derivatives have local maximum or minimum at image edges due to large local intensity changes. Therefore, the second-order derivatives have zero-crossings (e.g. transitions from positive to negative values and vice versa) at edge locations. Thus, an approach to edge detection is to estimate the Laplacian operator output and to find zero-crossing positions. An estimator of the Laplacian operator is given by:

$$\nabla^2 f(x, y) \cong f(x, y) - \frac{1}{4} [f(x, y+1) + f(x, y-1) + f(x+1, y) + f(x-1, y)] \quad (7.7)$$

Differentiation is a high pass operation. Thus, second-order differentiation tends to enhance image noise. The Laplacian operator creates false edges, especially in areas where the image variance is small, because small intensity perturbations (noise) tend to produce false zero-crossings only.

7.2.4 Texture boundary locator (TBL)

The TBL method was proposed by Bhanu et al (1997). Texture gradients are obtained by use of a texture boundary locator (TBL) algorithm. The TBL algorithm is described below.

For most regions in natural scenes, it has been observed that on either side of the boundary between two adjacent regions there occurs gradual transition from the mean of the image intensities of one of the regions to that of its neighbor. The TBL

algorithm calculates the texture gradient of an image, which is the local rate of change of a texture attribute of the image.

The textural attribute is derived from the mean μ and standard deviation σ of each $N \times N$ window of the image, where N is obtained as a function of the image features to be detected. The sole requirement imposed on the gradient image is that it should have a large magnitude wherever major discontinuities occur.

In order to compute a texture gradient image, a $(2K + 1) \times (2K + 1)$ window is centered at each pixel, where K is a function of the size of the region of interest and/or the range of the scene objects from the sensor. The window geometry for an arbitrary image plane location P is showed in Figure 7-2.

The pixels at the centers of the four sides and the corners of the $(2K + 1) \times (2K + 1)$ window are labeled sequentially beginning at the top left corner as shown in the figure.

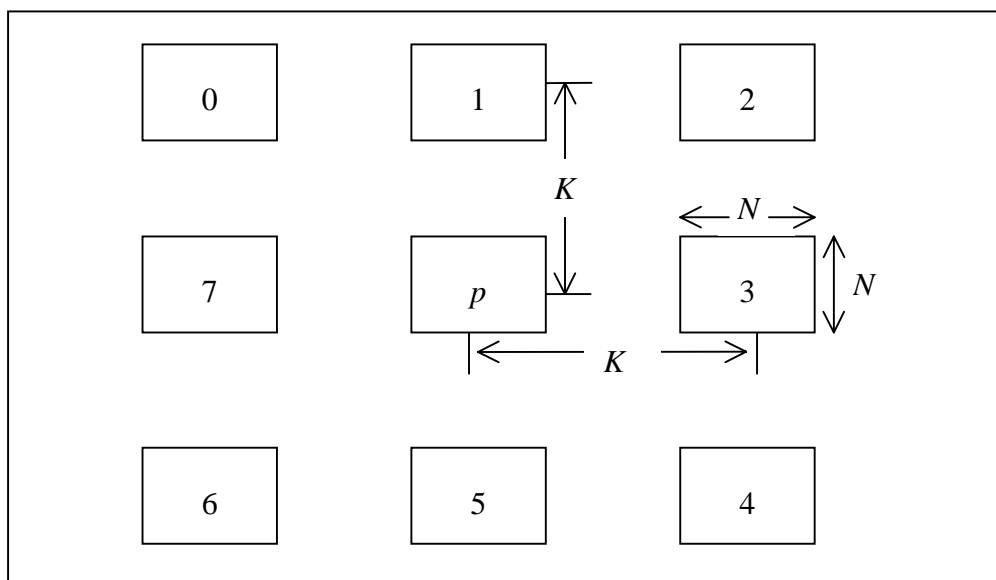


Figure 7-2 Window geometry for the texture boundary locator (TBL) algorithm (Source: Bhanu et al 1997)

The texture gradient at a pixel is obtained as:

$$\max_{0 \leq i \leq 3} \{(\mu_i - \mu_{i+1})^2 + (\sigma_i - \sigma_{i+4})^2\}^{1/2} \quad (7.8)$$

where:

μ_i and σ_i are the mean and the standard deviation of the image's intensities for an $N \times N$ window.

In the literature, it was reported that the edge images produced by the edge operators discussed above appear visually similar (Bhanu et al 1997). The Roberts operator, being two by two, responds best on sharp transitions in low-noise images. The other operators, being three by three, handle more gradual transitions and noisier images better. Normally, for the two-mask edge detectors, the larger magnitude is taken as the output value. This makes them somewhat sensitive to the orientation of the edge. The Sobel and Prewitt three-by-three edge operators can be generalized to eight orientations.

7.3 Edge Thresholding

Edge detectors produce a greyscale output image $e(k,l)$. This image carries information about the edge magnitude. If the edge detector output is large, a local edge is present. Otherwise, this pixel location corresponds to background. Therefore, a threshold operation is required after edge detection:

$$E(k,l) = \begin{cases} 1 & \text{if } e(k,l) \geq T \\ 0 & \text{otherwise} \end{cases} \quad (7.9)$$

The output of the thresholding is a binary image. Thresholding (7.9) is global because T is chosen based on global information and (7.9) is applied to the entire image.

The selection of thresholds is crucial to the output of edge detection procedure. This is because the edge detector output usually has regions possessing different statistical

properties. If the threshold is chosen too low, spurious region boundaries (thick edges) will appear alongside true ones in the resultant region boundary image. On the other hand, a high threshold value will cause pixels to be missing (e.g. thin or broken edges) from the region boundaries. The most simple threshold selection algorithm is the histogram method. Other schemes for fixing the threshold generally depend on some special property of the class of images being processed. Adaptive thresholding often is taken as a solution to this (Chow and Kaneko 1972; Nakagawa and Rosenfeld 1979; Yanowitz and Bruckstein 1989). But adaptive thresholding can not eliminate the problem of threshold selection (Pal and Pal 1993). A good strategy to produce meaningful segments would be to fuse region segmentation results and edge outputs (Yokoya and Levine 1989; Al-Hujazi and Sood 1990).

The histogram method was used in this study. In this method, the threshold is not absolute threshold for image intensities, but is upper percentage threshold for the cumulative distribution function of the accumulated texture gradient image's histogram. The threshold T can be chosen by inspecting the edge detector output histogram, so that only a small percentage of the pixels $e(k,l)$ above it.

The cumulative distribution function of an image's histogram is evaluated by deriving the image's histogram, normalising the histogram by the total number of pixels of the image and then integrating the normalised histogram bin counts from the lowest intensity value of the image. Three thresholds at the upper 15, 25, and 35% are found to be sufficient to define the true region boundaries. The use of a greater number of thresholds did not improve the quality of the detected boundaries significantly (Bhanu et al 1997).

7.4 Thinning of Binary Edge Images

The edge detection and thresholding operation produces a binary image that has 1s at edge locations. This binary image is called edge map or edge image. An edge image usually has thick edges and, therefore, must be thinned to produce sharp edges.

Thinning or skeletonization of binary images is generally considered as the process of iterative removal of contour pixels that are neither essential for preserving the connectivity or topology of the image, nor representative of any significant features of the figure (Govindan and Shivaprasad 1987). Edge-thinning operations enable large reductions in memory storage and data processing. Edge thinning has found many applications in areas like fingerprint classification, recognition of hand-written and printed characters, computer aided design, automated cartography, and facsimile transmission (Bhattacharya and Lu 1997).

The technique of thinning is used in many pattern recognition systems as a preprocessing step to represent the abstract nature of an object and investigate its geometric and topological properties. Various sequential, parallel, hybrid and other thinning algorithms are proposed in the literature.

Blum (1964) first defined a simple thinning procedure and called it the medial axis transformation (MAT). He also used the term skeleton as a synonym for medial axis. Persoon and Fu (1977) proposed a skeletonization method using Fourier descriptors. Naccache and Shinghal (1984) compared 14 existing algorithms and suggested a new algorithm. A comprehensive review of existing thinning algorithms can be found in Lam et al (1992).

A sequential thinning algorithm performs the pixel-removal work pixel by pixel in the image plane, and the removal decision depends on the result obtained so far in the current iteration as well as those of the previous iterations. A parallel thinning algorithm, on the other hand, processes all the pixels of the image simultaneously, and the removal decision depends only on the result of the previous iterations (Wu and Tsai 1992).

Ideally, a thinning algorithm should produce a connected skeleton with a structure of unit thickness. There are however several problems in the thinning process (Shinji 1983). Examples include:

- The phenomenon of shrinking medical lines,
- The subtle changes on the border of a pattern may yield noisy branches or affect the positions of medial lines.

- Two distinct branching points may result from thinning crossing lines, and the neighborhood of a branching point may result in Y-shape distortion.

A good thinning algorithm should have the following characteristics (Wu and Tsai 1992):

- (1) It should preserve the connectivity of the object shape;
- (2) It should not produce excessive erosion;
- (3) It should be noise insensitive; and
- (4) It should produce a good representation of the original shape.

The fast parallel algorithm proposed by Chen and Hsu (1988) is a modified version of the Zhang-Suen algorithm (1984). The Chen-Hsu algorithm preserves the original merits such as the contour noise immunity and good effect in thinning crossing lines; and overcomes the original demerits such as the serious shrinking and line connectivity problems from the standpoint of 8-neighbor connectivity. As a table is established for the thinning criteria in this method, only one pass is needed by table mapping to decide whether a pixel is deleted or not. The problem of efficiency is reduced to the number of iterations instead of the algorithm complexity.

A binary image is defined by a matrix IT where each pixel $IT(i, j)$ is either 1 or 0. The pattern consists of those pixels that have value 1. A 3×3 window is used in the Chen-Hsu algorithm (Figure 7-3). The new value of pixel $P(i, j)$ at the n -th iteration depends on its own value as well as those of its eight neighboring pixels at the $(n-1)$ -th iteration, so that all image elements can be processed simultaneously.

P7 (i-1, j-1)	P0 (i-1, j)	P1 (i-1, j+1)
P6 (i, j-1)	P (i, j)	P2 (i, j+1)
P5 (i+1, j-1)	P4 (i+1, j)	P3 (i+1, j+1)

Figure 7-3 The 3×3 neighborhood of the pixel $P(i, j)$

The thinning process is divided into two sub-cycles. Cycle 1 will be executed at odd iterations while cycle 2 will be executed at even iterations.

The test conditions for cycle 1 are shown in Figure 7-4.

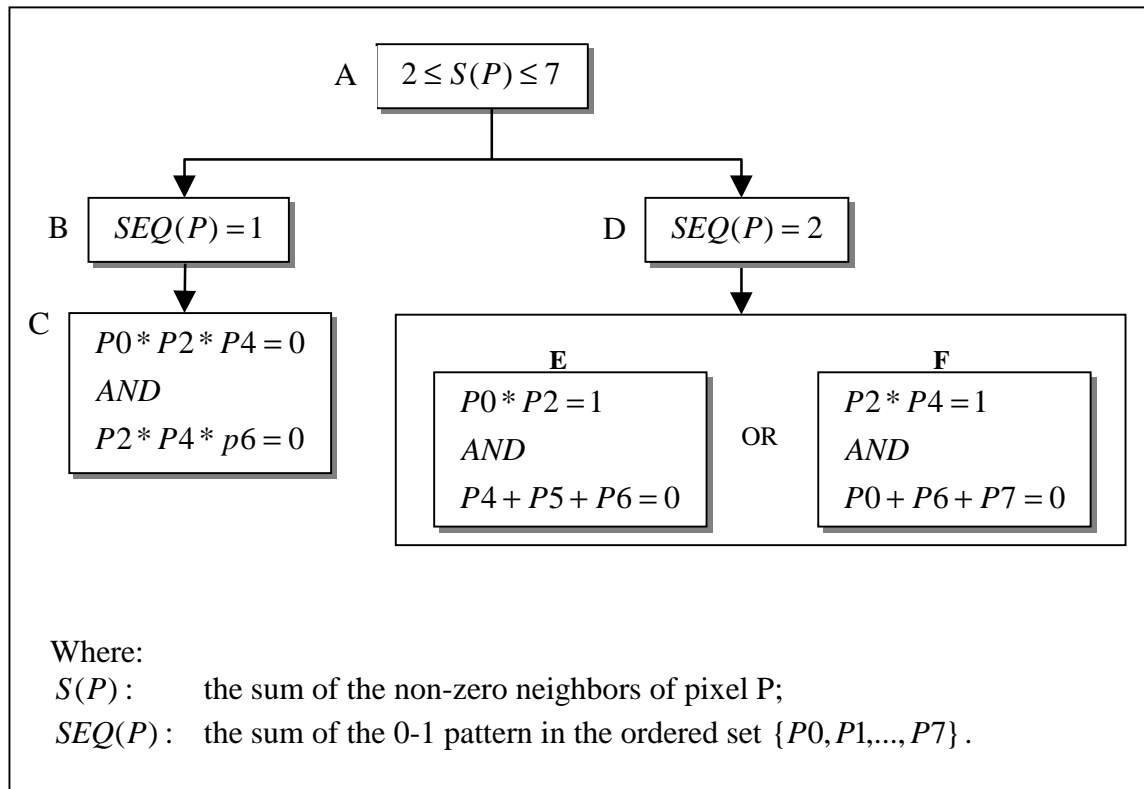


Figure 7-4 The flow of cycle 1 of the Chen-Hsu algorithm

The flow of cycle 1 is described as follows:

- If condition A is satisfied, $SEQ(P)$ will be checked, otherwise, pixel remains unchanged;
- If condition B is satisfied, then condition C will be checked. If condition D is satisfied, then condition E or F will be checked. If both condition B and D fail, then pixel P remains unchanged;
- If condition C is satisfied, then pixel P will be deleted. Otherwise it remains unchanged;
- If either condition E or F is satisfied, then pixel P is deleted. Otherwise, it remains unchanged.

The test conditions of cycle 2 are shown in Figure 7-5. The execution steps of cycle 2 is exactly the same as that for cycle 1.

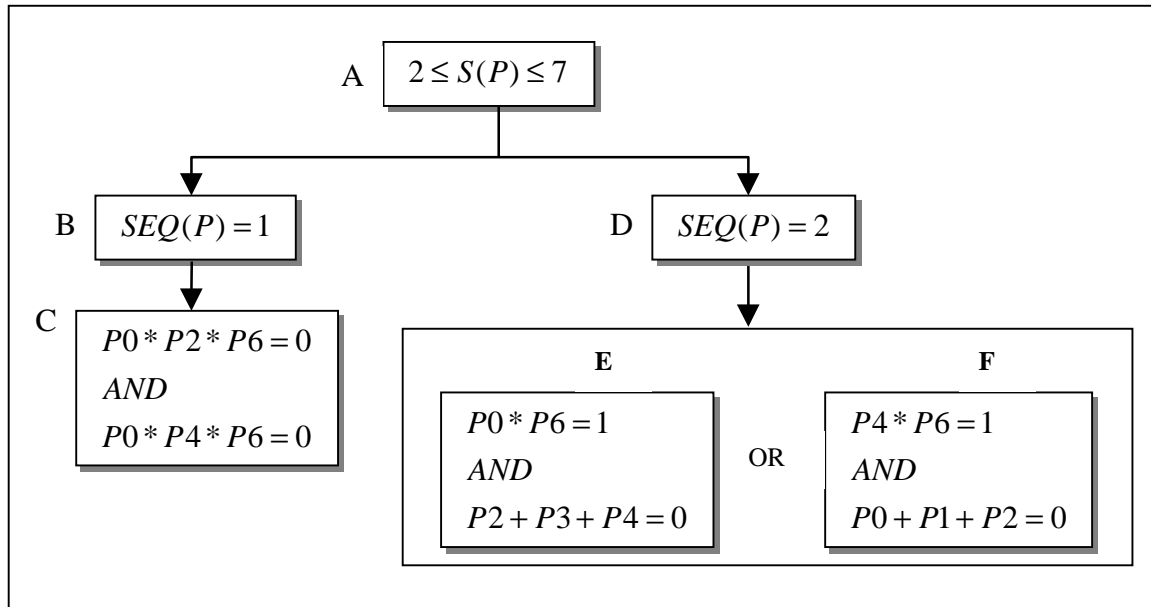


Figure 7-5 The flow of cycle 2 of the Chen-Hsu algorithm

7.5 Implementation and Results

7.5.1 Generation of edge map

The generation of edge map was conducted in two steps.

The first step is the implementation of edge detection algorithms. Sobel, Prewitt and TBL edge detectors were tested. It was found that the TBL edge detector provides pretty good results and is relatively robust to noise. Therefore, the TBL edge detector was used for the extraction of edge elements form the IRS-1C PAN image.

The second step is edge thresholding. The edges generated by the TBL algorithm were thresholded by using histogram thresholding method. Testing results suggest that the selection of the threshold is very crucial, because low intensity variation may

correspond to edges of interest in some part of the image, while high intensity variation appears in other part.

The programs for the TBL algorithm and the histogram thresholding algorithm were written using C. These two algorithms were conducted together. The following combinations of parameters $K = 1, 2, 3$; $N = 3, 5, 7$; $T = 15, 25$, and 35% were tested. Figures 7-6-1, 7-6-2 and 7-6-3 present a series of edge maps of various K , N , and T combinations.

As can be seen in Figures 7-6-1, 7-6-2 and 7-6-3, thick edges and not connected edge segments are two main problems with this edge detector. Thus these edges must be thinned to produce unit width edges; this is done in the following section.

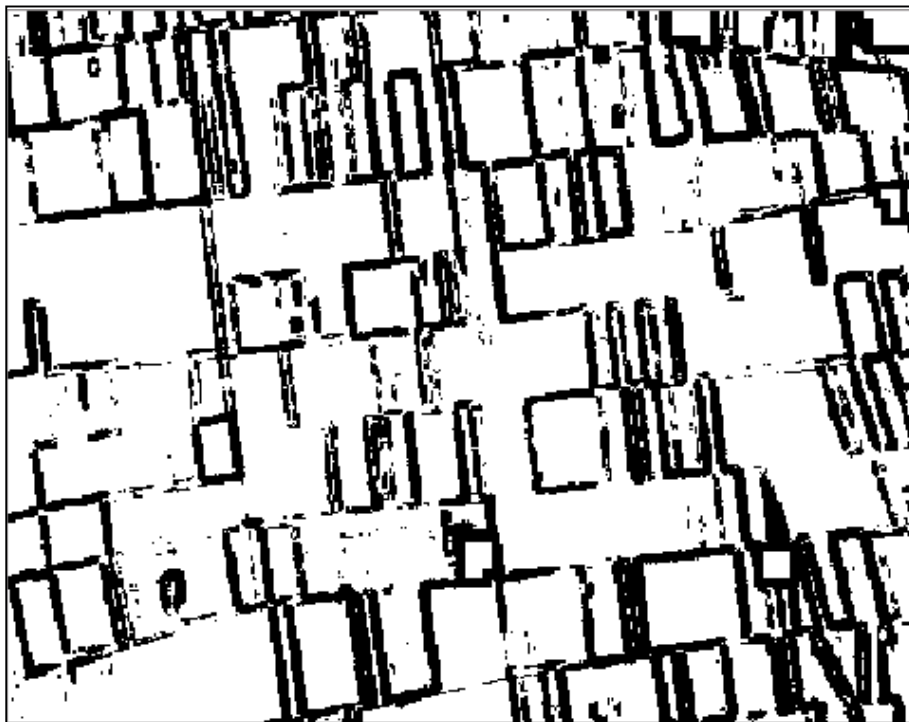


Figure 7-6-1 Result of TBL algorithm: $K = 1, N = 3, T = 10\%$



Figure 7-6-2 Result of TBL algorithm: $K = 1$, $N = 3$, $T = 15\%$

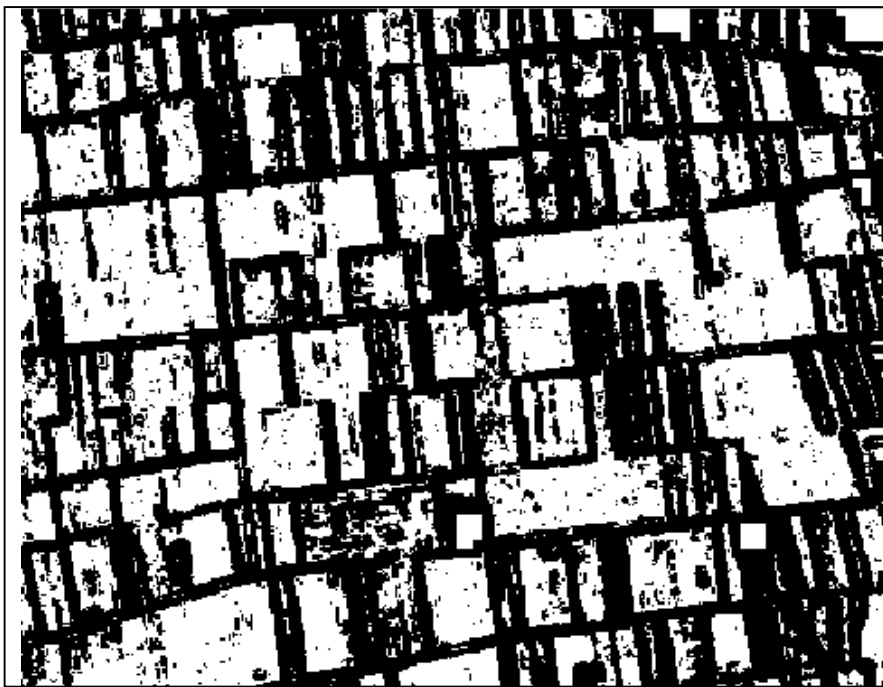


Figure 7-6-3 Result of TBL algorithm: $K = 1$, $N = 3$, $T = 20\%$

7.5.2 Generation of pixel-width contour map

The fast parallel thinning algorithm proposed by Chen and Hsu (1988) was performed on the thick edge maps. The operation of this algorithm resulted in a pixel-width contour map. Figures 7-7-1, 7-7-2 and 7-7-3 present the thinned edge maps that correspond to the thick edge maps displayed in Figures 7-6-1, 7-6-2 and 7-6-3. As can be seen in Figure 7-7-1, 7-7-2 and 7-7-3, the Chen-Hsu algorithm performed pretty well as it preserved the 8-neighbor connectivity and generated many closed contours.



Figure 7-7-1 Result of Chen-Hsu algorithm: $K = 1$, $N = 3$, $T = 10\%$



Figure 7-7-2 Result of Chen-Hsu algorithm: $K = 1$, $N = 3$, $T = 15\%$



Figure 7-7-3 Result of Chen-Hsu algorithm: $K = 1$, $N = 3$, $T = 20\%$

Testing results show that the fast parallel thinning algorithm yielded the best result of contour map with the combination of $K = 1$, $N = 3$ and $T = 15\%$.

As seen in Figures 7-7-1, 7-7-2 and 7-7-3, there are a lot of speckle noises. These noises have been reduced significantly by using Lee-Sigma filter (Figure 7-8). Lee-Sigma filter uses the average of all pixel values within the moving window that fall within the designated range of standard deviations.



Figure 7-8 Contour map after using Lee-Sigma filter

Figure 7-9 shows an example of an asphalt road. An example of a field pathway is presented in Figure 7-10. Both of these roads could be good detected, though the field pathway is narrow.



Figure 7-9 Asphalt road



Figure 7-10 Field pathway

Chapter 8 Fusion of Thematic Map and Edge Map Using Region-Growing Algorithm

8.1 The Basic Concept

In real remote sensing applications, the thematic map obtained from conventional statistical classifiers such as the Gaussian Maximum Likelihood classification is often very noisy and has weakly defined boundaries between different classes on the image. To overcome these defects, many approaches have been developed. Information fusion is one of the often used methods.

For image segmentation, the importance of data integration from different algorithmic processes has been stressed by several authors (Pavlidis and Liow 1990; Gambotto 1993). Due to noise and other factors, neither region segmentation nor edge detection provides perfect information. Therefore, a good strategy to produce meaningful segments is to fuse region segmentation results and edge outputs (Yokoya and Levine 1989; Al-Hujazi and Sood 1990; Pal and Pal 1993).

Haralick and Shapiro (1985) present a method that combines the thematic map with the edge map. The resulting thematic map has all the contour pixels set to zero, and the noncontour pixels are identified by their class code, as in the original thematic map. Other examples of integrating region growing and edge detection include Pavlidis and Liow (1990) and Gambotto (1993).

A key feature of the image data used in this study is that the IRS-1C panchromatic imagery data has a spatial resolution of 5.8 m, which is much higher than the 23 m resolution of the IRS-C multispectral imagery data. As shown in Figure 7-8, the extraction of edge elements from the IRS-1C PAN image produced very satisfactory results. Due to the high-resolution feature of the IRS-1C PAN data, the edge extraction operation has not only detected very fine edges, but has also succeeded in closing most of the edges. After checking with the rectified panchromatic image it was

found that the obtained edge map corresponds quite well to the ground truth (Figure 8-1).

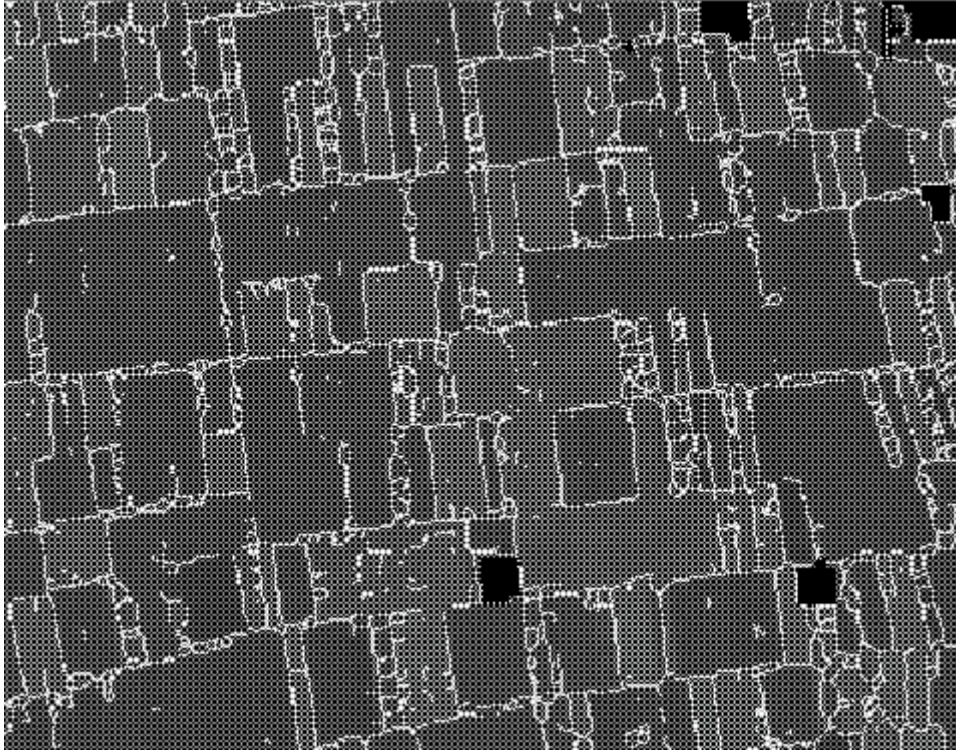


Figure 8-1 A subset of an overlay of the contour map with the rectified PAN image

This chapter presents a method for integrating the land-use classification map and the edge map. The purpose of this information fusion operation is to construct homogeneous regions over the noisy thematic map. This operation makes good sense because adding detailed and reliable edge information to the noisy land-use classification map can generate sharp interregion boundaries and reduce mixed pixels between interregion boundaries.

The fusion of the land-use classification map and the edge map is achieved by using a region-growing technique. The image data used in this fusion operation include the thematic map obtained from the Gaussian Maximum Likelihood algorithm, the

smoothed thematic map obtained from the probabilistic relaxation algorithm and the contour map resulted from edge extraction procedure (Figure 8-2).

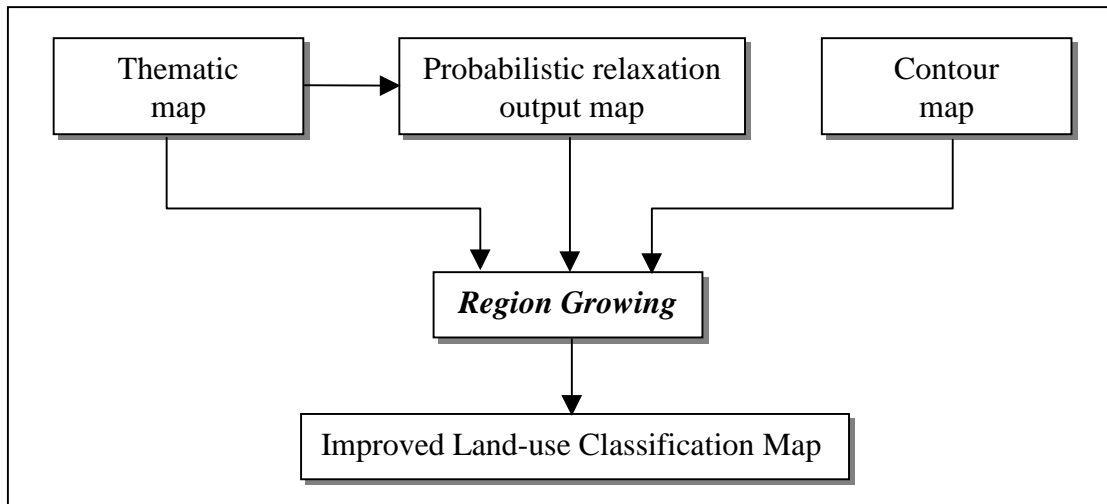


Figure 8-2 Information fusion procedure: the region-growing approach is applied over the thematic map and constrained by the contour map and the smoothed map

8.2 Region-growing Algorithms

A region in an image is a group of connected pixels with similar properties. Regions are important for the interpretation of an image because they may correspond to objects in a scene. There are two approaches to partitioning an image into regions: region-based segmentation and boundary estimation using edge detection.

Region growing is an important image segmentation approach. In the region-growing approach, all pixels that correspond to an object are grouped together and are marked to indicate that they belong to one region. Pixels are assigned to regions using some criterion that distinguishes them from the rest of the image. Region-growing techniques are useful for segmenting complex scenes using complex object definitions.

Two very important principles in segmentation are homogeneity and proximity (Jain et al 1995). Two pixels may be assigned to the same region if they have similar

intensity characteristics or if they are close to one another. For example, a specific measure of value similarity between two pixels is the difference between the gray values, and a specific measure of spatial proximity is Euclidean distance. The variance of gray values in a region and the compactness of a region can also be used as measures of value similarity and spatial proximity of pixels within a region, respectively.

Region growing process is iterated by alternately recomputing the object membership properties for the enlarged regions and then dissolving weak boundaries. Region-growing algorithms are computationally more expensive than the simpler techniques, but region growing is able to utilize several image properties directly and simultaneously in determining the final boundary location. The region-growing approach shows the greatest promise in the segmentation of natural scenes, where strong *a priori* knowledge is not available.

Many region-growing techniques are proposed in the literature. For example, Haralick and Shapiro (1992) describe three often used region-growing schemes: single-linkage region growing, hybrid-linkage region growing, centroid-linkage region growing.

Pitas (1993) described an efficient region-growing algorithm. This approach starts from some pixels (seeds) representing distinct image regions and grows them, until they cover the entire image. The pixel seeds are usually chosen by the user in a supervised mode. At least one seed, S_i , $i = 1, \dots, N$, per image region R_i is chosen. Two rules are needed for implementing region growing, i.e., a rule describing a growth mechanism and a rule checking the homogeneity of the regions after each growth step. The growth mechanism is simple: at each stage (k) and for each region $R_i^{(k)}$, $i = 1, \dots, N$, it will be checked if there are unclassified pixels in the 8-neighborhood of each pixel of the region border. Before assigning such a pixel \mathbf{x} to a region $R_i^{(k)}$, it will be checked if the region homogeneity:

$$P(R_i^{(k)} \cup \{\mathbf{x}\}) = \text{TRUE}$$

is still valid.

8.3 Implementation and Results

8.3.1 A modified region-growing algorithm

In this study, a modified region-growing algorithm that was described by Pitas (1993) was developed. The modified algorithm is conducted in three steps.

First, automatic searching of seed pixels. When the whole image is scanned, a seed pixel is the first non-contour pixel that follows directly a contour pixel.

Second, performing region growing, resulting in connected homogeneous regions. Region growing algorithm starts with a seed pixel, and performs region growing in a 4-neighborhood for edge elements and an 8-neighborhood for non-edge elements. Two conditions are used in checking the homogeneity of the regions: 1) a contour on the edge map is reached and 2) a class change on the smoothed thematic map occurred. In other words, the algorithm makes "seed" regions grow until reaching a closed contour on the edge map or a class change on the smoothed thematic map.

Third, assigning the winning class to all pixels of each connected homogeneous region. The majority class of the connected region is first calculated. This class is defined as the winning class, and then is assigned to all pixels in the homogeneous region.

These three steps are repeated until all pixels in the image have a class label. The output of this operation is a map of homogeneous region and sharp inter-class boundaries. An image fusion program was written using C. Details of the region growing algorithm used in this study is shown in Figure 8-3.

8.3.2 Image fusion

Three knowledge sources were used in this fusion operation: 1) the original thematic map (Figure 8-4-1), 2) the smoothed thematic map (Figure 8-4-2), and 3) the contour map (Figure 8-4-3).

The improved thematic map is shown in Figure 8-4-4. As can be seen from the resulting image, important contours that have not been detected during the edge-detecting process are obtained from the relaxation thematic map in a coarse manner.

The fusion of the thematic map and the contour map provides a series of closed contours more or less corresponding to individual fields and containing a unique class. The benefit of this postprocessing approach is evident when it separates into two distinct fields what previously could be interpreted as a single greater field.

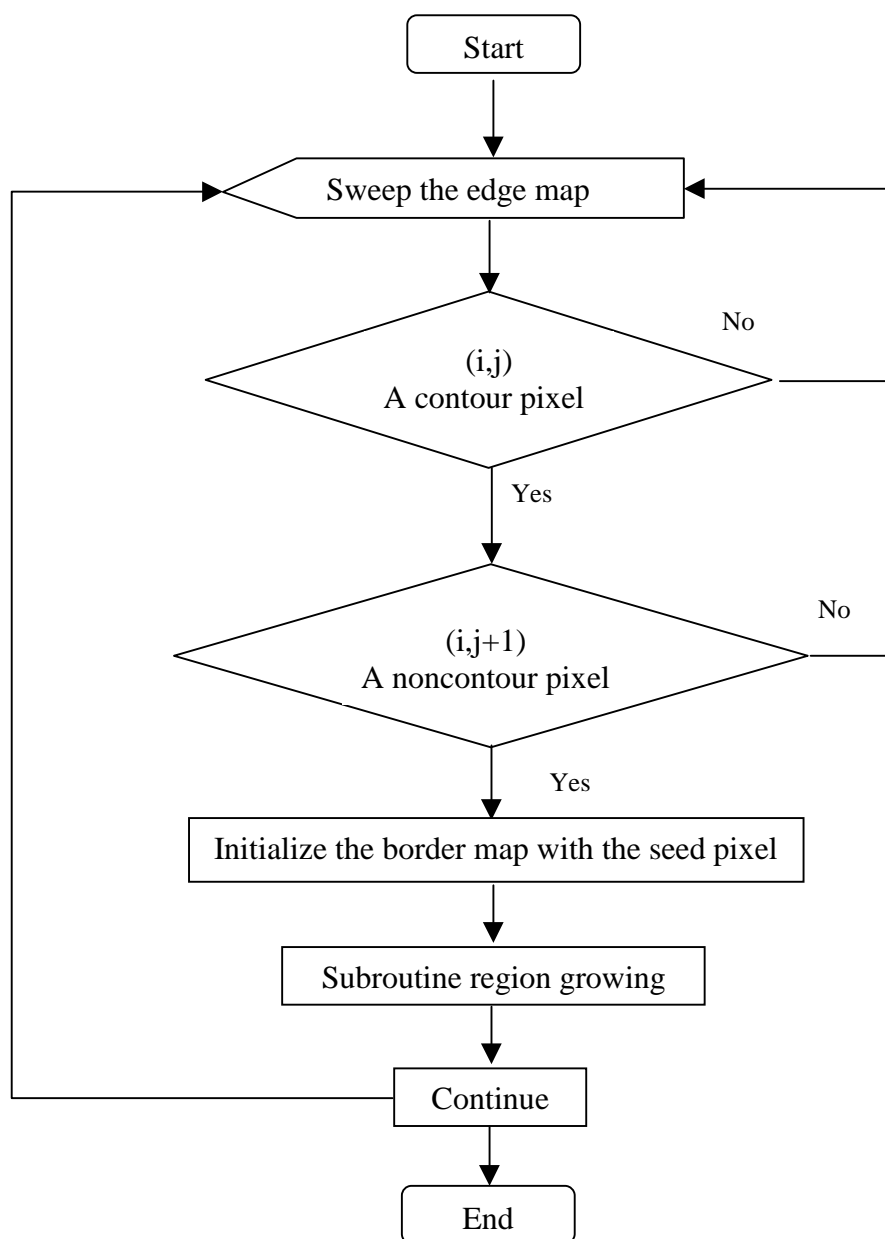


Figure 8-3-1 Fusion algorithm for the thematic map, contour map, and relaxed map

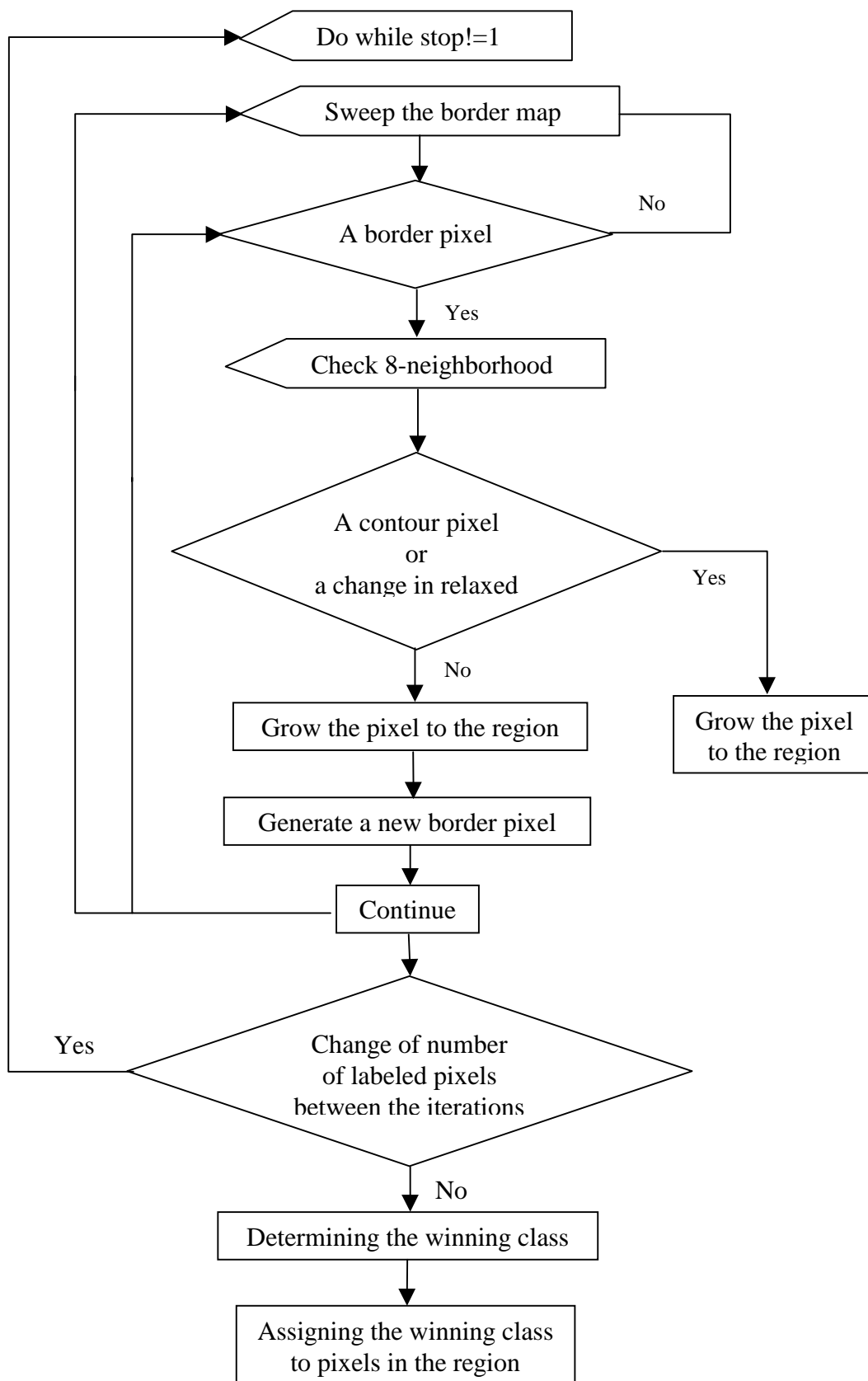


Figure 8-3-2 Subroutine region growing

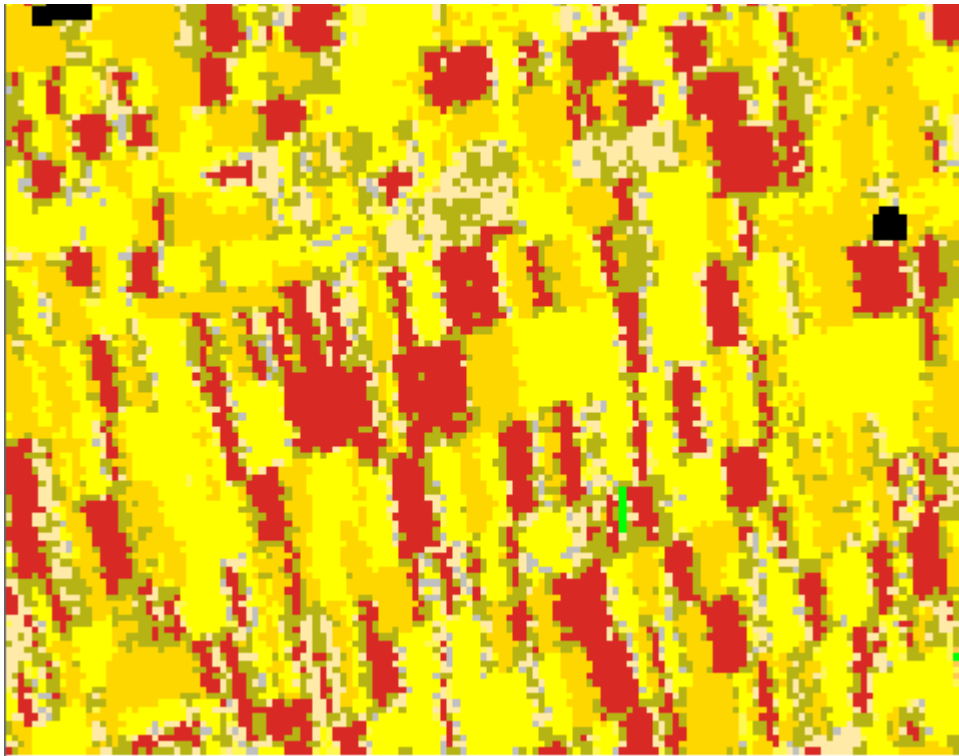


Figure 8-4-1 A subset of the original thematic map

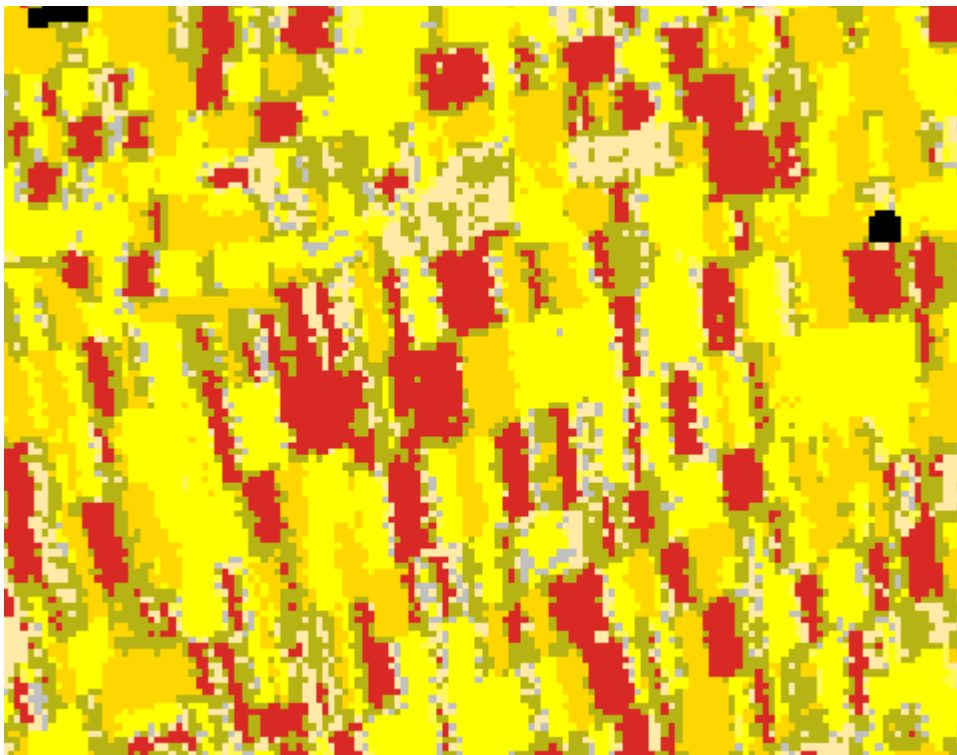


Figure 8-4-2 A subset of the smoothed map



Figure 8-4-3 A subset of the contour map

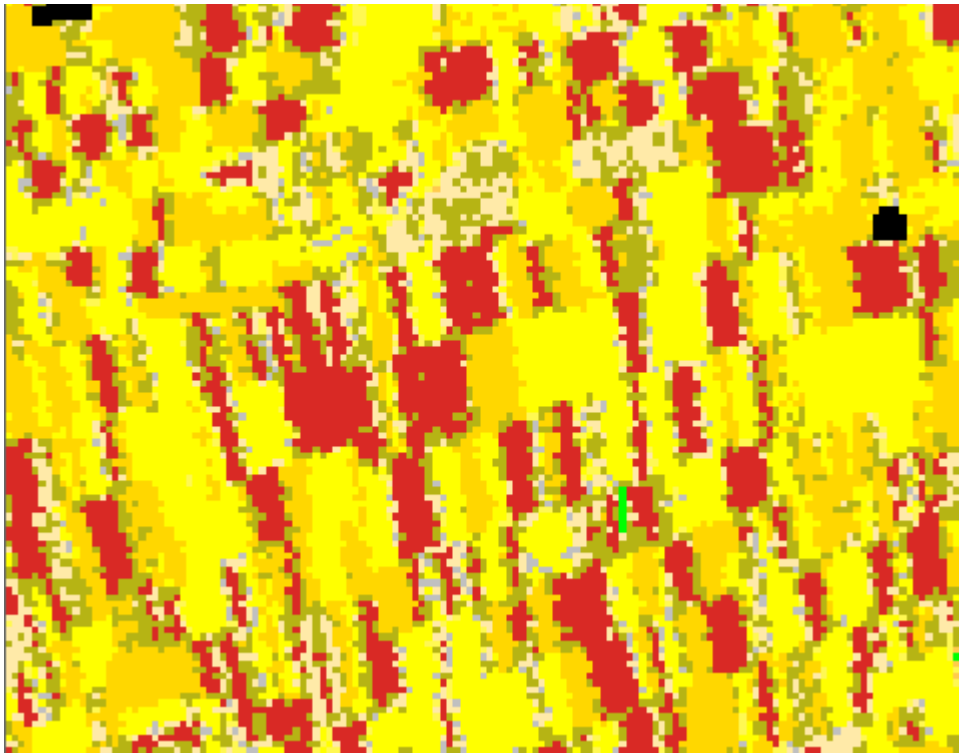


Figure 8-4-4 Improved thematic map by fusion of the thematic map, contour map and smoothed map

Chapter 9 Summary

In this study, we presented a new approach for the extraction and representation of land-use information based on high-resolution IRS-1C imagery data. A key feature of the proposed method is the combined use of spectral and contextual classification techniques.

The integration scheme involves a hybrid spectral classification algorithm combining Gaussian Maximum Likelihood classification and ISODATA clustering, probabilistic relaxation, extraction of pixel-width edge elements to obtain robust region boundaries, and postprocessing information fusion by use of region-growing techniques. These techniques are integrated in a way such that they work in a cooperative and complimentary manner.

Achieving more detailed and reliable land-use information by making fuller use of the enhanced spatial information content of the 5.8-m ground resolution IRS-1C PAN imagery is a major focus of this study. To achieve this objective, this study has incorporated a great deal of recent methodological development in such fields as computer vision, pattern recognition, image understanding, GIS, as well as satellite image processing.

The main techniques used and the results obtained in this study are summarized as follows.

- 1) In the preprocessing stage, GPS techniques were used to rectify IRS-1C PAN image. The total RMS error is 1.14 pixels, which corresponds to about 6.6m on the ground. This result suggests that the use of DGPS has significantly improved the accuracy of image rectification. The rectified PAN image was then used as a reference image for the rectification of multispectral IRS-1C images, which was done by use of the "image-to-image" registration method.
- 2) IHS and PCS methods were employed for merging the IRS-1C PAN and multispectral images. The resultant merge images show that the IHS method produced better color environment and more spatial details.

- 3) A GIS layer – ATKIS data – was used to separate urban and rural areas. This knowledge-based image segmentation resulted in two coarse homogeneous regions, which provide two separate data sets for the subsequent land-use classification operations. The separation of urban and agricultural areas proved to be useful for fixing the confusing pixel problem, that is, reducing potential misclassifications of urban and agricultural land-use types.
- 4) For the classification of land-use types in the study area, a three-level, hierarchical land-use classification system was designed. For the rural areas, a total number of 400 training samples were selected. A signature file containing 36 signatures was constructed.
- 5) Parallelepiped, Minimum Distance, Mahalanobis Distance, and Maximum Likelihood/Bayesian algorithms and ISODATA methods were performed on the three bands of LISS-III imagery data of the agriculture file. It was found that for the agricultural file, the hybrid method combining ISODATA clustering and the Maximum Likelihood/Bayesian algorithm produced the best results. Fourteen classes were extracted for the rural areas. The ISODATA clustering method was found to be suitable for the classification of urban land-use types. Five classes were extracted for the urban areas.
- 6) A probabilistic relaxation algorithm is performed on the thematic map obtained from Gaussian Maximum Likelihood classification operation. This algorithm reclassifies image pixels according to their spatial relationship to neighboring pixels. Results show that the probabilistic relaxation operation has resulted in a significant reduction of the "salt-and-pepper" noise appearance in the original thematic map. Furthermore, the number of mixed pixels has reduced. Consequently, regions in the image have become more homogeneous while line elements are maintained.
- 7) Image segmentation techniques that involve edge detection, edge thresholding and edge thinning were applied to the 5.8-m ground resolution IRS-1C PAN imagery to extract edge elements. Various edge operators including TBL, Sobel, Prewitt edge detectors were tested. Results show that the TBL edge detector provides

good results and is relatively robust to noise. The TBL detector and the Chen-Hsu thinning algorithm have not only produced very fine edges, but have also succeeded in closing most of the edges. After checking with the rectified panchromatic image it was found that the obtained edge map corresponds pretty well to the ground truth.

- 8) The strategy of extracting edge elements from high-resolution PAN image has proved extremely useful. It was found that the resulting edges lend robustness to the classification system against the mixture-pixel problem by capturing detailed spatial information that is not available from multispectral bands.
- 9) A modified region-growing algorithm was used for postprocessing information fusion. The purpose of this fusion operation was to construct homogeneous regions over the noisy thematic map. Three knowledge sources were used in this operation: (1) the original thematic map obtained from Gaussian Maximum Likelihood algorithm, (2) the smoothed thematic map generated from the probabilistic contextual relaxation algorithm, and (3) the contour map obtained from TBL edge detector and Chen-Hsu edge thinning algorithm.
- 10) The postprocessing image fusion strategy has proved to be particularly effective for generating sharp interclass boundaries and reducing mixed pixels between interregional boundaries. Important contours that had not been detected in the edge-detecting process were compensated from the smoothed thematic map in a coarse manner. The fusion of the thematic map and the contour map provides a series of closed contours quite closely corresponding to individual fields and containing a unique class. The benefit of this fusion method is particularly evident when it separates into two distinct fields what previously could be interpreted as a single greater field.

For the operation of the proposed method, a software package is developed using programming language C. This software package comprises the GML algorithm, a probabilistic relaxation algorithm, TBL edge detector, an edge thresholding algorithm, a fast parallel thinning algorithm, and a region-growing information fusion algorithm.

Literature

Abeyta, A.M., and J. Franklin, 1998. The Accuracy of Vegetation Stand Boundaries Derived from Image Segmentation in a Desert Environment, *Photogrammetric Engineering & Remote Sensing*, 64(1):59-66.

Achen, M., 1993. *Untersuchungen ueber Nutzungsmöglichkeiten von Satellitenbilddaten fuer eine oekologisch orientierte Stadtplanung: Am Beispiel Heidelberg*, Dissertation, Heidelberger Geographische Arbeiten, Heft 91, Universitaet Heidelberg.

Acheroy, V.L., 1998. Feature Extraction Using the Constrained Gradient, *Journal of Photogrammetry & Remote Sensing*, 53:85-94.

Al-Hujazi, E.H., and A.K. Sood, 1990. Integration of Edge and Region based Techniques for Range Image Segmentation, *SPIE, Vol. 1381, Intelligent Robots and Comput. Vision-IX: Algorithms and Techniques*, pp. 589-599.

Amadsun, M., and R.A. King, 1988. Low Level Segmentation of Multispectral Images via Agglomerative Clustering of Uniform Neighborhoods, *Pattern Recognition*, 21:261-268.

Ashton, E.A., and A. Schaum, 1998. Algorithms for the Detection of Subpixel Targets in Mutlispectral Imagery, *Photogrammetric Engineering & Remote Sensing*, 64(7):723-731.

Ballard, D.H., and C. M. Brown, 1982. *Computer Vision*, Prentice-Hall, New Jersey.

Baraldi, A., and F. Parmiggiani, 1994. A Nagao-Matsuyama Approach to High-Resolution Satellite Image Classification, *IEEE Transactions on Geoscience and Remote Sensing*, 32(4):749-758.

Bässmann, H., and P.W. Besslich, 1989. *Konturorientierte Verfahren in der digitalen Bildverarbeitung*, Springer-Verlag, Berlin.

Bernstein, R., 1983. Chapter 21: Image Geometry and Rectification, *Manual of Remote Sensing*, American Society of Photogrammetry (R.N. Colwell, editor), American Society of Photogrammetry, Falls Church, Virginia.

Bhanu, B., P. Symosek, and S. Das, 1997. Analysis of Terrain Using Multispectral Images, *Pattern Recognition*, 30(2):197-215.

Bhattacharya, P., and X. Lu, 1997. A Width-Independent Sequential Thinning Algorithm, *International Journal of Pattern Recognition and Artificial Intelligence*, 11(3):393-403.

Bischof, H., W. Scheider, and A.J. Pinz, 1992. Multispectral Classification of Landsat-Images Using Neural Networks, *IEEE Transactions on Geoscience and Remote Sensing*, 30:482-493.

Blum, H., 1964. A Transformation for Extracting New Descriptors of Shape, *Symposium on Models for Perception of Speech and Vision Form*, MIT Press, Cambridge, pp. 362-380.

Bruzzone, L., C. Conese, F. Maselli, and F. Roli, 1997. Multisource Classification of Complex Rural Areas by Statistical and Neural-Network Approaches, *Photogrammetric Engineering & Remote Sensing*, 63(5):523-533.

Canters, F., 1997. Evaluating the Uncertainty of Area Estimates Derived from Fuzzy Land-Cover Classification, *Photogrammetric Engineering & Remote Sensing*, 63(4):403-414.

Carlotto, M.J., 1998. Spectral Shape Classification of Landsat Thematic Mapper Imagery, *Photogrammetric Engineering & Remote Sensing*, 64(9):905-913.

Castleman, K.R., 1996. *Digital Image Processing*, Prentice-Hall, New Jersey.

Chalifoux, S., F. Cavayas, and J.T. Gray, 1998. Map-Guided Approach for the Automatic Detection on Landsat TM Images of Forest Stands Damaged by the Spruce Budworm, *Photogrammetric Engineering & Remote Sensing*, 64(6):629-635.

Chavez, P.S., and J. Bowell, 1988. Comparison of the Spectral Information Content of Landsat Thematic Mapper and SPOT for Three Different Sites in the Phoenix, Arizona Region, *Photogrammetric Engineering & Remote Sensing*, 54(12):1699-1708.

Chavez, P.S., S.C. Sides, and J.A. Anderson, 1991. Comparison of Three Different Methods to Merge Multiresolution and Multispectral Data: Landsat TM and SPOT Panchromatic, *Photogrammetric Engineering & Remote Sensing*, 57(3):295-303.

Chen, C.S., and W.H. Hsu, 1990. A New One-Pass Algorithm and Its Parallel Hardware Implementation, *Pattern Recognition Letters*, 11(7):471-477.

Chen, Y.S., and W.H. Hsu, 1988. A Modified Fast Parallel Algorithm for Thinning Digital Patterns, *Pattern Recognition Letters*, 7(2):99-106.

Chen, Y.S., and W.H. Hsu, 1989. A Systematic Approach for Designing 2-Subcycle and Pseudo 1-Subcycle Parallel Thinning Algorithms, *Pattern Recognition*, 22(3):267-282.

Chen, Y.S., and W.H. Hsu, 1990. A Comparison of Some One-Pass Parallel Thinnings, *Pattern Recognition Letters*, 11(1):35-41.

Chou, J., R.C. Weger, J.M. Ligtenberg, K.S. Kuo, R.M. Welch, and P. Breeden, 1994. Segmentation of Polar Scenes Using Multispectral Texture Measures and Morphological Filtering, *International Journal of Remote Sensing*, 15(5):1019-1036.

Chow, C.K., and T. Kaneko, 1972. Automatic Boundary Detection of the Left-ventricle from Cineangiograms, *Comput. Biomed.*, 5:388-410.

Colwell, R.N. (editor), 1984. *Manual of Remote Sensing*, American Society of Photogrammetry, Falls Church, Virginia.

Congalton, R.G., M. Balogh, C. Bell, K. Green, J.A. Milliken, and R. Ottman, 1998. Mapping and Monitoring Agricultural Crops and Other Land Cover in the Lower Colorado River Basin, *Photogrammetric Engineering & Remote Sensing*, 64(11):1107-1113.

Current Science, 1996. Special Section: IRS-1C, Vol. 70, No. 7.

DeKruger, D., and B.R. Hunt, 1994. Imaging Processing and Neural Networks for Recognition of Cartographic Area Features, *Pattern Recognition*, 27(4):461-483.

Deng, W., and S.S. Lyengar, 1996. A New Probabilistic Relaxation Scheme and Its Application to Edge Detection, *IEEE Transactions on Pattern Analysis and Machine Intelligence*, 18(4):432-437.

Deppe, F., 1998. Forest Area Estimation Using Sample Surveys and Landsat MSS and TM Data, *Photogrammetric Engineering & Remote Sensing*, 64(4):285-292.

DiZenzo, S., S.D. DeGloria, R. Bernstein, and H.G. Kolsky, 1987. Gaussian Maximum Likelihood and Contextual Classification Algorithms for Multi Crop Classification, *IEEE Transactions on Geoscience and Remote Sensing*, 25:805-814.

Draeger, W.C., T.M. Holm, D.T. Lauer, and R.J. Thompson, 1997. The Availability of Landsat Data: Past, Present, and Future, *Photogrammetric Engineering & Remote Sensing*, 63(7):869-875.

Duda, R.O., and P.E. Hart, 1973. *Pattern Classification and Scene Analysis*, Wiley, New York.

Eklundh, J.O., H. Yamamoto, and R. Rosenfeld, 1980. A Relaxation Method for Multispectral Pixel Classification, *IEEE Transactions on Pattern Analysis and Machine Intelligence*, 2:72-75.

ERDAS Field Guide, 1997.

Farag, A.A., and E.J. Delp, 1995. Edge Linking by Sequential Search, *Pattern Recognition*, 28(5):611-633.

Faugeras, O.D., and M.M. Berthod, 1981. Improving Consistency and Reducing Ambiguity in Stochastic Labeling: An Optimization Approach, *IEEE Transactions on Pattern Analysis and Machine Intelligence*, 3:412-424.

Fernandes, R.A., and M.E. Jemigan, 1992. Unsupervised Multispectral Segmentation of Multispectral Imagery, *Proc. IEEE-SP Intl. Symp. Time-Frequency and Time-scal Analysis*, pp. 547-550.

Fiset, R., F. Cavayas, M.C. Mouchot, B. Solaiman, and R. Desjardins, 1998. Map-Image Matching Using a Multi-Layer Perception: The Case of the Road Network, *Journal of Photogrammetry & Remote Sensing*, 53:76-84.

Foody, G.M., 1999. The Continuum of Classification Fuzziness in Thematic Mapping, *Photogrammetric Engineering & Remote Sensing*, 65(4):443-451.

Foschi, P.G., and D.K. Smith, 1997. Detecting Subpixel Woody Vegetation in Digital Imagery Using Two Artificial Intelligence Approaches, *Photogrammetric Engineering & Remote Sensing*, 63(5):493-500.

Franklin, S.E., and D.R. Peddle, 1989. Spectral Texture for Improved Class Discrimination in Complex Terrain, *International Journal of Remote Sensing*, 10(8):1437-1443.

Freund, J.E., and R. E. Walpole, 1987. *Mathematical Statistics*, Prentice Hall, New Jersey.

Fu, K.S., 1978. Pattern Recognition in Remote Sensing of the Earth's Resources, *Digital Image Processing for Remote Sensing* (R. Bernstein, editor), IEEE Press, New York, pp. 297-305.

Fu, K.S., and J.K. Mui, 1981. A Survey on Image Segmentation, *Pattern Recognition*, 13:3-16.

Fu, K.S., and A. Rosenfeld, 1976. Pattern Recognition and Image Processing, *IEEE Trans. Comput.* 25:1336-1346.

Gahn, M., 1994. Umweltdokumentation mit Hilfe von Color-Infrarot-Luftbildern, *Umweltinformation und Karte Tagungsband*, 43, Deutscher Kartographentag, Trier, pp. 81-93.

Galbiati, L.J., 1990. *Machine Vision and Digital Image Processing Fundamentals*, Prentice-Hall, New Jersey.

Gambotto, J., 1993. A New Approach to Combining Region Growing and Edge Detection, *Pattern Recognition Letters*, 14(11):869-875.

Gascuel, O., B.B. Meunier, G. Caraux, P. Gallinari, A. Guenoche, Y. Guerneur, Y. Lechevallier, C. Marsala, L. Miclet, J. Nicolas, R. Nock, M. Ramdani, M. Sebag, B. Tallur, G. Venturini, and P. Vitte, 1993. Twelve Numerical, Symbolic and Hybrid Supervised Classification Methods, *International Journal of Pattern Recognition and Artificial Intelligence*, pp. 517-571.

Goldberg, M., D.G. Goodenough, M. Alvo, and G.M. Karam, 1985. A Hierarchical Expert System for Updating Forestry Maps with Landsat Data, *Proc. IEEE* 73(6):1054-1063.

Gong, P., and P.J. Howarth, 1990. The Use of Structural Information for Improving Land-Cover Classification Accuracies at the Rural-Urban Fringe, *Photogrammetric Engineering & Remote Sensing*, 56:67-73.

Gong, P., D.J. Marceau, and P.J. Howarth, 1992. A Comparison of Spatial Feature Extraction Algorithms for Land-Use Classification with SPOT HRV Data, *Remote Sensing of Environment*, 40:137-151.

Gonzalez, R.C., and P. Wintz, 1987. *Digital Image Processing*, Addison- wesley, Massachusetts.

Göpfert, W., 1987. *Raumbezogene Informationssysteme*, Herbert Wichmann Verlag, Karlsruhe.

Govindan, V.K., and A.P. Shivaprasad, 1987. A Pattern Adaptive Thinning Algorithm, *Pattern Recognition*, 20(6):623-637.

GPS Patherfinder Series, 1994. *Datalogging with TDC1 Asset SurveyorTM (TDC1 Asset SurveyorTM Software User's Guide)*.

GPS Patherfinder Series, 1994. *Pro XL System Operation Manual*.

Grandell, J., J. Pullianinen, and M. Hallikainen, 1998. Subpixel Land Use Classification and Retrieval of Forest Stem Volume in the Boreal Forest Zone by Employing SSM/I Data, *Remote Sensing of Environment*, 63:140-154.

Gross, H.N., and J.R. Schott, 1998. Application of Spectral Mixture Analysis and Image Fusion Techniques for Image Sharpening, *Remote Sensing of Environment*, 63:85-94.

Haberäcker, P., 1989. *Digitale Bildverarbeitung: Grundlagen und Anwendungen*, Carl Hanser Verlag, München.

Hall, E.L., 1979. *Computer Image Processing and Recognition*, Academic Press, New York.

Hancock, E.R., and J. Kittler, 1990. Edge-Labeling Using Dictionary-Based Relaxation, *IEEE Transactions on Pattern Analysis and Machine Intelligence*, 12(2):165-181.

Haralick, R.M., and H. Joo, 1986. A Context Classifier, *IEEE Transactions on Geoscience and Remote Sensing*, 24:997-1007.

Haralick, R.M., and L.G. Shapiro, 1985. Survey: Image Segmentation, *Computer Vision, Graphics and Image Processing*, 29:100-132.

Haralick, R.M., and L.G. Shapiro, 1992. *Computer and Robot Vision*, Addison-Wesley, Massachusetts.

Haslett, J., 1985. Maximum Likelihood Discriminant Analysis on the Plane Using a Markovian Model of Spatial Context, *Pattern Recognition*, 18:287-296.

Haydn, R., G.W. Dalke, and J. Henkel, 1982. Application of the IHS Transform to the Processing of Multisensor Data and Image Enhancement, *Proceedings, International Symposium on Remote Sensing of Arid and Semi-Arid Lands*, Cairo, Egypt, pp. 599-616.

Hopfield, J.J., 1982. Neural networks and physical systems with emergent collective computational abilities, *Proc. National Academy of Sciences, USA* 79 2554-2558.

Hord, R.M., 1982. *Digital Image Processing of Remotely Sensed Data*, Academic Press, New York.

Huguenin, R.L., M.A. Karaska, D.V. Blaricom, and J.R. Jensen, 1997. Subpixel Classification of Bald Cypress and Tupelo Gum Trees in Thematic Mapper Imagery, *Photogrammetric Engineering & Remote Sensing*, 63(6):717-725.

IRS-1C Data User's Handbook, 1995. Edited by National Remote Sensing Agency (NRSA), Hyderabad.

Jain, A.K., 1989. *Fundamentals of Digital Image Processing*, Prentice-Hall, New Jersey.

- Jain, R., R. Kasturi, and B.G. Schunck, 1995. *Machine Vision*, McGraw-Hill, New York.
- James, M., 1987. *Pattern Recognition*, BSP Professional Books, Oxford.
- Jähne, B., 1989. *Digitale Bildverarbeitung*, Springer-Verlag, Berlin.
- Jeng, J.F., and S. Sahni, 1992. Serial and Parallel Algorithms for the Medial Axis Transform, *IEEE Transactions on Pattern Analysis and Machine Intelligence*, 14(12):1218-1224.
- Jensen, J.R., 1986. *Digital Image Processing*, Prentice-Hall, New Jersey.
- Jensen, J.R., and D.C. Cowen, 1999. Remote Sensing of Urban/Suburban Infrastructure and Socio-Economic Attributes, *Photogrammetric Engineering & Remote Sensing*, 65(5):611-622.
- Jhung, Y., and P.H. Swain, 1996. Bayesian Contextual Classification Based on Modified M -Estimates and Markov Random Fields, *IEEE Transactions on Geoscience and Remote Sensing*, 34(1):67-75.
- Kalayeh, H.M., and D.A. Landgrebe, 1987. Stochastic Model Utilizing Spectral and Spatial Characteristics, *IEEE Transactions on Pattern Analysis and Machine Intelligence*, 9:457-461.
- Kanal, L., 1974. Patterns in Pattern Recognition: 1968-1974, *IEEE Trans. Inform. Theory*, 20:697-722.
- Kartikeyan, B., and B. Gopalakrishna, 1994. Contextual Techniques for Classification of High and Low Resolution Remote Sensing Data, *International Journal of Remote Sensing*, 15(5):1037-1051.
- Kartikeyan, B., K.L. Majumder, and A.R. Dasgupta, 1995. An Expert System for Land Cover Classification, *IEEE Transactions on Geoscience and Remote Sensing*, 33(1):58-66.
- Kasturirangan, K., 1996. Indian Remote Sensing Satellite (IRS)-1C-The Beginning of a New Era, *Current Science*, 70(7):495-500.
- Kettig, R.L., and D.A. Landgrebe, 1976. Classification of Multispectral Image Data by Extraction and Classification of Homogeneous Objects, *IEEE Transactions on Geoscience Electronics*, 14:19-26.
- Khazenie, N., and M.M. Grawford, 1990. Spatial-temporal Autocorrelated Model for Contextual Classification, *IEEE Transactions on Geoscience and Remote Sensing*, 28:529-539.
- Khuen, C.A., 1997. Commercial Applications for High Resolution Geospatial Imagery, *Photogrammetric Engineering & Remote Sensing*, pp. 933-941.
- Kloer, B.R., 1994. Hybrid Parametric/Non-parametric Image Classification, *The ACSM-ASPRS Annual Convention*, Reno, Nevada.

- Knick, S.T., J.T. Rotenberry, and T.J. Zarriello, 1997. Supervised Classification of Landsat Thematic Mapper Imagery in a Semi-Arid Rangeland by Nonparametric Discriminant Analysis, *Photogrammetric Engineering & Remote Sensing*, 63(1):79-86.
- Kusaka, T., and Y. Kawata, 1991. Hierarchical Classification of Landsat TM Image Using Spectral and Spatial Information, *International Geoscience and Remote Sensing Symposium (IGARSS'91)*, pp. 2187-2190.
- Kushwaha, S.P.S., S. Kuntz, and G. Oesten, 1994. Applications of Image Texture in Forest Classification, *International Journal of Remote Sensing*, 15(11):2273-2284.
- Lam, L., S.W. Lee, and C.Y. Suen, 1992. Thinning Methodologies-A Comprehensive Survey, *IEEE Transactions on Pattern Analysis and Machine Intelligence*, 14(9):869-885.
- Landgrebe, D.A., 1980. The Development of a Spectral-Spatial Classifier for Earth Observational Data, *Pattern Recognition*, 12:165-175.
- Lee, K.S., W.D. Philpot, and S.W. Pacala, 1992. Calibration of a Forest Ecosystem Model Using Remote Sensing and GIS, *Proceedings, ASPRS/ACSM/RT 92', Monitoring and Mapping Global Change*, ASPRS/ACSM, Washington, D.C., 4:20-29.
- Li, R., 1998. Potential of High-Resolution Satellite Imagery for National Mapping Products, *Photogrammetric Engineering & Remote Sensing*, 64(12):1165-1169.
- Liedtke, C.E., and M. Ender, 1989: *Wissensbasierte Bildverarbeitung*, Springer-Verlag, Berlin.
- Lillesand, T.M., and R.W. Kiefer, 1994. *Remote Sensing and Image Interpretation* (third edition), John Wiley & Sons, New York.
- Low, A., 1991. *Introductory Computer Vision and Image Processing*, McGraw-Hill, London.
- Macleod, R.D., and R.G. Congalton, 1998. A Quantitative Comparison of Change-Detection Algorithms for Monitoring Eelgrass from Remotely Sensed Data, *Photogrammetric Engineering & Remote Sensing*, 64(3):207-216.
- Mallet, Y., D. Coomans, J. Kautsky, and O. De Vel, 1997. Classification Using Adaptive Wavelets for Feature Extraction, *IEEE Transactions on Pattern Analysis and Machine Intelligence*, 19(10):1058-1066.
- Marr, D., 1982. *Vision*, Freeman, San Francisco.
- Masarilla, L., E.H. Zahzah, and J. Desachy, 1993. Combination of Remote Sensing and Geocoded Data for Satellite Image Interpretation Based on Neural Networks, *Proc. Intl. Geosci. Remote Sensing Symp. '93*, Vol II, pp. 725-727.
- Mather P.M., 1991. *Computer Applications in Geography*, John Wiley & Sons, New York.

- Martin, M.E., S.D. Newman, J.D. Aber, and R.G. Congalton, 1998. Determining Forest Species Composition Using High Spectral Resolution Remote Sensing Data, *Remote Sensing of Environment*, 65:249-254.
- Maselli, F., M.A. Gilabert, and C. Conese, 1998. Integration of High and Low Resolution NDVI Data for Monitoring Vegetation in Mediterranean Environments, *Remote Sensing of Environment*, 63:208-218.
- Matsuyama, T., 1987. Knowledge-based Aerial Image Understanding Systems and Expert Systems for Image Processing, *IEEE Transactions on Geoscience and Remote Sensing*, 25(3):305-316.
- McCloy, K.R., 1995. *Resource Management Information Systems*, Taylor & Francis, London.
- McLachlan, G.J., 1992. *Discriminant Analysis and Statistical Pattern Recognition*, John Wiley & Sons, New York.
- Merickel, M.B., J.C. Landgrebe, and S.S. Shen, 1984. A Spatial Processing Algorithm to Reduce the Effects of Mixed Pixels and Increase the Separability between Classes, *Pattern Recognition*, 17:525-533.
- Messev, V., 1998. The Use of Census Data in Urban Image Classification, *Photogrammetric Engineering & Remote Sensing*, 64(5):431-438.
- Metternicht, G.I., and J.A. Zinck, 1998. Evaluating the Information Content of JERS-1 SAR and Landsat TM Data for Discrimination of Soil Erosion Features, *Journal of Photogrammetry & Remote Sensing*, 53:143-153.
- Moigne, J.L., and J.C. Tilton, 1995. Refining Image Segmentation by Integration of Edge and Region Data, *IEEE Transactions on Geoscience and Remote Sensing*, 33(3):605-615.
- Moller-Jensen, L., 1990. Knowledge-based Classification of an Urban Area Using Texture and Context Information in Landsat-TM Imagery, *Photogrammetric Engineering & Remote Sensing*, 56(6):899-904.
- Naccache, N.J., and R. Shinghal, 1984. STPA: A Proposed Algorithm for Thinning Binary Patterns, *IEEE Trans. Syst. Man Cybernet.* 14:409-418.
- Nagao, M., and T. Matsuyama, 1979. Edge Preserving Smoothing, *Computer Vision, Graphics and Image Processing*, 9:394-407.
- Nagao, M., and T. Matsuyama, 1980. *A Structural Analysis of Complex Aerial Photographs*, Plenum Press, New York.
- Nakagawa, Y., and A. Rosenfeld, 1979. Some Experiments on Variable thresholding, *Pattern Recognition*, 11:191-204.
- NASA, 1974. *Skylab Earth Resource Data Catalog*, Document No. 3300-00586, Government Printing Office, Washington D.C.

NASA, 1976. *Landsat Data Users Handbook*, Document No. 76SDS4258, Goddard Space Flight Center, Greenbelt, MD.

National Remote Sensing Agency, 1995. *IRS-1C Data Users Handbook*, Hyderabad.

Needham, B.H., 1986. Chapter 9: Availability of Remotely Sensed Data and Information from the U.S. National Oceanic and Atmospheric Administration's Satellite Data Service Division, *Satellite Remote Sensing for Resource Development*, Gaithersburg, Graham & Trotman, Inc., Maryland.

Pal, N.R., and S.K. Pal, 1993. A Review on Image Segmentation Techniques, *Pattern Recognition* 26(9): 1277-1294.

Pal, S.K., and P.P. Wang (editors), 1996. *Genetic Algorithms for Pattern Recognition*, CRC Press, Boca Raton.

Paola, J.D., and R.A. Schowengerdt, 1997. The Effect of Neural-Network Structure on a Multispectral Land-Use /Land-Cover Classification, *Photogrammetric Engineering & Remote Sensing*, 63(5):535-544.

Pavlidis, T., 1977. *Structural Pattern Recognition*, Springer Verlag, New York.

Pavlidis, T., and Y. Liow, 1990. Integrating Region Growing and Edge Detection, *IEEE Transactions on Pattern Analysis and Machine Intelligence*, 12(3):225-233.

Pearl, J., 1984. *Heuristics - Intelligent Search Strategies for Computer Problem Solving*, Addison-Wesley, Massachusetts.

Peddle, D.R., F.G. Hall, and E.F. LeDrew, 1999. Spectral Mixture Analysis and Geometric-Optical Reflectance Modeling of Bored Forest Biophysical Structure, *Remote Sensing of Environment*, 67:288-297.

Peleg, S., 1980. A New Probabilistic Relaxation Scheme, *IEEE Transactions on Pattern Analysis and Machine Intelligence*, 2:362-369.

Persoon, E., and K.S. Fu, 1977. Shape Description Using Fourier descriptors, *IEEE Trans. Syst. Man Cybernet*, 7:170-179.

Pitas, I., 1993. *Digital Image Processing Algorithms*, Prentice Hall, London.

Richards, J.A., 1994. *Remote Sensing Digital Image Analysis: An Introduction*, Springer-Verlag, Berlin.

Richards, J.A., D.A. Landgrebe, and P.H. Swain, 1981a. Pixel Labeling by Supervised Probabilistic Relaxation, *IEEE Transactions on Pattern Analysis and Machine Intelligence*, 3:188-191.

Richards, J.A., D.A. Landgrebe, and P.H. Swain, 1981b. On the Accuracy of Pixel Relaxation Labelling, *IEEE Trans. Systems, Man and Cybernetics*, 11:303-309.

- Richards, J.A., D.A. Landgrebe, and P.H. Swain, 1982. A Means for Utilizing Ancillary Information in Multispectral Classification, *Remote Sensing of Environment*, 12:463-477.
- Ridd, M.K., and J. Liu, 1998. A Comparison of Four Algorithms for Change Detection in an Urban Environment, *Remote Sensing of Environment*, 63:95-100.
- Rion, R., and F. Seyler, 1997. Texture Analysis of Tropical Rain Forest Infrared Satellite Images, *Photogrammetric Engineering & Remote Sensing*, 63(5):515-521.
- Rosenfeld, A., and A.C. Kak, 1982. *Digital Picture Processing*, Academic Press, New York.
- Rosenfeld, A., and J.S. Weszka, 1976. Picture Recognition, *Digital Pattern Recognition* (K.S. Fu, W.D. Keidel, and H. Wolter, editors), Springer-Verlag, New York, pp. 135-166.
- Rutkowski, W.S., S Peleg, and A. Rosenfeld, 1981. Shape Segmentation Using Relaxation, *IEEE Transactions on Pattern Analysis and Machine Intelligence*, 3(4):368-375.
- Salvador, R., 1999. A Parametric Model for Estimating Relations between Unprecisely Located Field Measurements and Remotely Sensed Data, *Remote Sensing of Environment*, 67:99-107.
- Schowengerdt, R., 1983. *Techniques for Image Processing and Classification in Remote Sensing*, Academic Press, New York.
- Segl, K., 1996. *Integration von Form- und Spektralmerkmalen durch Künstliche neuronale Netze bei der Satellitenbildklassifizierung*, Ph.D. Dissertation, Verlag der Bayerischen Akademie der Wissenschaften, Münch.
- Sharma, K.M.S., and A. Sarkar, 1998. A Modified Contextual Classification Technique for Remote Sensing Data, *Photogrammetric Engineering & Remote Sensing*, 64(4):273-280.
- Shinji, T., 1983. Thinning Algorithms for Digital Pictures and Their Application to Handprinted Characters Recognition, *Trans. IECE J66-D* (in Japanese), pp. 526-532.
- Solaiman, B., R.K. Koffi, M. Mouchot, and A. Hillion, 1998. An Information Fusion Method for Multispectral Image Classification Postprocessing, *IEEE Transactions on Geoscience and Remote Sensing*, 36(2):395-406.
- Sossa, J.H., 1989. An Improved Parallel Algorithm for Thinning Digital Patterns, *Pattern Recognition Letters*, 10(2):77-80.
- Star, J., and J. Estes, 1990. *Geographic Information System: An Introduction*, Prentice-Hall, New Jersey.
- Strahler, A.H., 1980. The Use of Prior Probabilities in Maximum Likelihood Classification of Remotely Sensed Data, *Remote Sensing of Environment*, 10:135-163.
- Swain, P.H., 1985. Advanced Interpretation Techniques for Earth Data Information Systems, *Proc. IEEE* 73(6):1031-1039.

Swain, P.H., and S.M. Davis (editors.), 1978. *Remote Sensing: The Quantitative Approach*, McGraw-Hill, New York.

Swain, P.H., S.B. Vardeman, and J.C. Tilton, 1981. Contextual Classification of Multispectral Image Data, *Pattern Recognition*, 13(6):429-441.

Therrien, C.A., 1983. An Estimation-Theoretic Approach to Terrain Image Segmentation, *Computer Graphics Image Processing* 22:313-326.

Thomas, I.L., 1987 *Classification of Remotely Sensed Images*, Adam Hilger, Bristol.

Thormodsgrad, J.M., and J.W. Feuquay, 1987. Large Scale Image Mapping with SPOT, *Proceedings, SPOT-1 Utilization and Assessment Results*, Paris.

Tilton, J.C., S.B. Vardeman, and P.H. Swain, 1982. Estimation of Context for Statistical Classification of Multispectral Image Data, *IEEE Transactions on Geoscience and Remote Sensing*, 20(4):445-452.

Tom, C., L.D. Miller, and J.W. Christenson, 1978. Spatial Land Use Inventory, Modeling, and Projection/ Denver Metropolitan Area with Inputs from Existing Maps, Airphotos, and Landsat Imagery, *NASA Technical Memorandum 79710*, National Aeronautics and Space Administration, Greenbelt, Md.

Ton, J., J. Stricklen, and A.K. Jain, 1991. Knowledge-based Segmentation of Landsat Images, *IEEE Transactions on Geoscience and Remote Sensing*, 29(2):222-232.

Toussaint, G.C., 1978. The Use of Context in Pattern Recognition, *Pattern Recognition*, 10:189-204.

Toutin, T., 1998. SPOT and Landsat Stereo Fusion for Data Extraction over Mountainous Areas, *Photogrammetric Engineering & Remote Sensing*, 64(2):109-113.

Townsend, F.E., 1986. The Enhancement of Computer Classifications by Logical Smoothing, *Photogrammetric Engineering & Remote Sensing*, 52:213-221.

Vogelmann, J.E., T. Sohl, and S.M. Howard, 1998. Regional Characterization of Land Cover Using Multiple Sources of Data, *Photogrammetric Engineering & Remote Sensing*, 64(1):45-57.

Wald, L., T. Ranchin, and M. Mangolini, 1997. Fusion of Satellite Images of Different Spatial Resolutions: Assessing the Quality of Resulting Images, *Photogrammetric Engineering & Remote Sensing*, 63(6):691-699.

Wang, Y., 1998. Principles and Application of Structural Image Matching, *Journal of Photogrammetry & Remote Sensing*, 53:154-165.

Welch, R., and W. Ehlers, 1987. Merge Multiresolution SPOT HRV and Landsat TM data, *Photogrammetric Engineering & Remote Sensing*, 53(3):301-303.

Wharton, S.W., 1987. A Spectral-Knowledge-Based Approach for Urban Land-Cover Discrimination, *IEEE Transactions on Geoscience and Remote Sensing*, 25(3):272-282.

- Whichello, A.P., and H. Yan, 1996. Linking Broken Character Borders with Variable Sized Masks to Improve Recognition, *Pattern Recognition*, 29(8):1429-1435.
- Wickham, J.D., R.V. O'Neill, K.H. Riitters, T.G. Wade, and K.B. Jones, 1997. Sensitivity of Selected Landscape Pattern Metrics to Land-Cover Misclassification and Differences in Land-Cover Composition, *Photogrammetric Engineering & Remote Sensing*, 63(4):397-402.
- Wilson, P.A., 1997. Rule-Based Classification of Water in Landsat MSS Images Using the Variance Filter, *Photogrammetric Engineering & Remote Sensing*, 63(5):485-491.
- Winston, P.H., 1975. Learning structural descriptions from examples, *The psychology of Computer Vision*, Mc Graw Hill, New York, pp. 157-209.
- Wu, R.Y., and W.H. Tsai, 1992. A New One-Pass Parallel Thinning Algorithm for Binary Images, *Pattern Recognition Letters*, 13(10):715-723.
- Yanowitz, S.D., and A.M. Bruckstein, 1989. A New Method for Image Segmentation, *Computer Vision Graphics Image Processing*, 46:82-95.
- Yokoya, N., and M.D. Levine, 1989. Range Image Segmentation based on Differential Geometry: A Hybrid Approach, *IEEE Transactions on Pattern Analysis and Machine Intelligence*, 11(6):643-694.
- Yu, F.T.S., and S. Jutamulia (editors), 1998. *Optical Pattern Recognition*, Cambridge University Press, Cambridge.
- Yuan, D., J.R. Lucas, and D.E. Holland, 1998. A Landsat MSS Time Series Model and Its Application in Geological Mapping, *Journal of Photogrammetry & Remote Sensing*, 53:39-53.
- Zadeh, L.A., 1965. Fuzzy sets, *Information Control*, pp.338-353.
- Zhang, M.C., R.M. Haralick, and J.B. Campbell, 1990. Multispectral Image Context Classification Using Stochastic Relaxation, *IEEE Trans. Systems Man Cybernet, SMC* 20(1):128-140.
- Zhang, T.Y., and C.Y. Suen, 1984. A Fast Parallel Algorithm for Thinning Digital Patterns, *Commun, ACM* 27, pp. 236-239.
- Zhang, Y.J., 1996. A Survey of Evaluation Methods for Image Segmentation, *Pattern Recognition* 29(8):1335-1346.
- Zhang, Y.Y., and P.S.P. Wang, 1995. Analysis and Design of Parallel Thinning Algorithms - A Generic Approach, *International Journal of Pattern Recognition and Artificial Intelligence*, 9(5):735-752.
- Zhu, A.X., 1997. Measuring Uncertainty in Class Assignment for Natural Resource Maps under Fuzzy Logic, *Photogrammetric Engineering & Remote Sensing*, 63(10):1195-1202.

Lebenslauf

Name: SUN
Vorname: Wanxiao

Geboren am: 08.10.1965 in Fushun
Staatsangehörigkeit: Chinesisch
Familienstand: Verheirated, 1 Kind
Anschrift: Jakob-Welder-Weg 30, 55128 Mainz

Ausbildungsgang

1972 – 1977 Grundschule Dong Fanghong, Fushun

1977 – 1982 Gymnasium No. 2 in Fushun

1982 – 1986 Nanjing University
Studium der Geographie
Studienfächer: Computer aided Kartographie
Abschluß: Bachelor Degree

1986 - 1989 Nanjing Institute of Geography and Limnology; Chinese Academy of
Sciences Studienfächer: Geographische Informations Systeme und
Fernerkundung
Abschluß: Master Degree

1989 – 1992 Nanjing Institute of Geography and Limnology; Chinese Academy of
Sciences Wissenschaftliche Angestellte

1992 – 1994 Deutschkurse an der Johannes Gutenberg-Universität, Mainz

1995 – 1996 Geographisches Institut der Johannes Gutenberg-Universität, Mainz
Mitarbeit an der Stadt-Biotopkartierung Mainz

1997 – 1999 Graduiertenkolleg der Johannes Gutenberg-Universität, Mainz

Fremdsprachen: Deutsch, Englisch: fließend in Wort und Schrift

Mainz, den 30.11.1999